

Supporting Information

Synthesis and Reactivity of Zr MOFs Assembled from P^NN^NP-Ru Pincer Complexes

Abebu A. Kassie[†], Pu Duan[‡], Matthew B. Gray[†], Klaus Schmidt-Rohr[‡], Patrick M. Woodward[†], Casey R. Wade^{*†}

[†]Department of Chemistry and Biochemistry, The Ohio State University, Columbus, Ohio 43210, United States

[‡]Department of Chemistry, Brandeis University, Waltham, Massachusetts 02453, United States

Contents

Figure S1. ¹ H NMR spectrum of [Bu ₄ L-RuH(CO)(PPh ₃)]Cl in DMSO-d ₆ .	S3
Figure S2. ³¹ P{ ¹ H} NMR spectrum of [Bu ₄ L-RuH(CO)(PPh ₃)]Cl in DMSO-d ₆ .	S4
Figure S3. ¹³ C{ ¹ H} NMR spectrum of [Bu ₄ L-RuH(CO)(PPh ₃)]Cl in DMSO-d ₆ .	S5
Figure S4. ¹ H NMR spectrum of [Bu ₄ L-RuH(CO)(PPh ₃)]TFA in DMSO-d ₆ .	S6
Figure S5. ³¹ P{ ¹ H} NMR spectrum of [Bu ₄ L-RuH(CO)(PPh ₃)]TFA in DMSO-d ₆ .	S7
Figure S6. ¹ H NMR spectrum of [H ₄ L-Ru(TFA)(CO)(PPh ₃)]TFA in DMSO-d ₆ .	S8
Figure S7. ³¹ P{ ¹ H} NMR spectrum of [H ₄ L-Ru(TFA)(CO)(PPh ₃)]TFA in DMSO-d ₆ .	S9
Figure S8. ¹³ C{ ¹ H} NMR spectrum of [H ₄ L-Ru(TFA)(CO)(PPh ₃)]TFA in DMSO-d ₆ .	S10
Figure S9. ¹ H NMR spectrum of [Bu ₄ L-RuCl(CO) ₂]Cl in DMSO-d ₆ .	S11
Figure S10. ³¹ P{ ¹ H} NMR spectrum of [Bu ₄ L-RuCl(CO) ₂]Cl in DMSO-d ₆ .	S12
Figure S11. ¹³ C{ ¹ H} NMR spectrum of [Bu ₄ L-RuCl(CO) ₂]Cl in DMSO-d ₆ .	S13
Figure S12. ¹ H NMR spectrum of [H ₄ L-RuCl(CO) ₂]TFA in DMSO-d ₆ .	S14
Figure S13. ³¹ P{ ¹ H} NMR spectrum of [H ₄ L-RuCl(CO) ₂]TFA in DMSO-d ₆ .	S15
Figure S14. ¹³ C{ ¹ H} NMR spectrum of [H ₄ L-RuCl(CO) ₂]TFA in DMSO-d ₆ .	S16
Figure S15. ³¹ P{ ¹ H} NMR spectrum of <i>cis/trans</i> -Bu ₄ L-RuCl ₂ (CO) in DMSO-d ₆ .	S17
Figure S16. ¹ H NMR spectrum of <i>cis/trans</i> -Bu ₄ L-RuCl ₂ (CO) in DMSO-d ₆ .	S18
Figure S17. ¹ H NMR spectrum of <i>cis/trans</i> -H ₄ L-RuCl ₂ (CO) in DMSO-d ₆ .	S19
Figure S18. ³¹ P{ ¹ H} NMR spectrum of <i>cis/trans</i> -H ₄ L-RuCl ₂ (CO) in DMSO-d ₆ .	S20
Figure S19. ATR-IR spectra of Bu ₄ L-Ru-P ^N N ^N P pincer complexes	S21
Figure S20. ATR-IR spectra of H ₄ L-Ru-P ^N N ^N P pincer complexes	S22
Figure S21. ATR-IR spectra of RuCl ₂ (CO) ₃ (HCO ₂ H) and RuCl ₂ (CO) ₃ (THF)	S23
Synchrotron X-ray Powder Diffraction, Structure Solution, and Rietveld Refinement of 1	S24
Table S1. Fractional coordinates of the asymmetric unit for framework structure 1.	S24
Pawley refinement of 1.	S25
Table S2. Pawley refinement parameters for 1 in <i>P6/mmm</i> space group.	S25
Figure S22. CsF- and acid-digested ³¹ P{ ¹ H} NMR spectra of 1, 2 and 3.	S26
Figure S23. CsF-digested ¹ H NMR spectrum (DMSO-d ₆ /D ₂ O) of 1 after MeOH solvent exchange.	S27
Figure S24. CsF-digested ¹ H NMR spectrum (DMSO-d ₆ /D ₂ O) of 1 after activation.	S28
Figure S25. CsF-digested ³¹ P{ ¹ H} NMR spectrum (DMSO-d ₆ /D ₂ O) of 1 after activation.	S29
Figure S26. ³¹ P{ ¹ H} NMR spectrum for MOF reaction supernatant of 1.	S30
Figure S27. Solid-state NMR spectra of 1, 2 and 3.	S31

Figure S28. Acid-digested ^1H NMR spectrum ($\text{CF}_3\text{CO}_2\text{H}/\text{DMSO}-d_6$) of 2 after THF washing.	S32
Figure S29. Acid-digested ^1H NMR spectrum ($\text{CF}_3\text{CO}_2\text{H}/\text{DMSO}-d_6$) of 2 after activation.....	S33
Figure S30. Acid-digested $^{31}\text{P}\{^1\text{H}\}$ NMR spectrum ($\text{CF}_3\text{CO}_2\text{H}/\text{DMSO}-d_6$) of 2 after activation.	S34
Figure S31. Acid-digested ^1H NMR spectrum ($\text{CF}_3\text{CO}_2\text{H}/\text{DMSO}-d_6$) of 3 after MeOH solvent exchange.....	S35
Figure S32. Solid-state ^{31}P and ^{13}C NMR spectra of MOF 3 synthesized with HCO_2H as the modulator.	S36
Figure S33. TGA for MeOH soaked sample of 1 measured at a ramp rate of $5\text{ }^\circ\text{C}/\text{min}$ under flowing N_2	S37
Figure S34. TGA for MeOH soaked sample of 3 measured at a ramp rate of $5\text{ }^\circ\text{C}/\text{min}$ under flowing N_2	S38
Figure S35. TGA for THF-exchanged sample of 2 measured at ramp rate of $5\text{ }^\circ\text{C}/\text{min}$ under flowing N_2	S39
Figure S36. XRPD patterns for as synthesized, THF and MeOH solvent exchanged samples of 2.	S40
Figure S37. N_2 adsorption isotherm (77 K) for MeOH soaked sample of 1	S41
Figure S38. N_2 adsorption isotherm (77 K) for THF soaked sample of 2	S42
Figure S39. N_2 adsorption isotherm (77 K) for MeOH soaked sample of 3	S43
Figure S40. XRPD patterns for activated samples of 1, 2 and 3.....	S44
Figure S41. ATR-IR spectra for samples of 1, 3 (MeOH soaked), and 2 (THF soaked).	S45
Figure S42. ATR-IR spectra for 2 before and after activation.	S46
Figure S43. Diffuse reflectance IR spectra of 2 at room temperature and have heating to 100 and $150\text{ }^\circ\text{C}$	S47
Figure S44. ATR-IR spectra of 2, 2-a, and 2-b.....	S48
Figure S45. XRPD patterns of 2, 2-a and 2-b.....	S49
Figure S46. XRPD patterns of 1 and 1-KO ^t Bu.....	S50
Figure S47. XRPD patterns of 3 and 3-KO ^t Bu.....	S51
Figure S48. ATR-IR spectra for $[\text{tBu}_4\text{L-RuCl}(\text{CO})_2]\text{Cl}$ reaction with KO ^t Bu and Me_3NO	S52
Figure S49. ATR-IR spectra for 2-b before and after catalysis, and regeneration of 2-b with Me_3NO	S53
Table S3. Hydrosilylation of aryl aldehydes catalyzed by 2-b	S54
Figure S50. ^1H NMR spectrum for hydrosilylation of benzaldehyde with 2-b.	S55
Figure S51. GC/MS chromatogram for the hydrosilylation of benzaldehyde with 2-b	S56
Figure S52. ^1H NMR spectrum for hydrosilylation of benzaldehyde with 2.....	S57
Figure S53. ^1H NMR spectrum for hydrosilylation of benzaldehyde with 2-a.....	S58
Figure S54. ^1H NMR spectrum for hydrosilylation of benzaldehyde with 2 treated with Me_3NO	S59
Figure S55. ^1H NMR spectrum for hydrosilylation of benzaldehyde with 1	S60
Figure S56. ^1H NMR spectrum for hydrosilylation of benzaldehyde with 1-KO ^t Bu.	S61
Figure S57. ^1H NMR spectrum for hydrosilylation of benzaldehyde with 3.....	S62
Figure S58. ^1H NMR spectrum for hydrosilylation of benzaldehyde with 3-KO ^t Bu.	S63
Figure S59. ^1H NMR spectrum for hydrosilylation of benzaldehyde with $[\text{tBu}_4\text{L-RuCl}(\text{CO})_2]\text{Cl}$	S64
Figure S60. ^1H NMR spectrum for hydrosilylation of benzaldehyde with <i>cis/trans</i> - $\text{tBu}_4\text{L-RuCl}_2(\text{CO})$	S65
Figure S61. ^1H NMR spectrum for hydrosilylation of benzaldehyde with $\text{tBu}_4\text{L-RuCl}(\text{CO})$	S66
Figure S62. ^1H NMR spectra before and after hot filtration for hydrosilylation of benzaldehyde with 2-b.....	S67
Figure S63. ^1H NMR spectrum for hydrosilylation of o-anisaldehyde with 2-b	S68
Figure S64. GC/MS chromatogram for the hydrosilylation of O-anisaldehyde with 2-b.....	S69
Figure S65. ^1H NMR spectrum for hydrosilylation of 4-methylbenzaldehyde with 2-b	S70

Figure S66. GC/MS chromatogram for the hydrosilylation of 4-methylbenzaldehyde with 2-b.....	S71
Figure S67. ¹ H NMR spectrum for hydrosilylation of 4-(Trifluoromethyl)benzaldehyde with 2-b.	S72
Figure S68. GC/MS chromatogram for the hydrosilylation of 4-(Trifluoromethyl)benzaldehyde with 2-b	S73
Figure S69. ¹ H NMR spectrum for for the hydrosilylation of 4-methoxybenzaldehyde with 2-b.	S74
Figure S70. GC/MS chromatogram for the hydrosilylation of 4-methoxybenzaldehyde with 2-b.	S75
Figure S71. ¹ H NMR spectrum for the hydrosilylation of 3,5-dibenzyloxybenzaldehyde with 2-b.....	S76
Figure S72. GC/MS chromatogram for the hydrosilylation of 3,5-dibenzyloxybenzaldehyde with 2-b.	S77
Figure S73. ¹ H NMR spectrum for the hydrosilylation of acetophenone with 2-b.....	S78
Figure S74. GC/MS chromatogram for the hydrosilylation of acetophenone with 2-b.	S79
REFERENCES.	S80

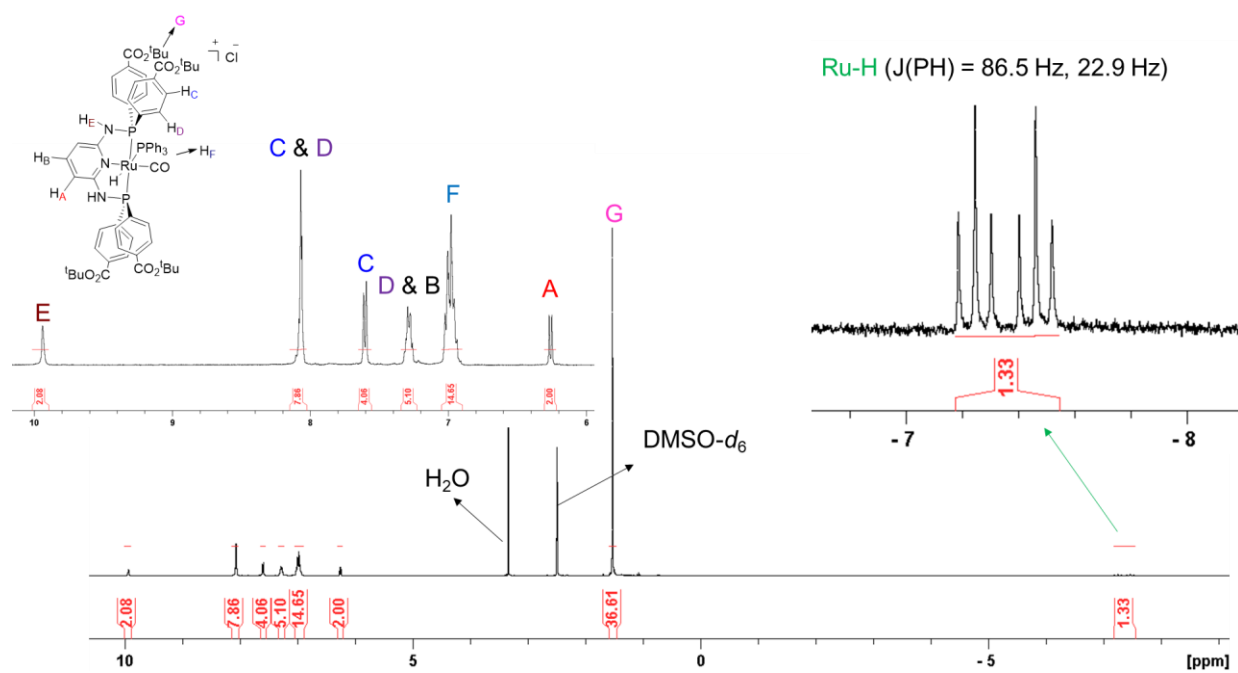


Figure S1. ^1H NMR spectrum of $[\text{tBu}_4\text{L-RuH(CO)(PPh}_3\text{)}]\text{Cl}$ in DMSO-d₆.

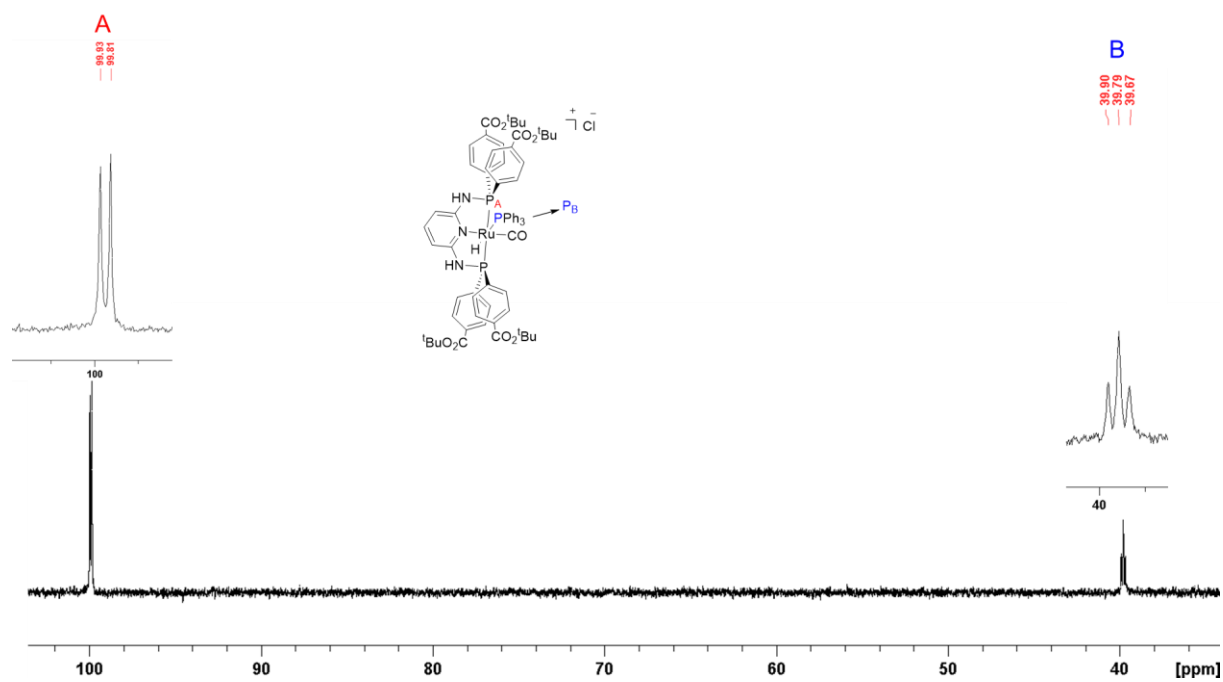


Figure S2. $^{31}\text{P}\{^1\text{H}\}$ NMR spectrum of $[\text{tBu}_4\text{L-RuH(CO)(PPh}_3\text{)}]\text{Cl}$ in DMSO-d_6 .

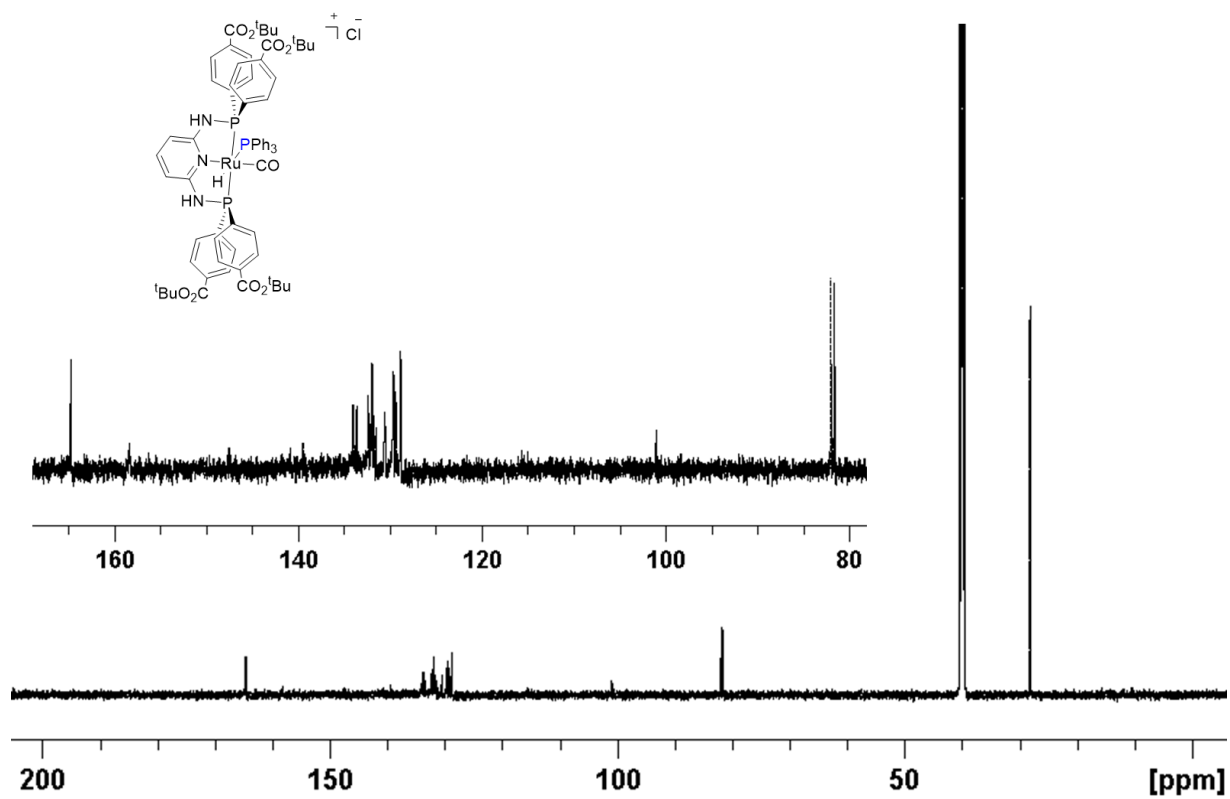


Figure S3. $^{13}\text{C}\{^1\text{H}\}$ NMR spectrum of $[\text{tBu}_4\text{L-RuH(CO)(PPh}_3\text{)]Cl}$ in DMSO-d_6 .

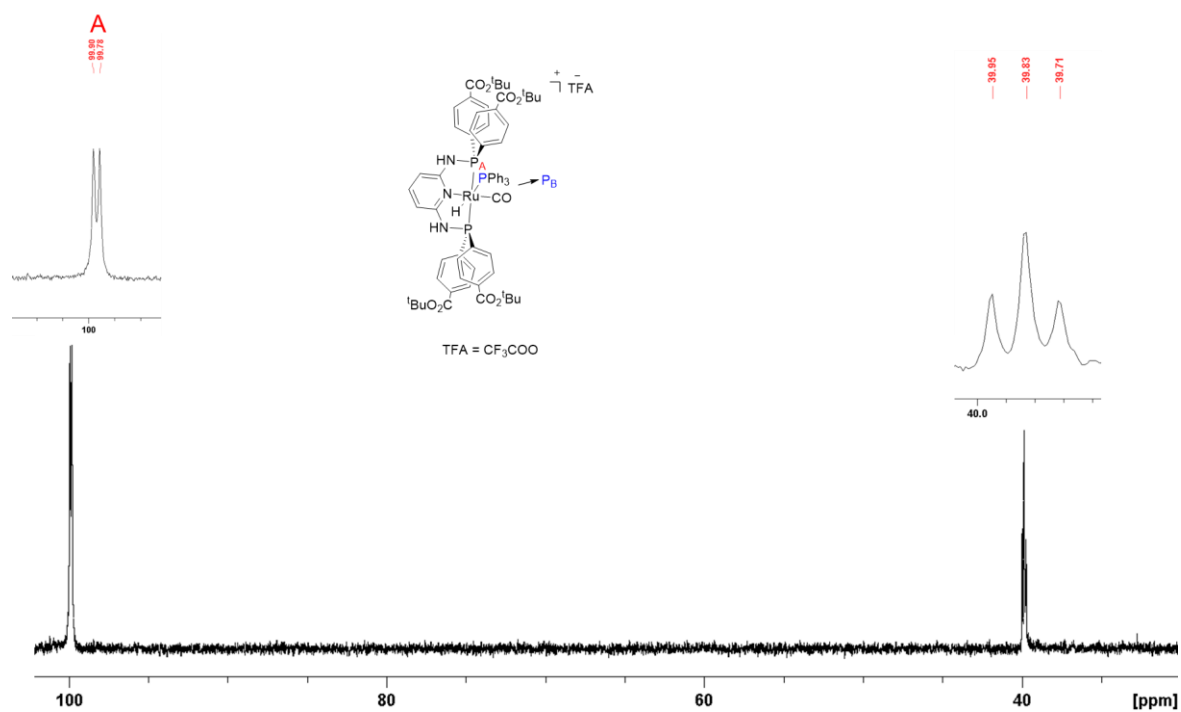


Figure S5. $^{31}\text{P}\{^1\text{H}\}$ NMR spectrum of $[\text{tBu}_4\text{L-RuH(CO)(PPh}_3\text{)]TFA}$ in DMSO-d_6 .

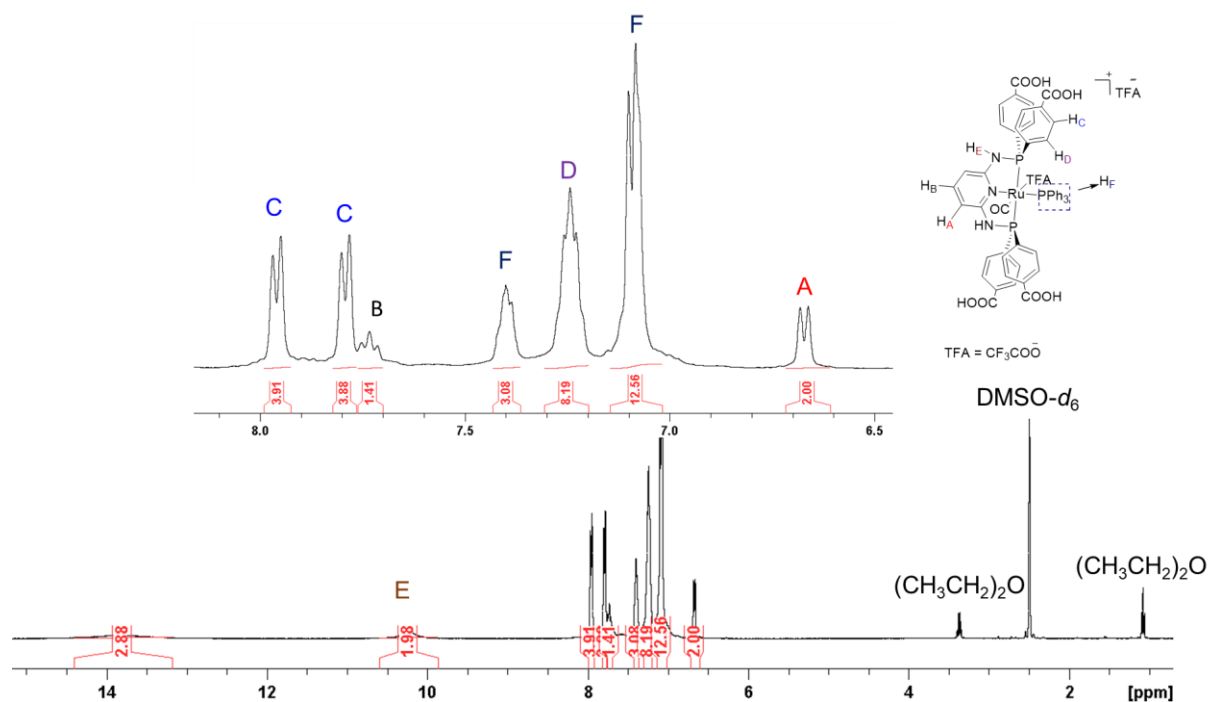


Figure S6. ^1H NMR spectrum of $[\text{H}_4\text{L-Ru}(\text{TFA})(\text{CO})(\text{PPh}_3)]\text{TFA}$ in $\text{DMSO-}d_6$.

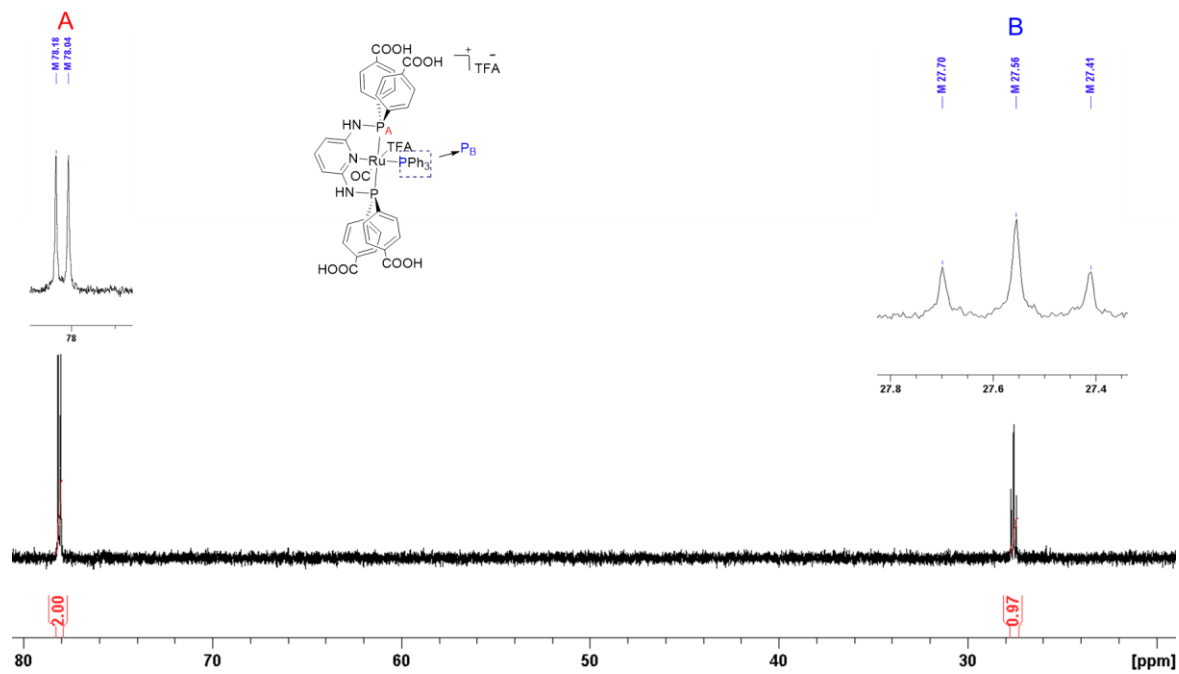


Figure S7. ^{31}P $\{^1\text{H}\}$ NMR spectrum of $[\text{H}_4\text{L-Ru}(\text{TFA})(\text{CO})(\text{PPh}_3)]\text{TFA}$ in DMSO-d_6 .

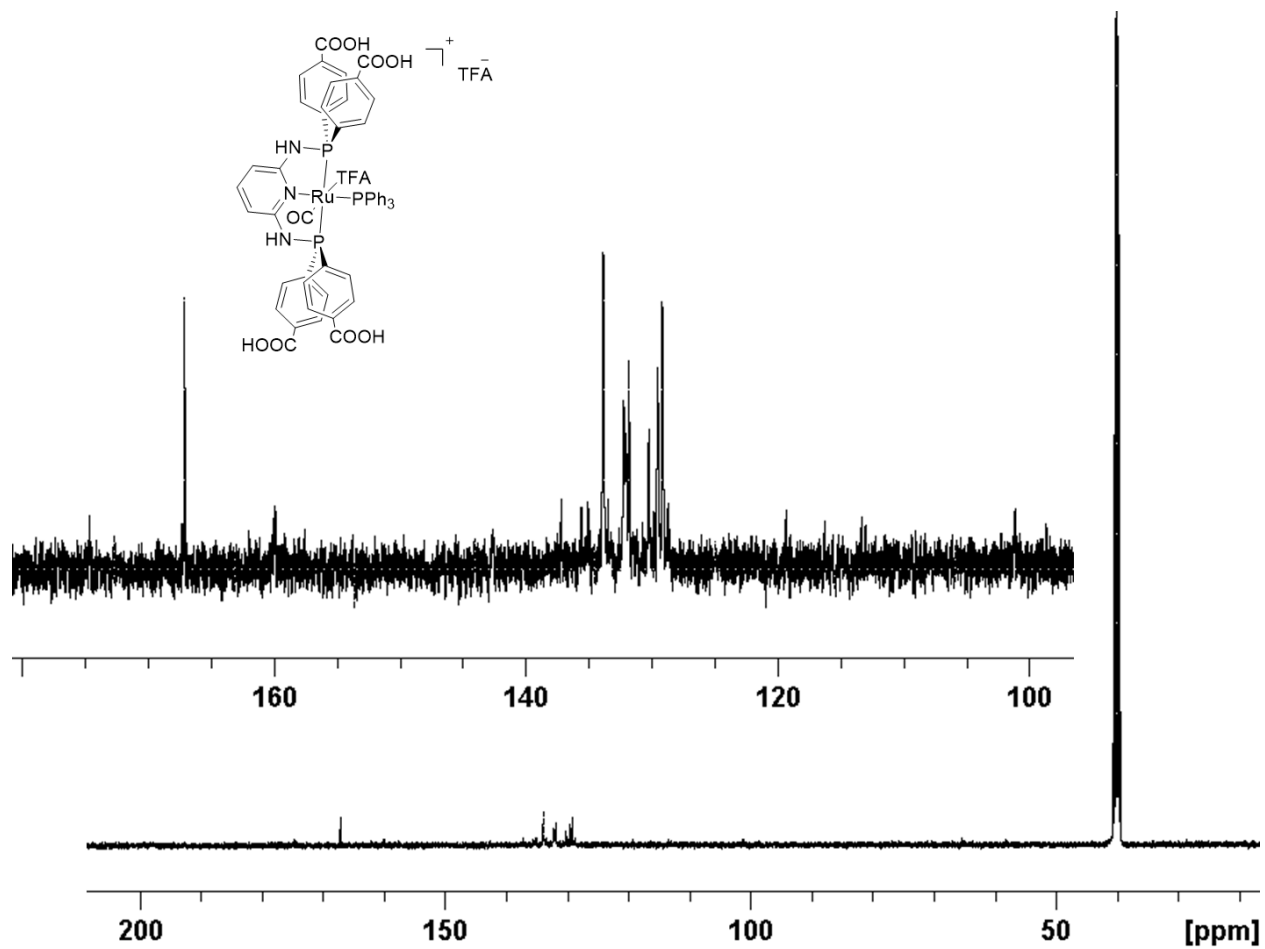


Figure S8. ^{13}C $\{^1H\}$ NMR spectrum of $[H_4L-Ru(TFA)(CO)(PPh_3)]TFA$ in $DMSO-d_6$.

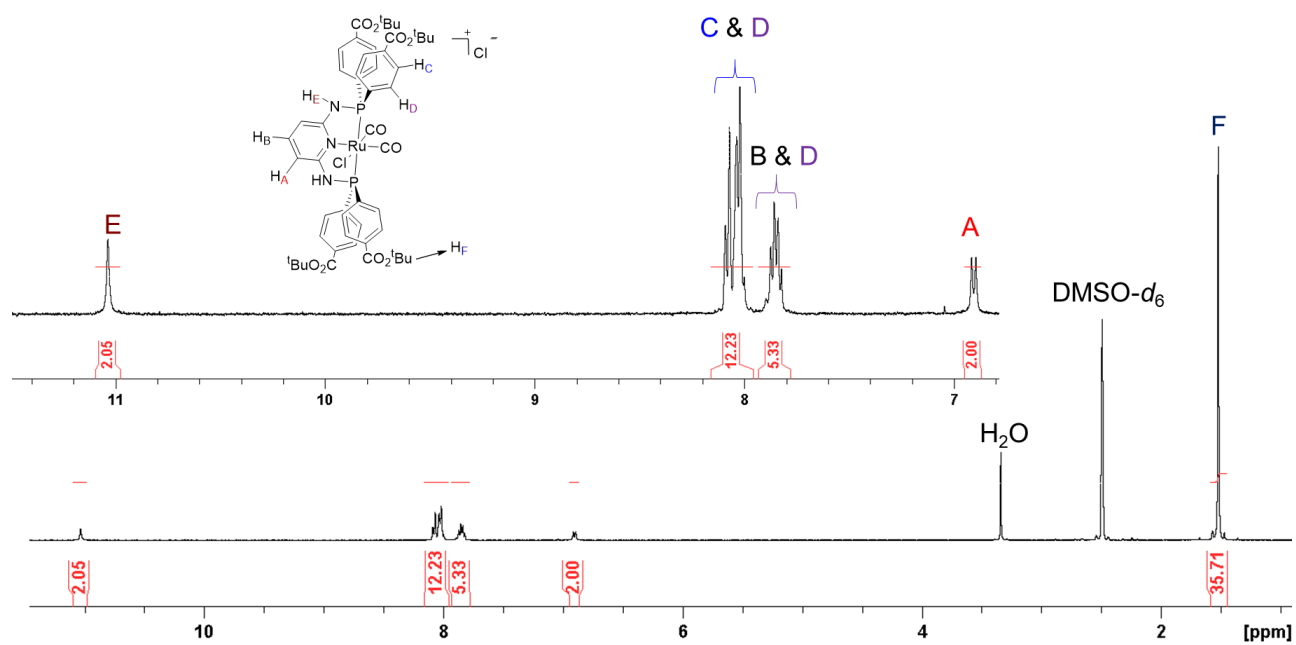


Figure S9. ^1H NMR spectrum of $[\text{tBu}_4\text{L-RuCl}(\text{CO})_2]\text{Cl}$ in $\text{DMSO-}d_6$.

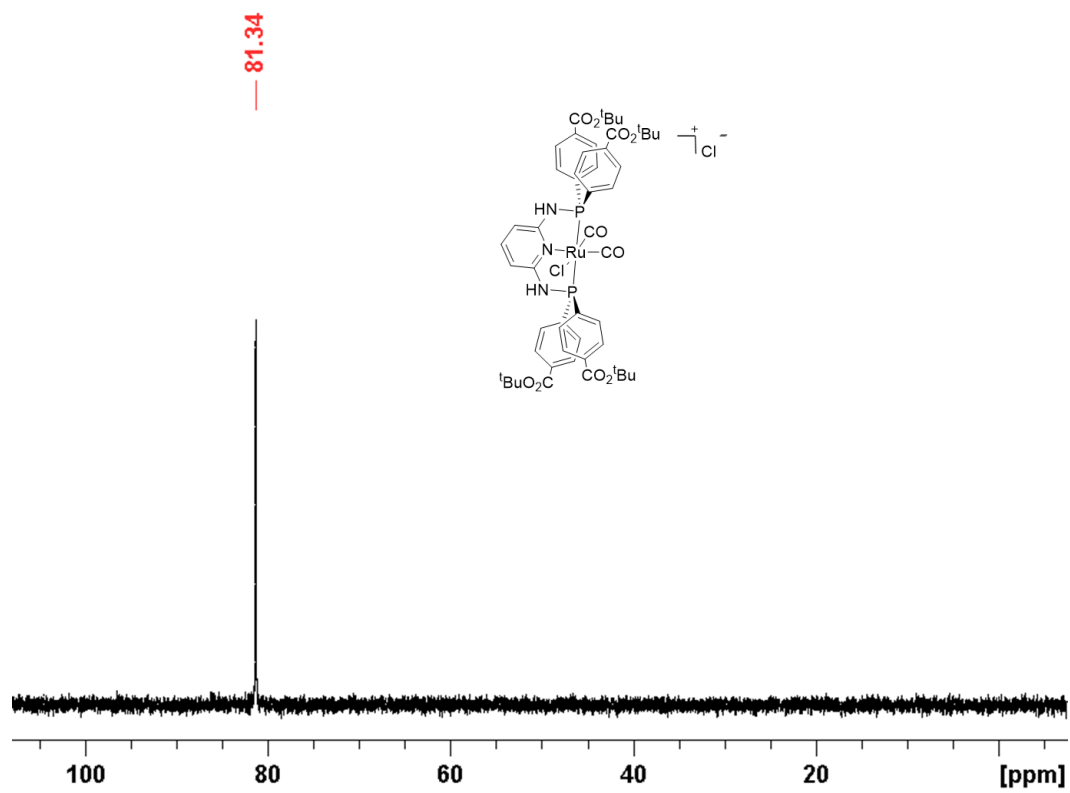


Figure S10. ^{31}P $\{^1\text{H}\}$ NMR spectrum of $[\text{tBu}_4\text{L-RuCl(CO)}_2]\text{Cl}$ in DMSO-d_6

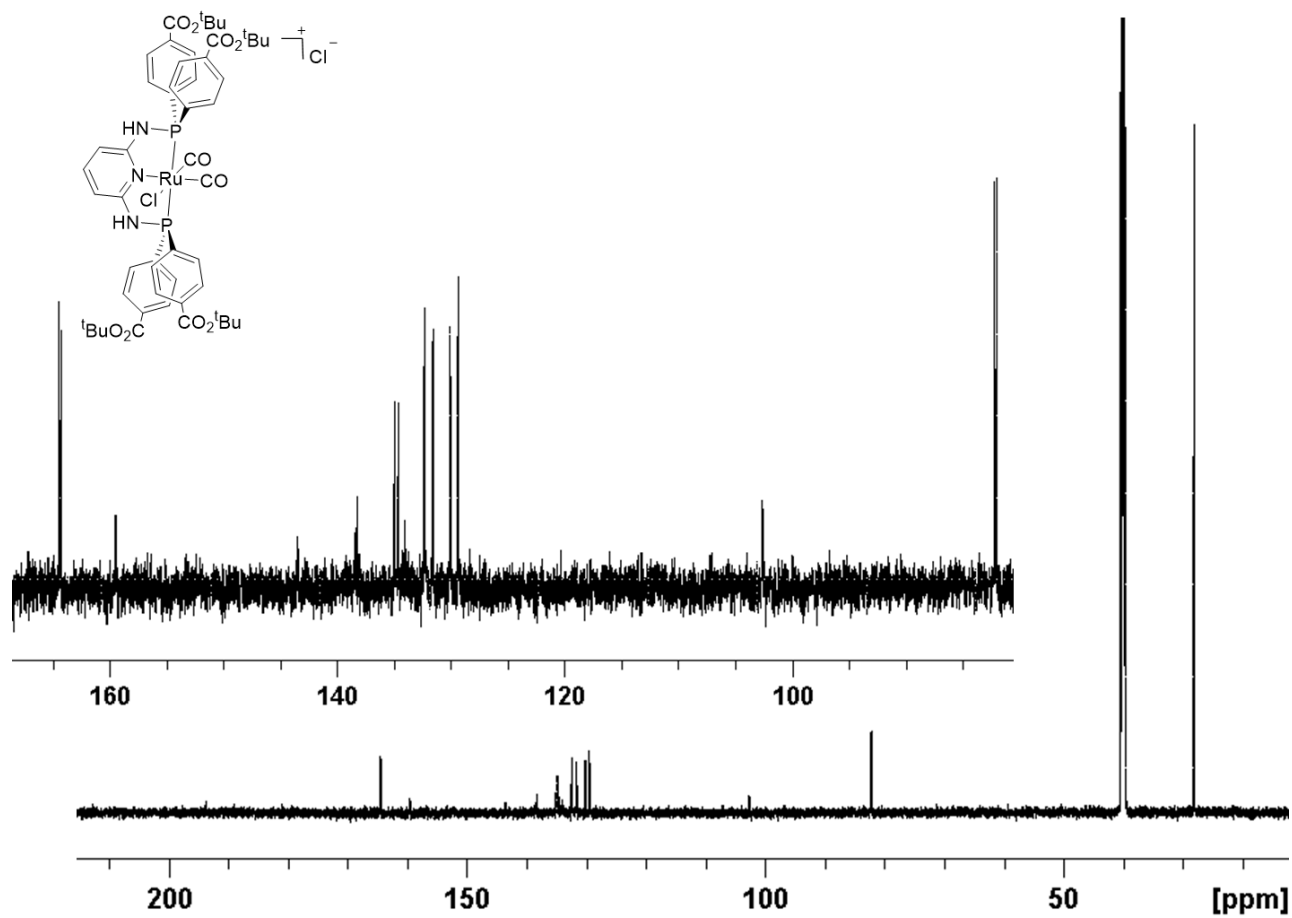


Figure S11. $^{13}\text{C} \{^1\text{H}\}$ NMR spectrum of $[\text{tBu}_4\text{L-RuCl}(\text{CO})_2]\text{Cl}$ in DMSO-d_6

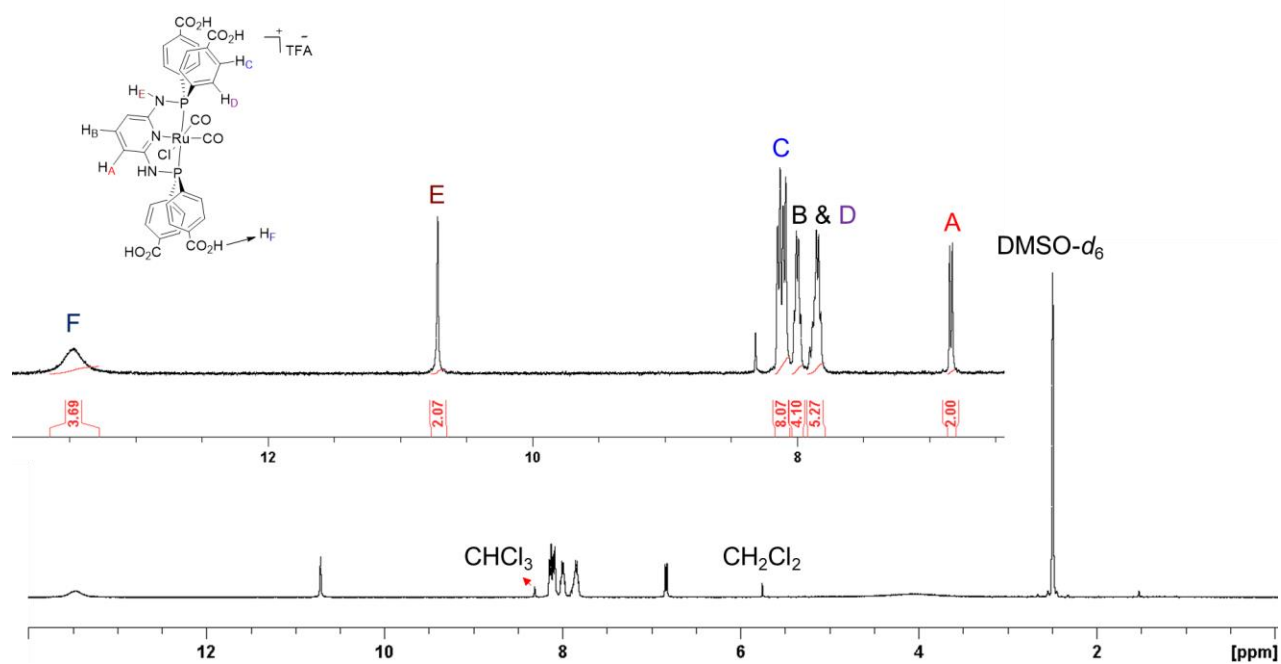


Figure S12. 1H NMR spectrum of $[H_4L-RuCl(CO)_2]TFA$ in $DMSO-d_6$.

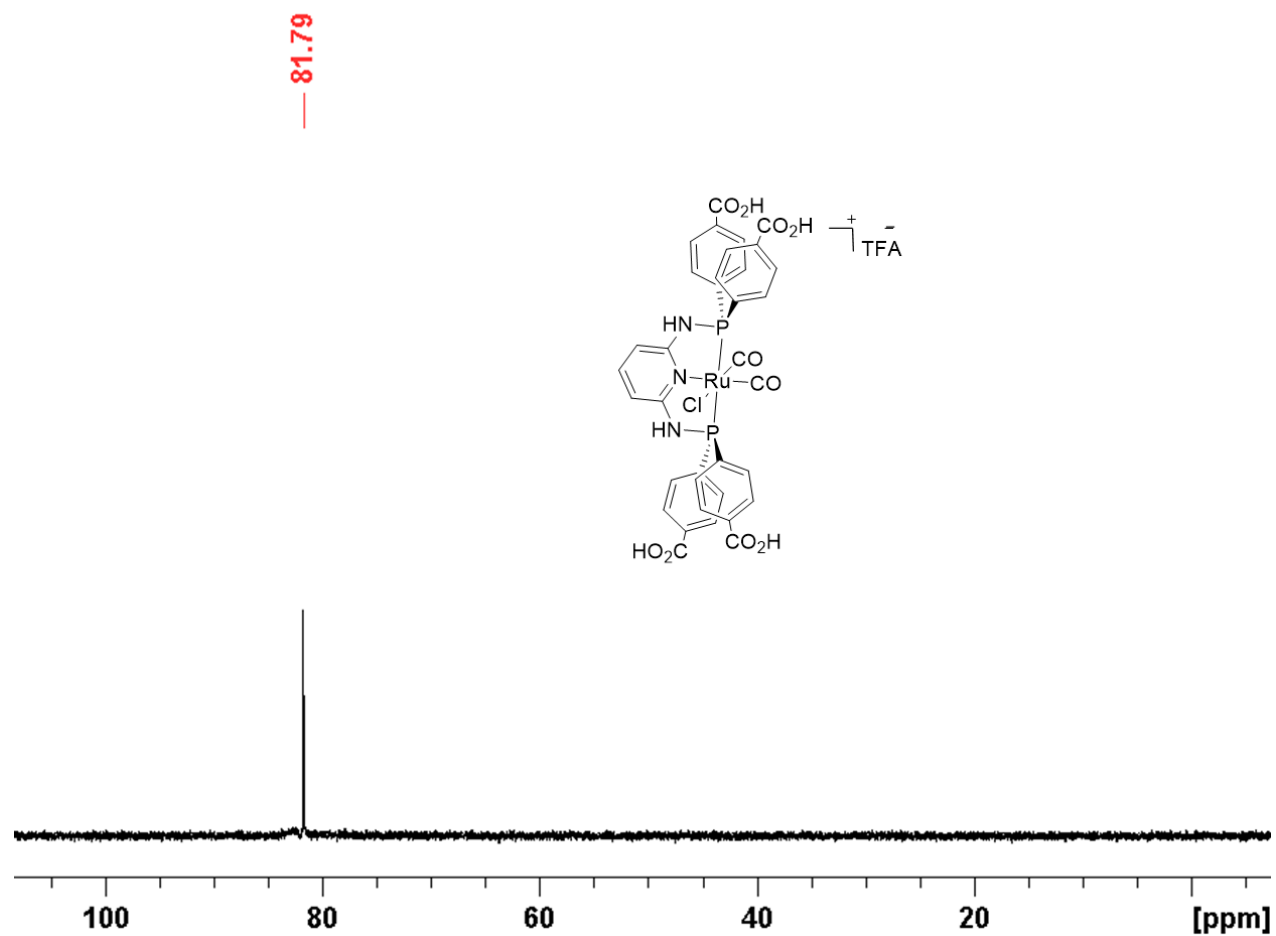


Figure S13. $^{31}P \{^1H\}$ NMR spectrum of $[H_4L-RuCl(CO)_2]TFA$ in $DMSO-d_6$.

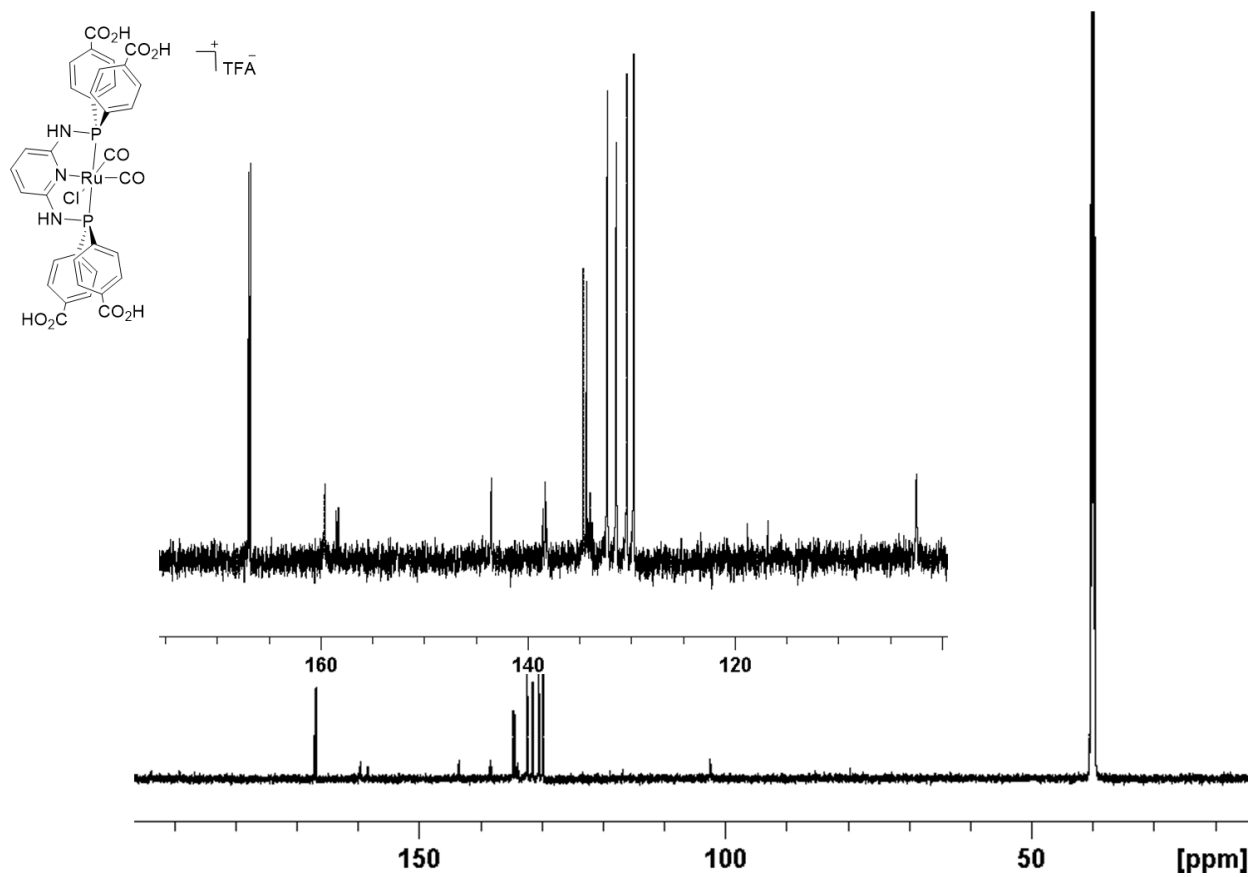


Figure S14. $^{13}C \{^1H\}$ NMR spectrum of $[H_4L-RuCl(CO)_2]TFA$ in DMSO- d_6 .

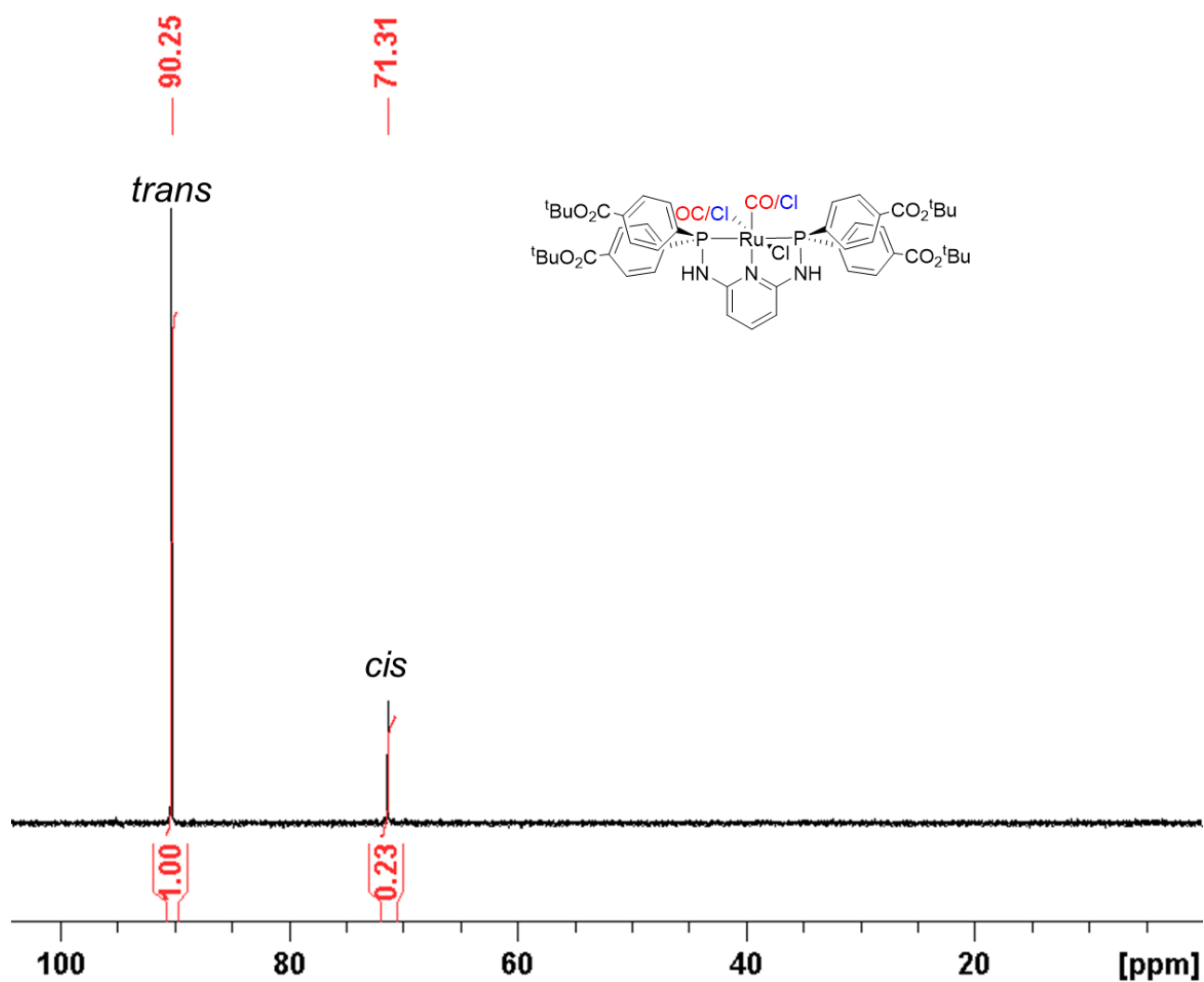


Figure S15. ^{31}P $\{^1\text{H}\}$ NMR spectrum of *cis/trans*- $^t\text{Bu}_4\text{L-RuCl}_2(\text{CO})$ in DMSO-d_6 .

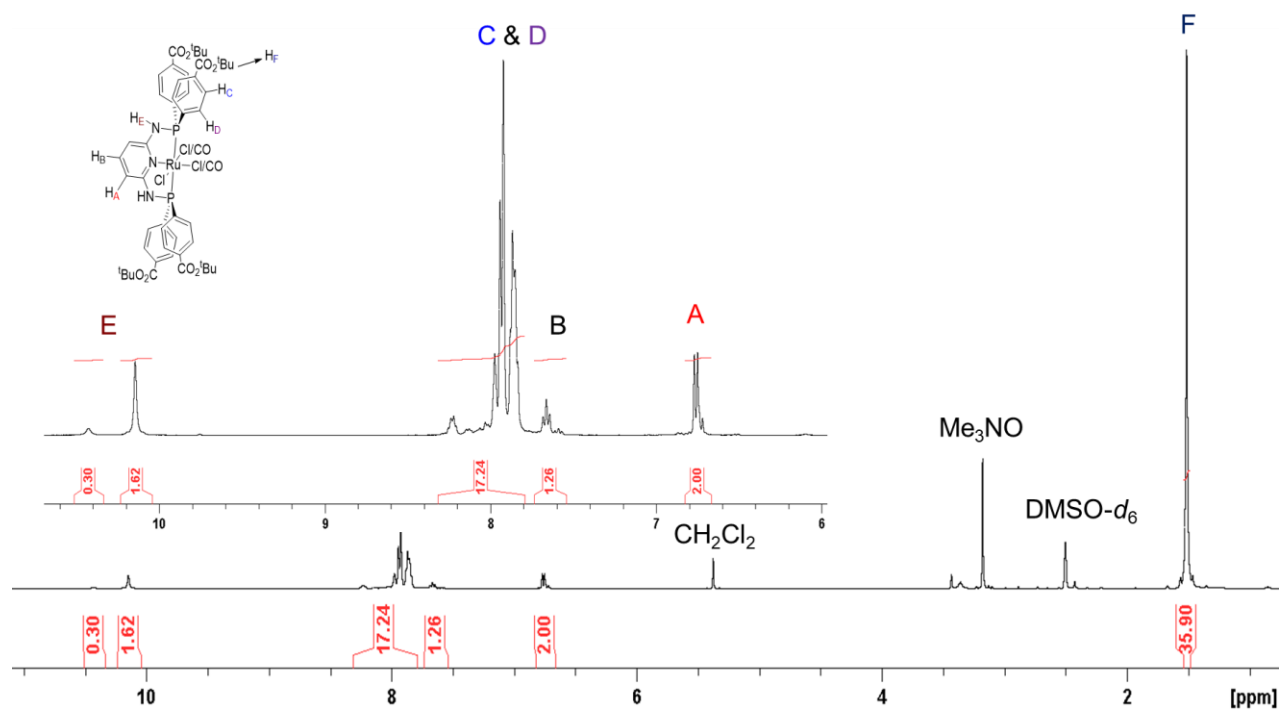


Figure S16. ^1H NMR spectrum of *cis/trans*- $^t\text{Bu}_4\text{L-RuCl}_2(\text{CO})$ in $\text{DMSO-}d_6$.

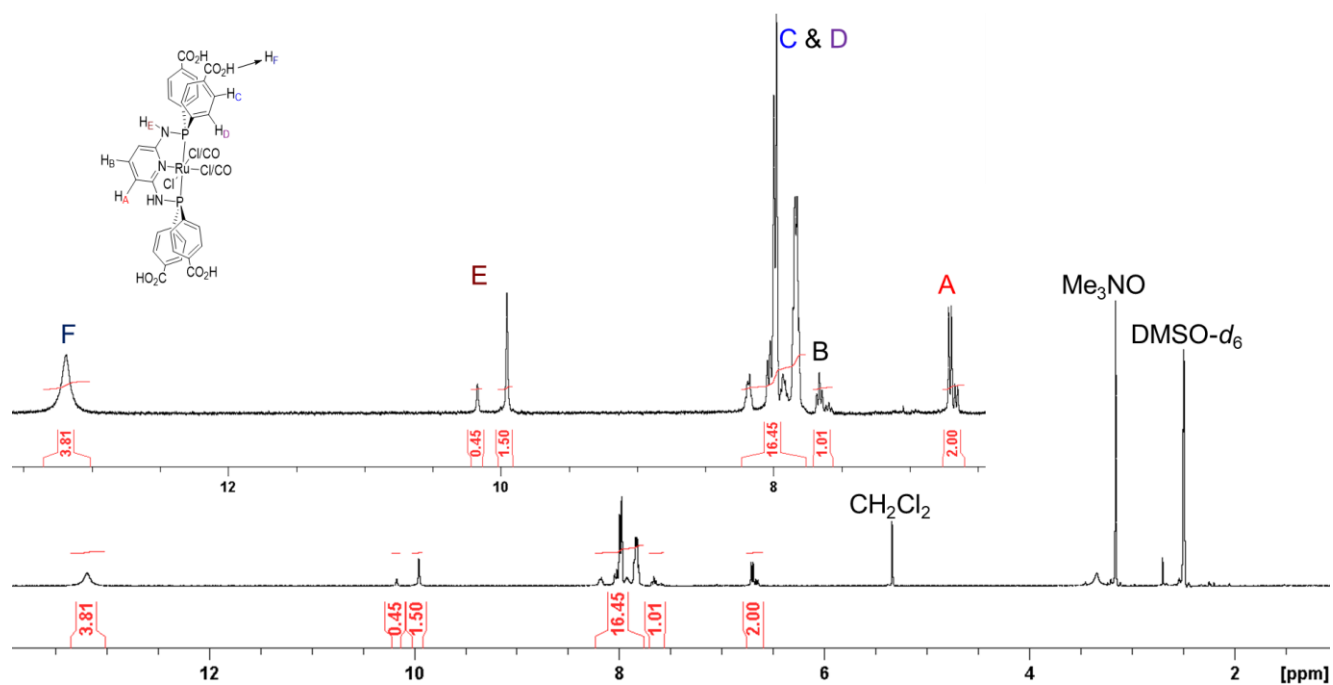


Figure S17. ^1H NMR spectrum of $\text{cis/trans-H}_4\text{L-RuCl}_2(\text{CO})$ in DMSO-d_6

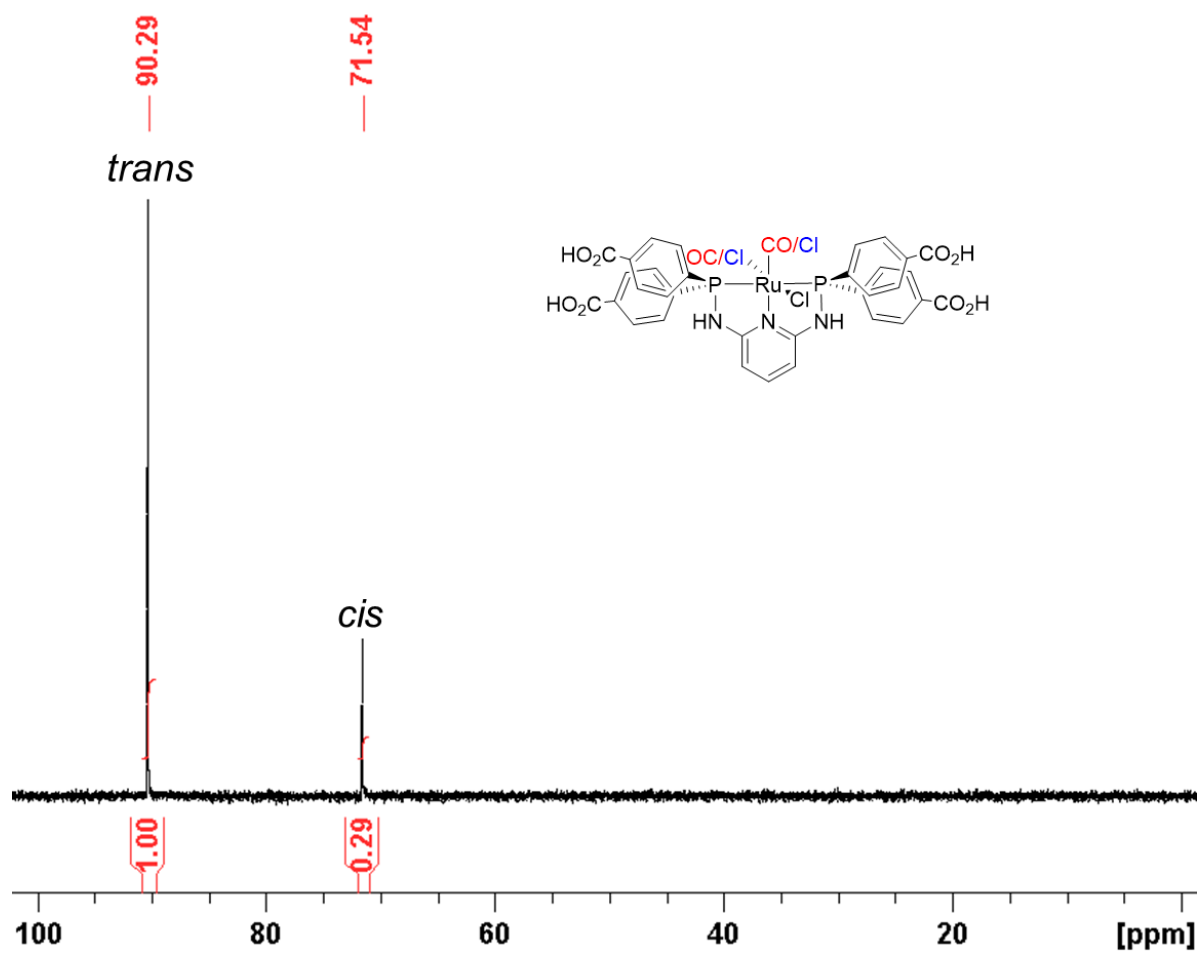


Figure S18. ^{31}P $\{^1\text{H}\}$ NMR spectrum of *cis/trans*- $\text{H}_4\text{L-RuCl}_2(\text{CO})$ in DMSO-d_6

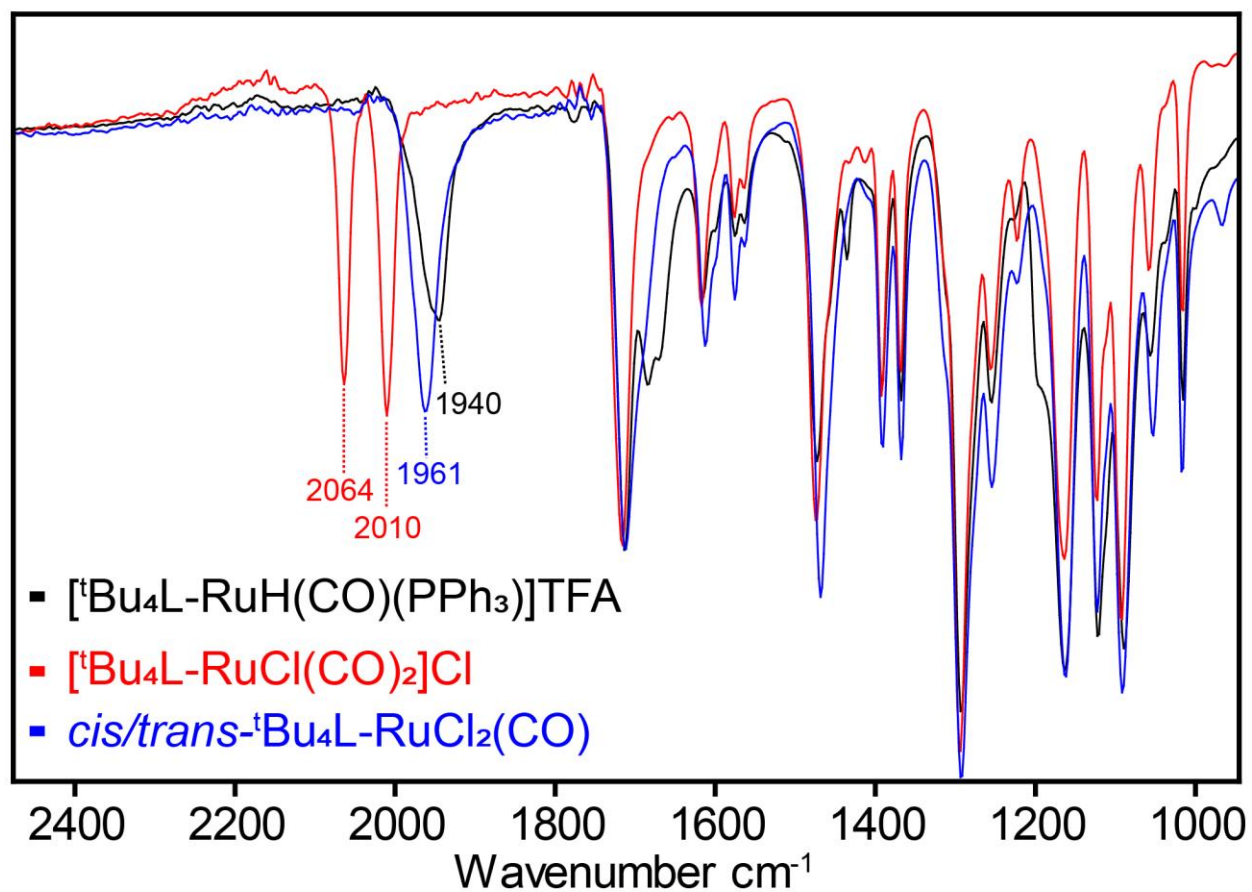


Figure S19. ATR-IR spectra of $\text{tBu}_4\text{L-Ru-P}^{\text{N}}\text{N}^{\text{N}}\text{P}$ pincer complexes

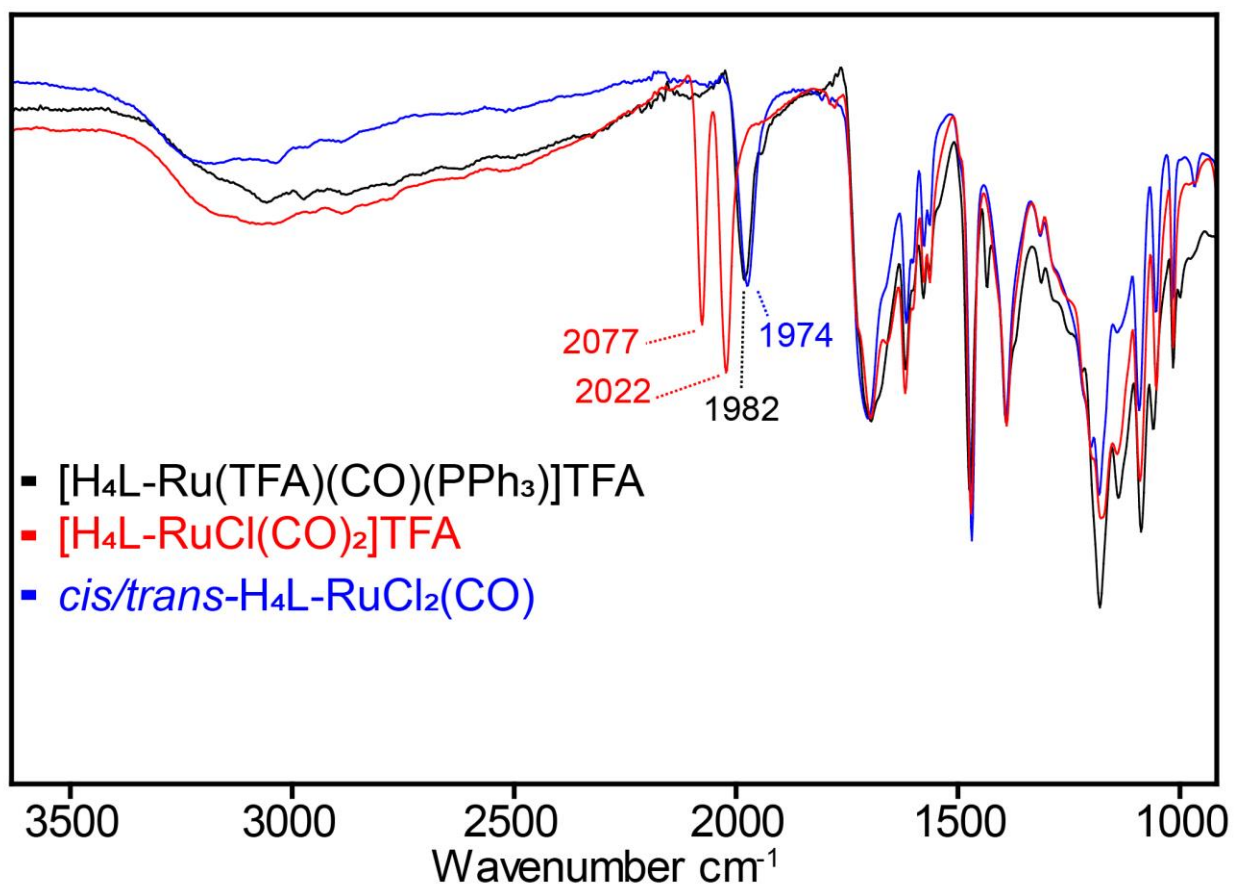


Figure S20. ATR-IR spectra of H₄L-Ru-P^NN^NP pincer complexes

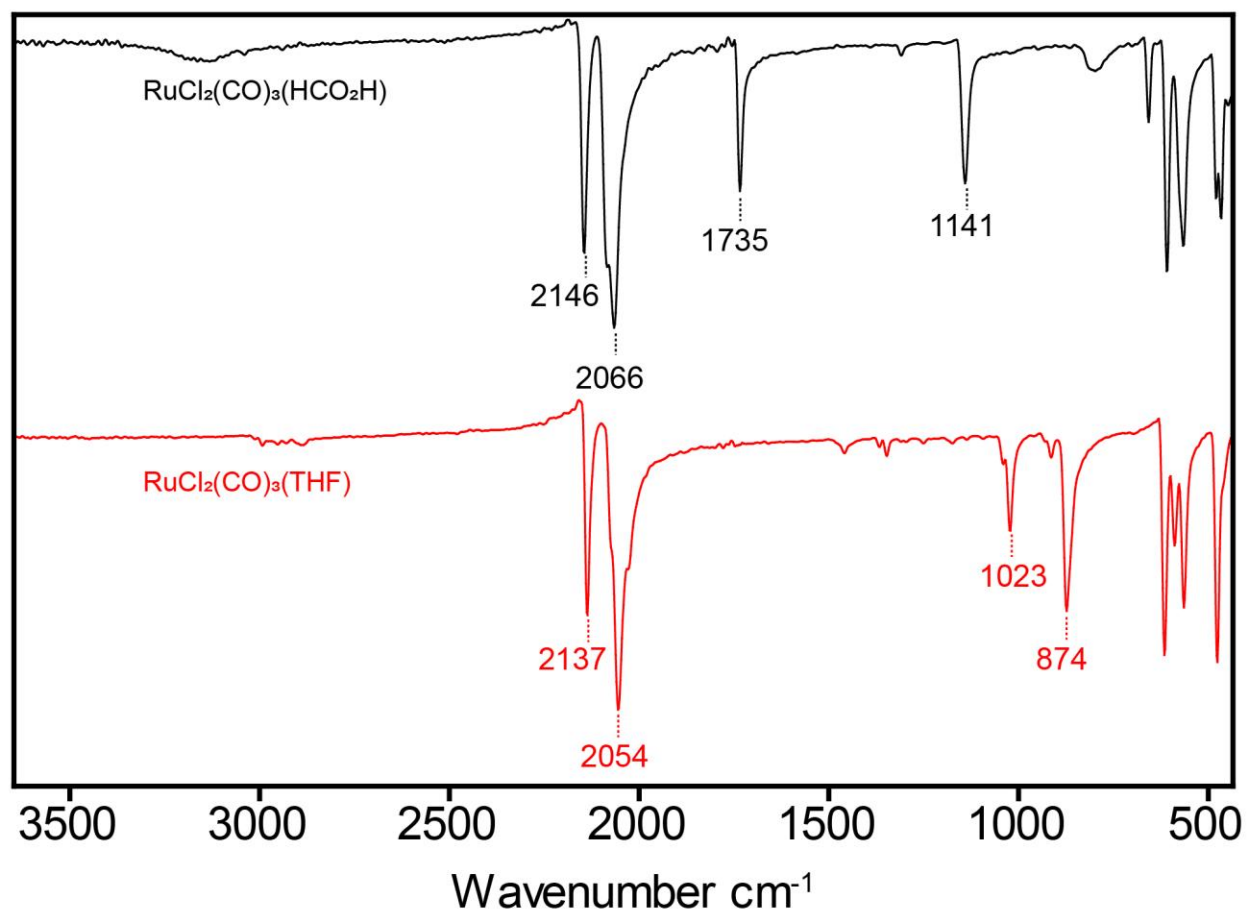


Figure S21. ATR-IR spectra of RuCl₂(CO)₃(HCO₂H) and RuCl₂(CO)₃(THF)

Synchrotron X-ray Powder Diffraction, Structure Solution, and Rietveld Refinement of **1**

Synchrotron X-ray Powder diffraction (SXPd) data for **1** was collected on the 11-BM beamline at the Advanced Photon Source (APS, Argonne National Laboratory). Measurements were taken on a powder sample sealed in a 0.8 mm ID Kapton capillary at 298 K using a photon wavelength of $\lambda = 0.414536$ Å. Subsequent Pawley fits and Rietveld refinement were performed using TOPAS-Academic (v6) over the data range $2\theta = 0.5 - 10.0^\circ$ and $0.5 - 20.0^\circ$, respectively. Indexing the SXPd data gave a hexagonal unit cell ($a = 31.937(7)$ Å, $c = 15.798(4)$ Å) with $P6/mmm$ as a possible space group. An initial structure model was constructed with $P6/mmm$ space group symmetry and Rietveld refinement was carried out using simulated annealing with two rigid bodies, a D_{4h} $Zr_6O_4(OH)_4(OAc)_4$ cluster and idealized $[L-RuCl_3]^{4-}$ linker. The position and orientation of each rigid body is constrained by symmetry; the torsion angles of the benzoate group were allowed to freely refine, as described previously.¹ Constraints were placed on the Zr-acetate and Zr-benzoate bond distances, to guarantee chemically reasonable Zr-O bond lengths. The best fit to the data provided $R_{wp} = 14.03$ with final lattice parameters of $a = 31.9437(6)$ Å, $c = 15.8051(3)$ Å.

Table S1. Fractional coordinates of the asymmetric unit for framework structure **1**.

Label	Element	Xfrac	Yfrac	Zfrac
Ru	Ru	0.186100	0.372200	0.000000
Cl _a	Cl	0.229870	0.459741	0.000000
Cl _b	Cl	0.110287	0.372200	0.000000
P1	P	0.181952	0.363905	-0.148726
N1	N	0.152066	0.304132	-0.147269
C1	C	0.137403	0.274806	-0.074540
C2	C	0.111950	0.223900	-0.076341
C3	C	0.099062	0.198124	0.000274
N2	N	0.149818	0.299637	0.000101
C11	C	0.151269	0.390328	0.205106
C12	C	0.161653	0.437831	0.190923
C13	C	0.136862	0.456403	0.236143
C14	C	0.101685	0.427469	0.295546
C15	C	0.091301	0.379966	0.309729
C16	C	0.116093	0.361394	0.264509
C17	C	0.075075	0.447403	0.344083
O11	O	0.054313	0.430335	0.409705
O12	O	0.076722	0.485714	0.307436
Zr1 _a	Zr	0.422372	0.422372	0.500000
Zr2 _a	Zr	0.468309	0.531691	0.610953
O1 _a	O	0.463860	0.463860	0.603326
O2 _a	O	0.506627	0.565653	0.500000
O3 _a	O	0.429834	0.570166	0.567662
C3 _a	C	0.418676	0.581324	0.500000

C3b	C	0.391499	0.608501	0.500000
O4a	O	0.519326	0.480674	0.745654
C4a	C	0.500000	0.500000	0.784719
C4b	C	0.500000	0.500000	0.879866

Pawley refinement of **1**

The Pawley refinement was performed using synchrotron X-ray powder diffraction data of **1**. The Pawley fits were carried out in $P6$, $P6/m$, and $P6/mmm$ space groups using a data range of $0.5 - 10^\circ 2\theta$, a 7 term Chebyshev polynomial, a $1/x$ term (low angle scattering), a PVII peak profile, a simple axial model term, a zero-point correction, and cell parameter refinement. An R_{wp} of ~ 12.6 was found for the Pawley fit, which is not significantly different than the Rietveld refined R_{wp} of 14.03 in $P6/mmm$, indicating the reasonableness of the Rietveld refined structure.

Table S2. Pawley refinement parameters for **1** in $P6/mmm$ space group.

Parameters	Value
$2\theta_{\min} (^\circ)$	0.5
$2\theta_{\max} (^\circ)$	10.0
$\lambda (^\circ)$	0.414536
$a (\text{\AA})$	31.937(7)
$c (\text{\AA})$	15.798(4)
R_{wp}	12.598
<i>Goodness of Fit</i>	1.972

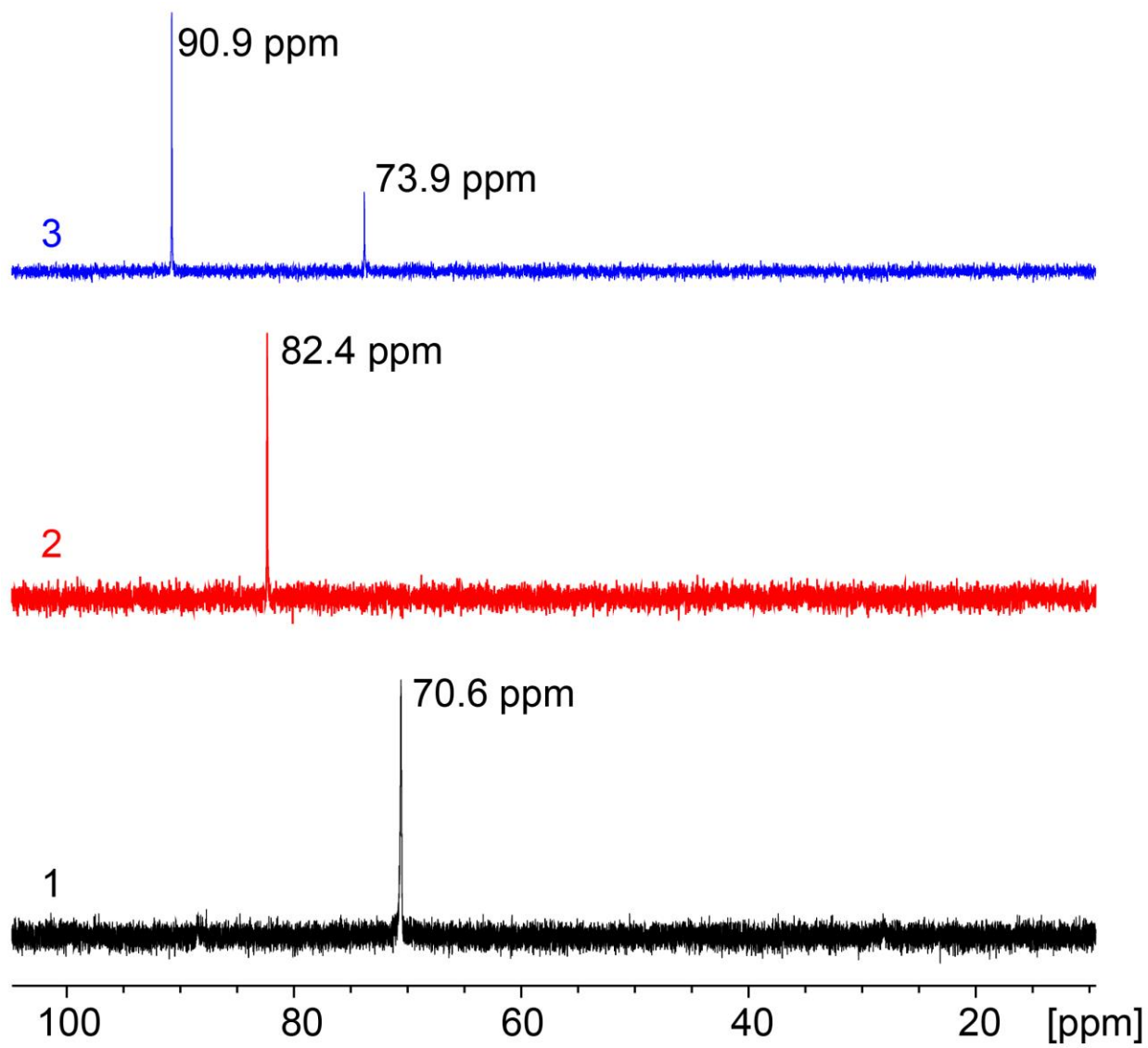


Figure S22. CsF- and acid-digested ^{31}P { ^1H } NMR spectra of **1**, **2** and **3**. **1** was digested with CsF/DMSO- d_6 /D $_2\text{O}$ while **2** and **3** were digested with $\text{CF}_3\text{CO}_2\text{H}$ /DMSO- d_6 .

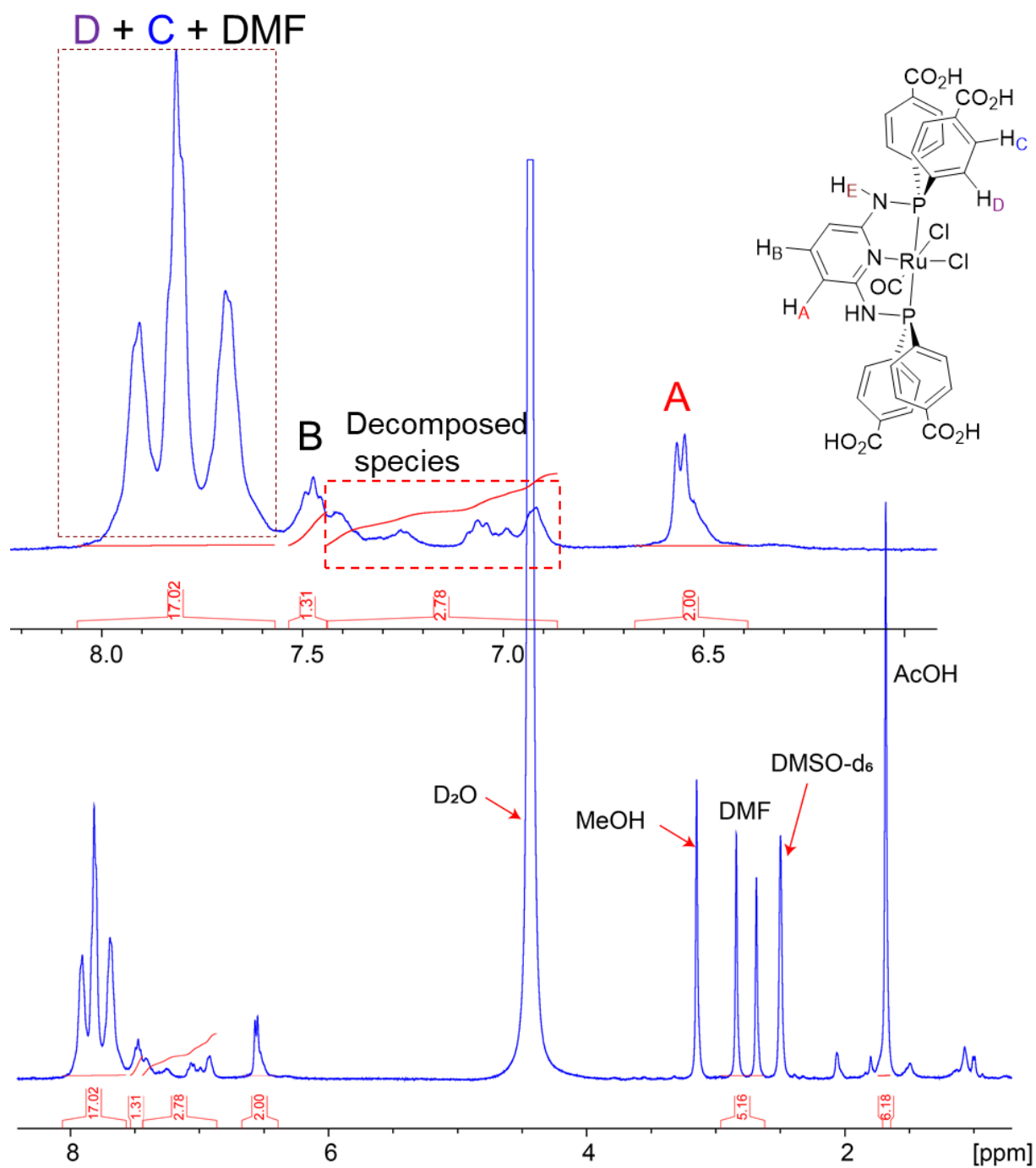


Figure S23. CsF-digested ^1H NMR spectrum ($\text{DMSO-d}_6/\text{D}_2\text{O}$) of **1** after MeOH solvent exchange.

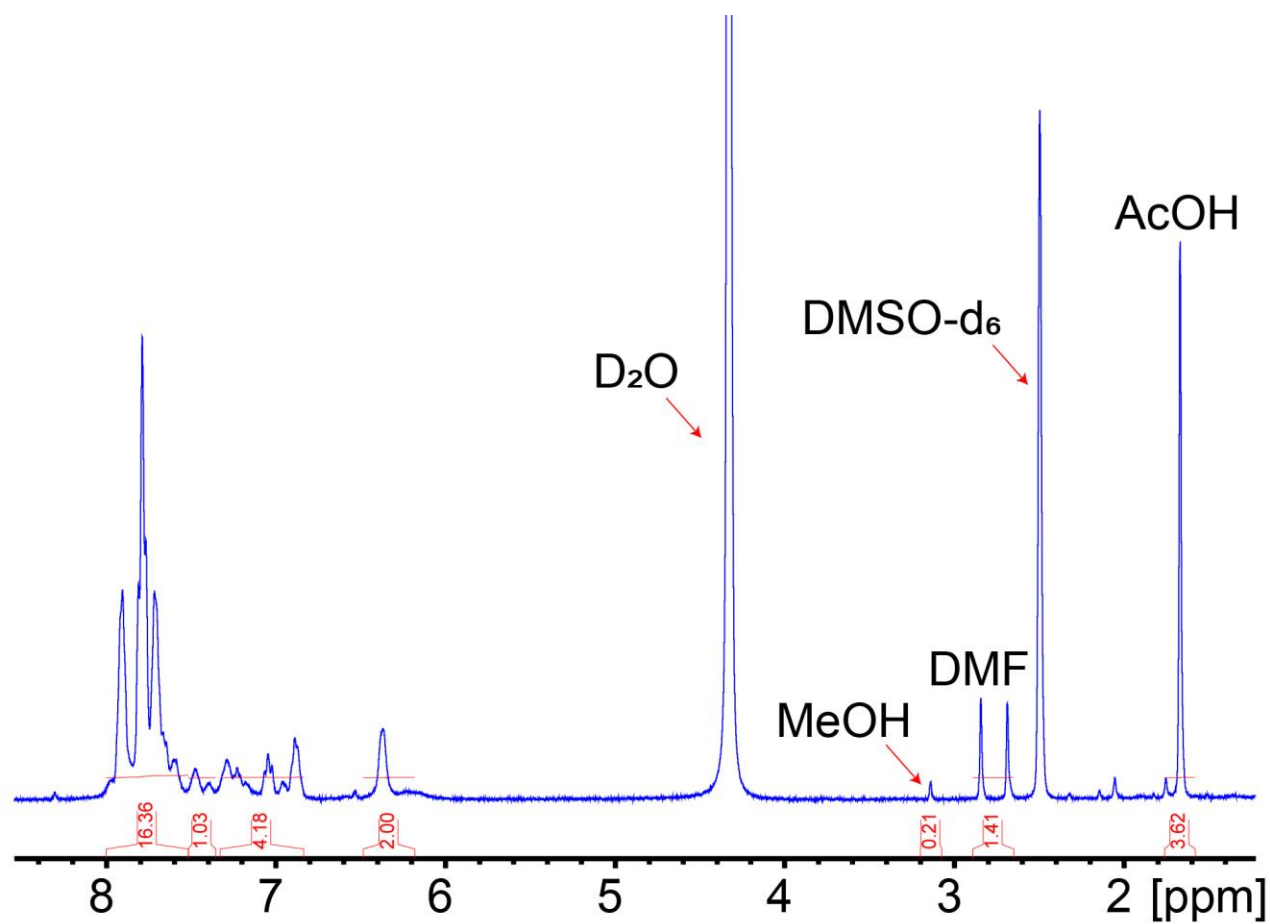


Figure S24. CsF-digested ^1H NMR spectrum ($\text{DMSO-d}_6/\text{D}_2\text{O}$) of **1** after activation.

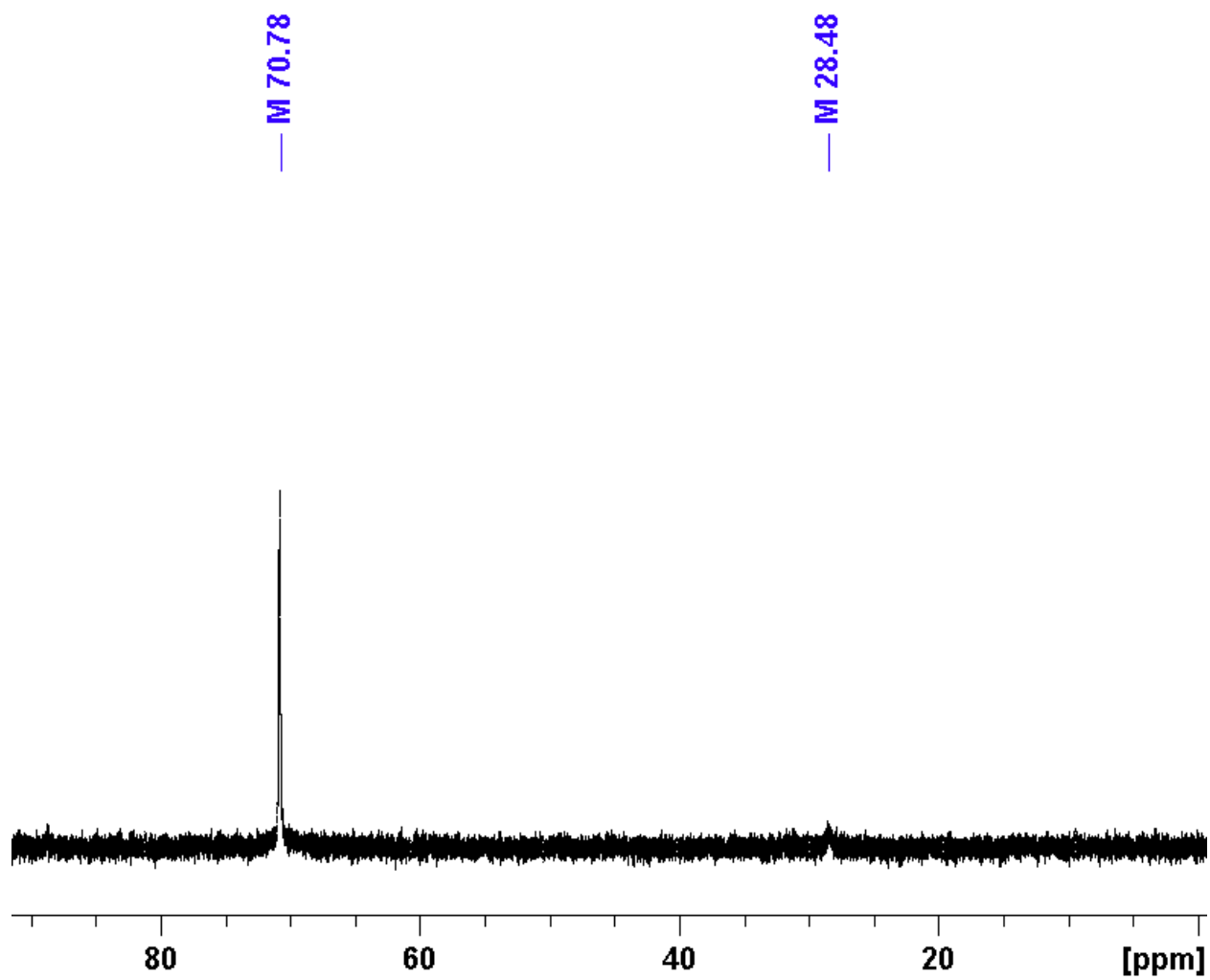


Figure S25. CsF-digested $^{31}\text{P}\{^1\text{H}\}$ NMR spectrum (DMSO- $\text{d}_6/\text{D}_2\text{O}$) of **1** after activation.

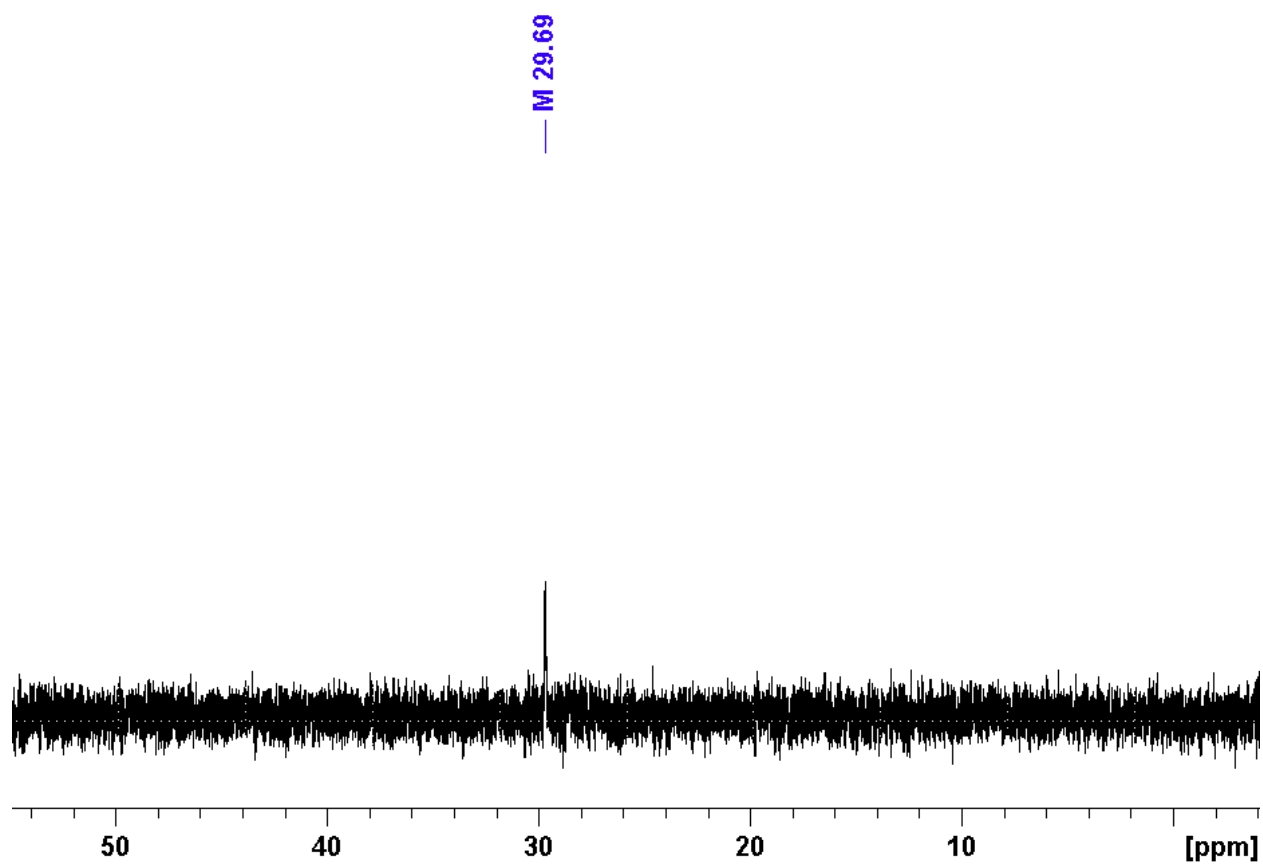


Figure S26. $^{31}\text{P}\{^1\text{H}\}$ NMR spectrum for MOF reaction supernatant of **1**.

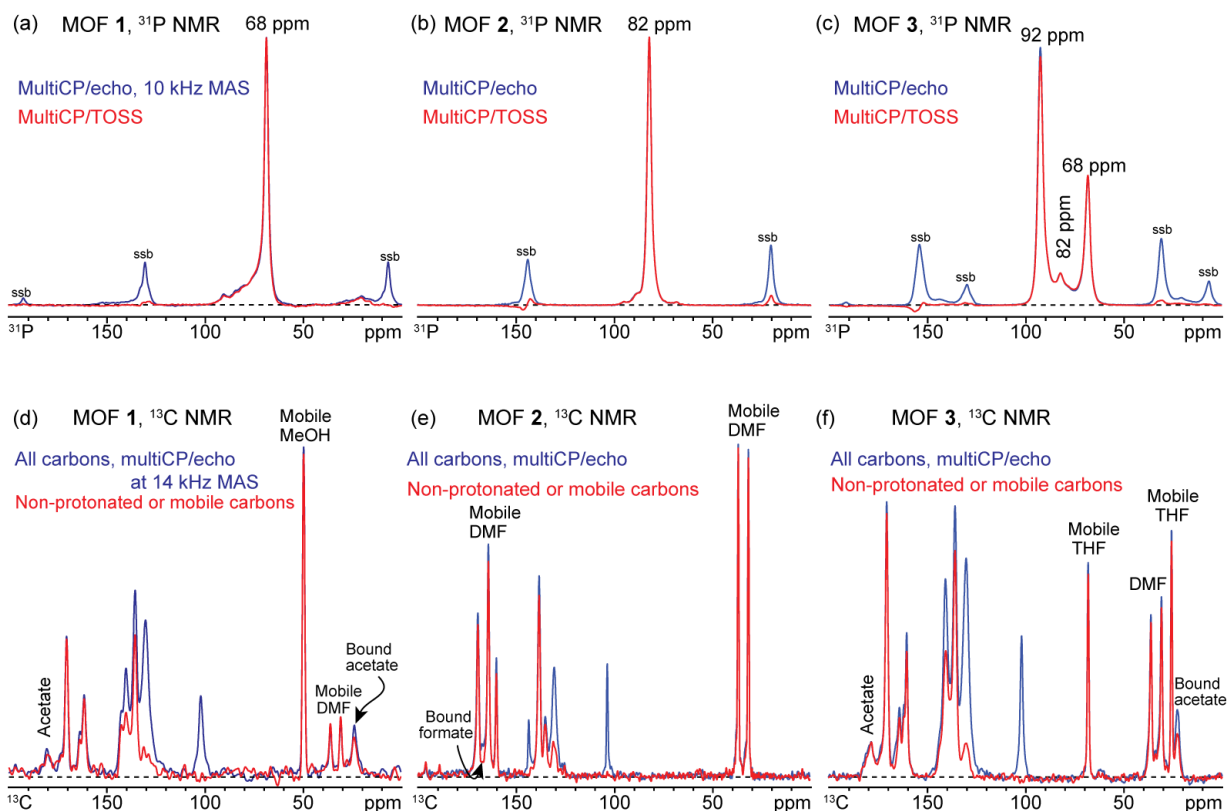


Figure S27. Solid-state NMR spectra of (a, d) 1, (b, e) 2 and (c, f) 3. (a-c): ^{31}P NMR spectra recorded at 10 kHz MAS without (top blue line) and with (bottom red line) total suppression of spinning sidebands. “ssb”: spinning sideband. (d-f) Quantitative multiCP ^{13}C NMR spectra without (top blue line) and with (bottom red line) recoupled ^1H dipolar dephasing, recorded at 14 kHz MAS. The spectrum in red shows nonprotonated carbons and highly mobile segments. Bound acetate and formate are identified by the signal reduction of their CH_n groups after dipolar dephasing, and by inhomogeneous line broadening. For rotating CH_3 groups in immobilized molecules, dephasing to 57% of the full signal is expected.

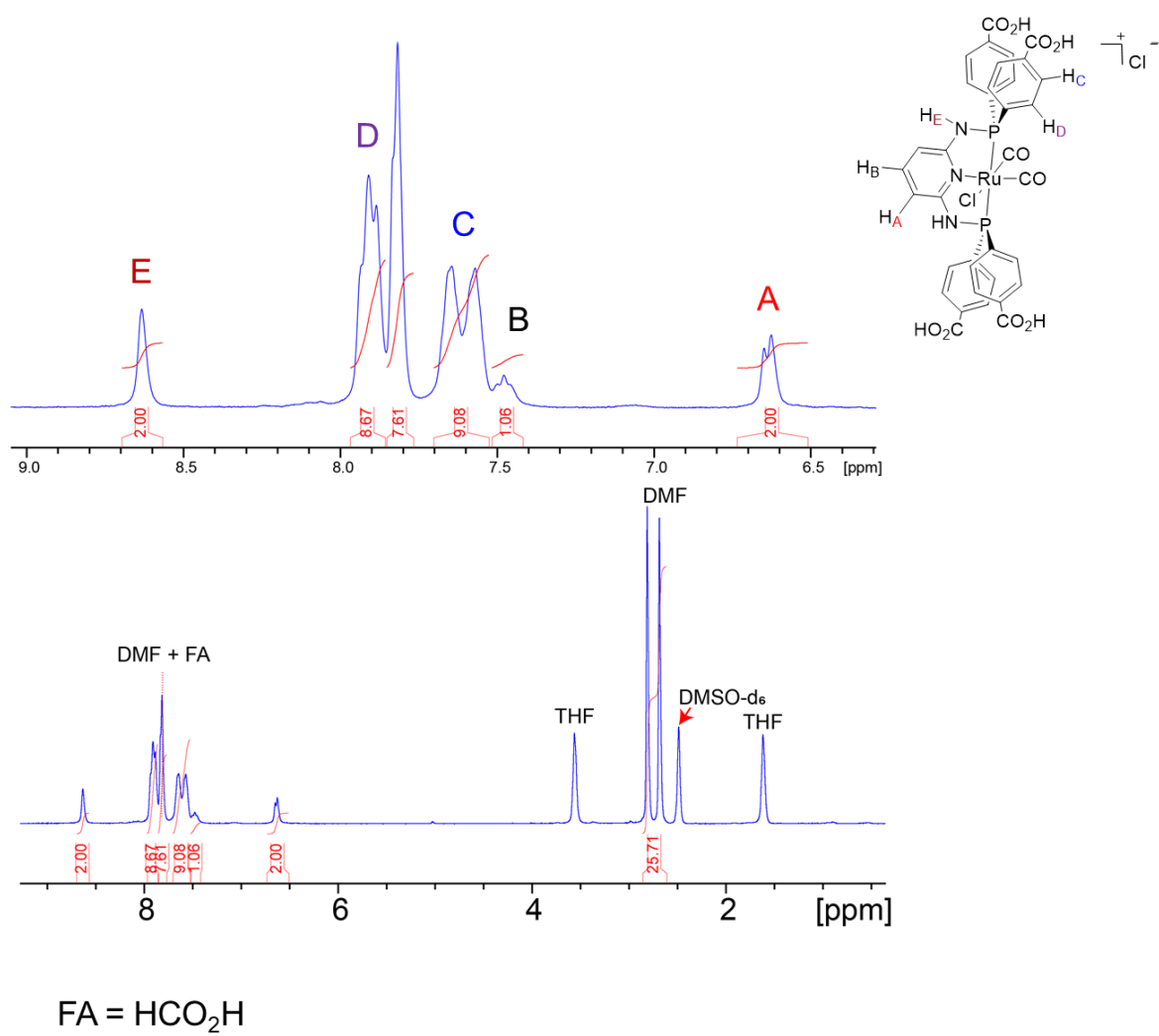


Figure S28. Acid-digested ^1H NMR spectrum ($\text{CF}_3\text{CO}_2\text{H}/\text{DMSO-d}_6$) of **2** after THF washing.

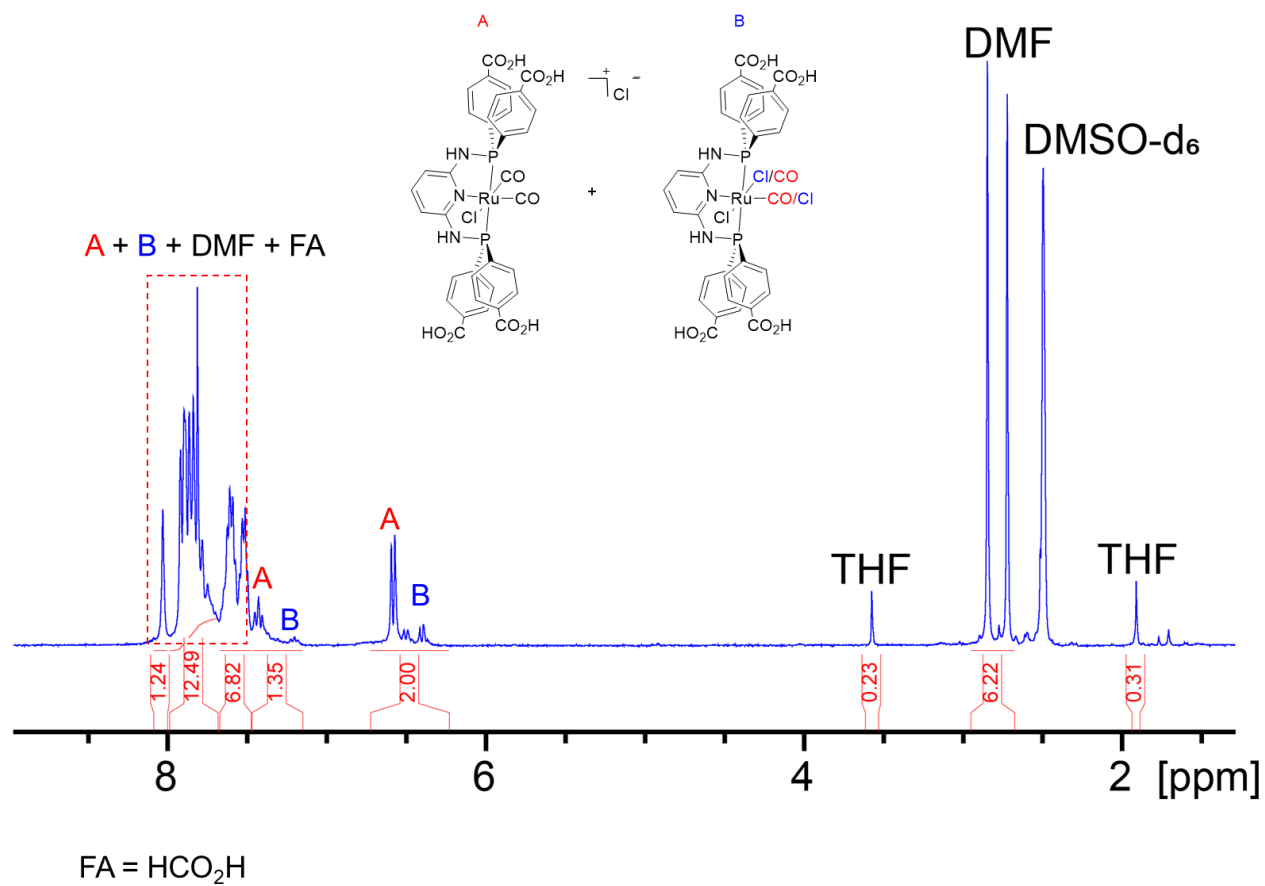


Figure S29. Acid-digested ^1H NMR spectrum ($\text{CF}_3\text{CO}_2\text{H}/\text{DMSO-}\text{d}_6$) of **2** after activation.

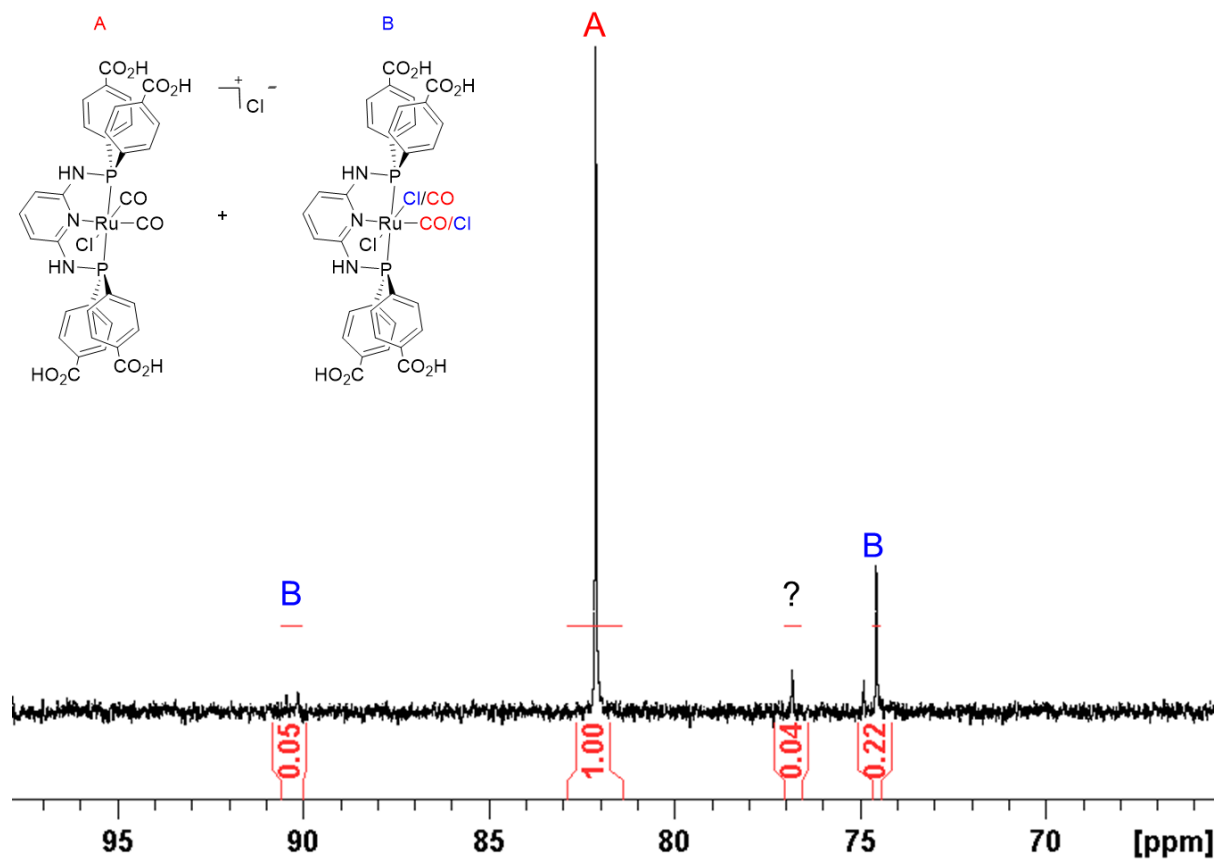


Figure S30. Acid-digested $^{31}\text{P}\{^1\text{H}\}$ NMR spectrum (CF₃CO₂H/DMSO-d₆) of **2** after activation.

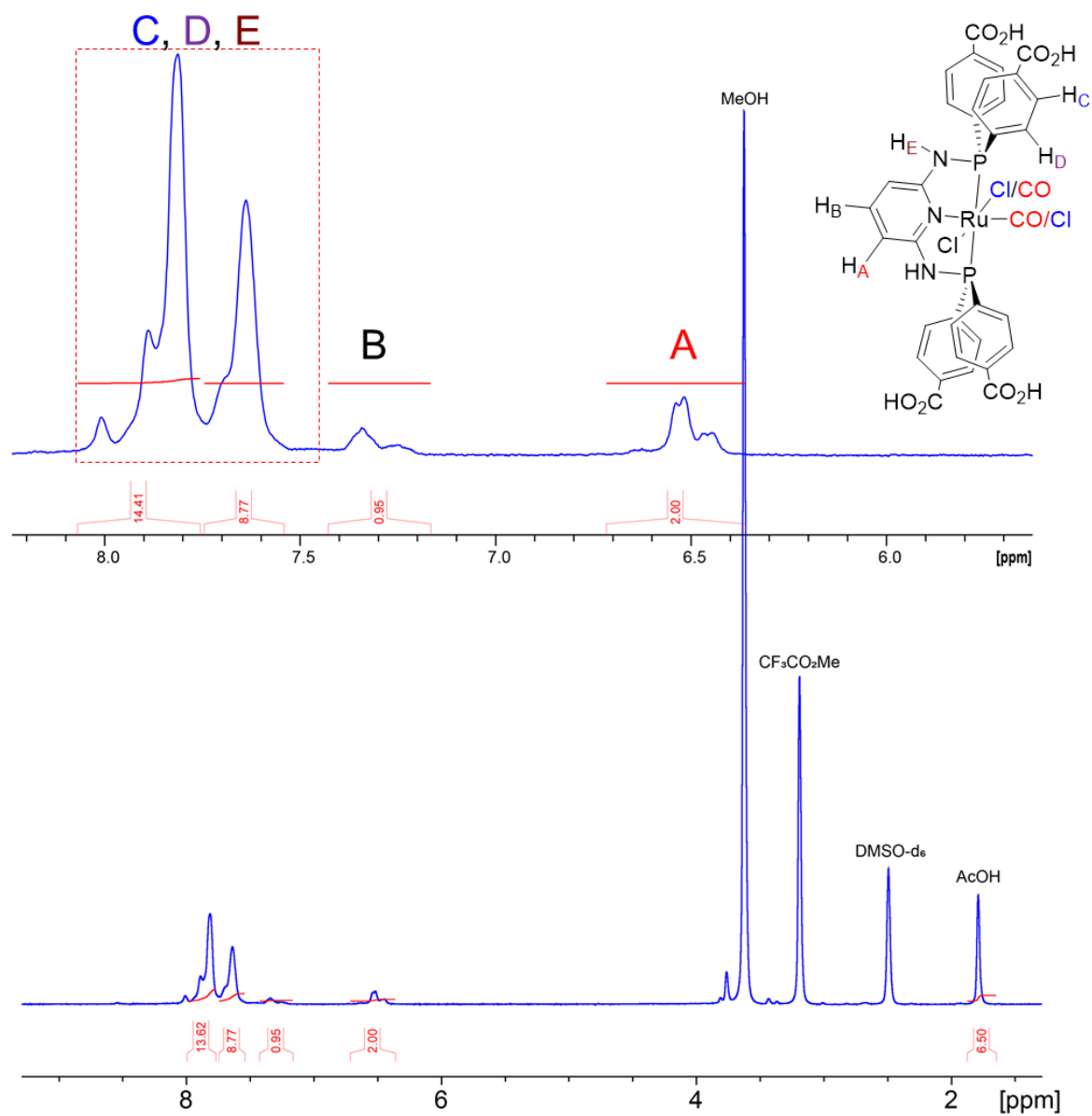


Figure S31. Acid-digested 1H NMR spectrum ($CF_3CO_2H/DMSO-d_6$) of **3** after MeOH solvent exchange.

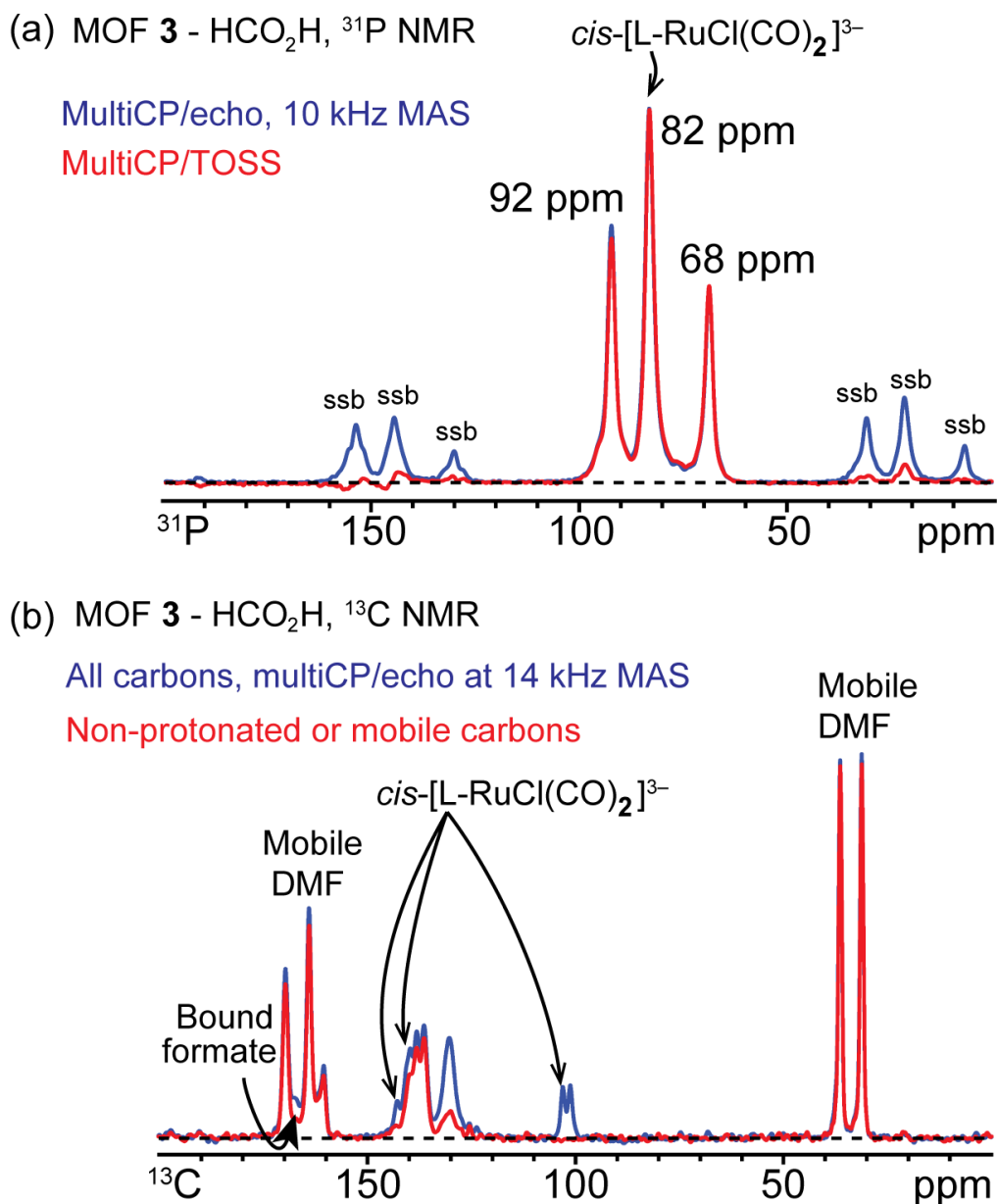


Figure S32. Solid-state ³¹P and ¹³C NMR spectra of MOF **3** synthesized with HCO₂H as the modulator. (a): ³¹P NMR spectra recorded at 10 kHz MAS without (top blue line) and with (bottom red line) total suppression of spinning sidebands. “ssb”: spinning sideband. (b) Quantitative multiCP ¹³C NMR spectra without (top blue line) and with (bottom red line) recoupled ¹H dipolar dephasing, recorded at 14 kHz MAS. Bound formate is identified by the signal reduction after dipolar dephasing.

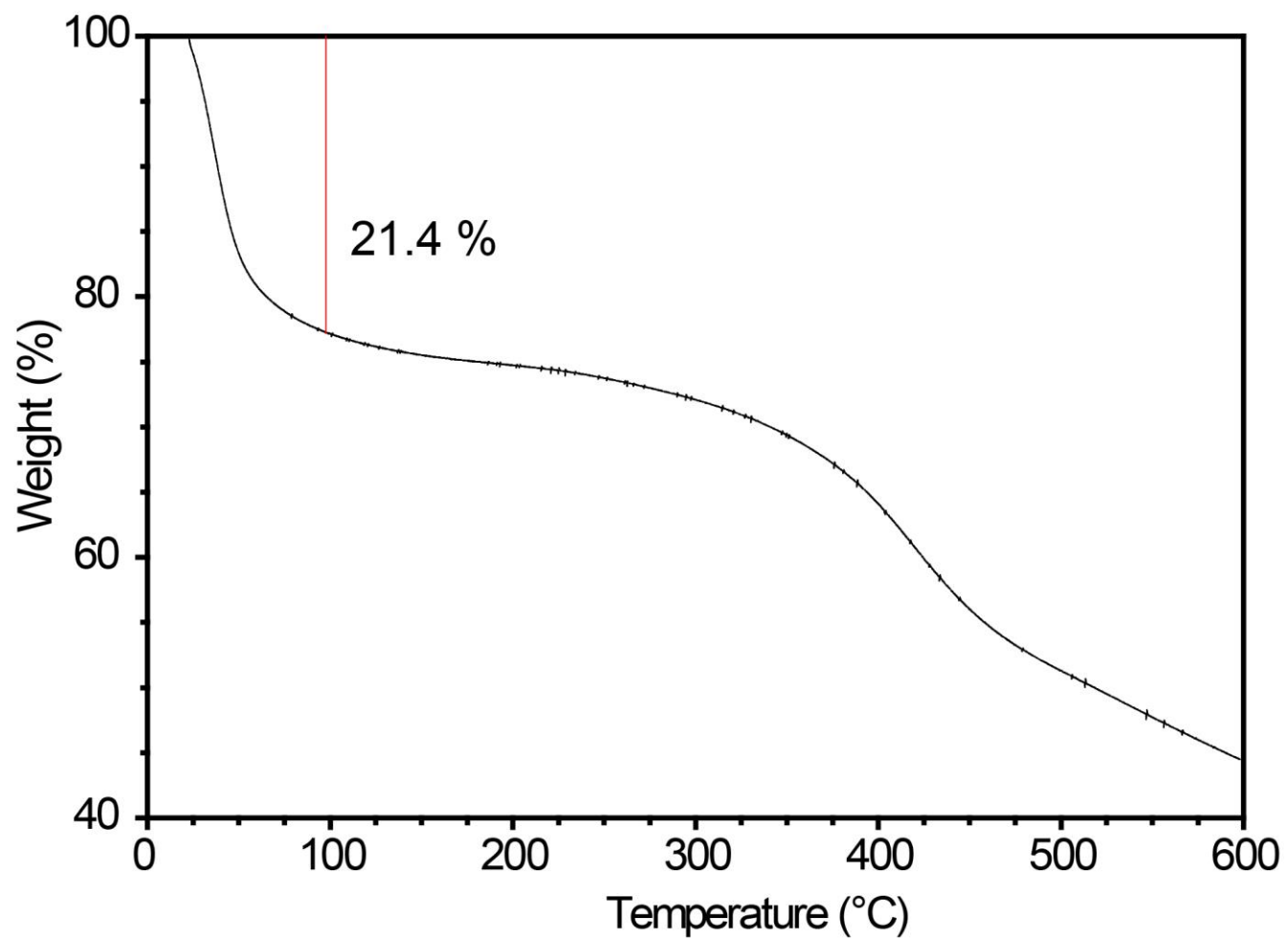


Figure S33. TGA for MeOH soaked sample of **1** measured at a ramp rate of 5 °C/min under flowing N₂ (50 mL/min).

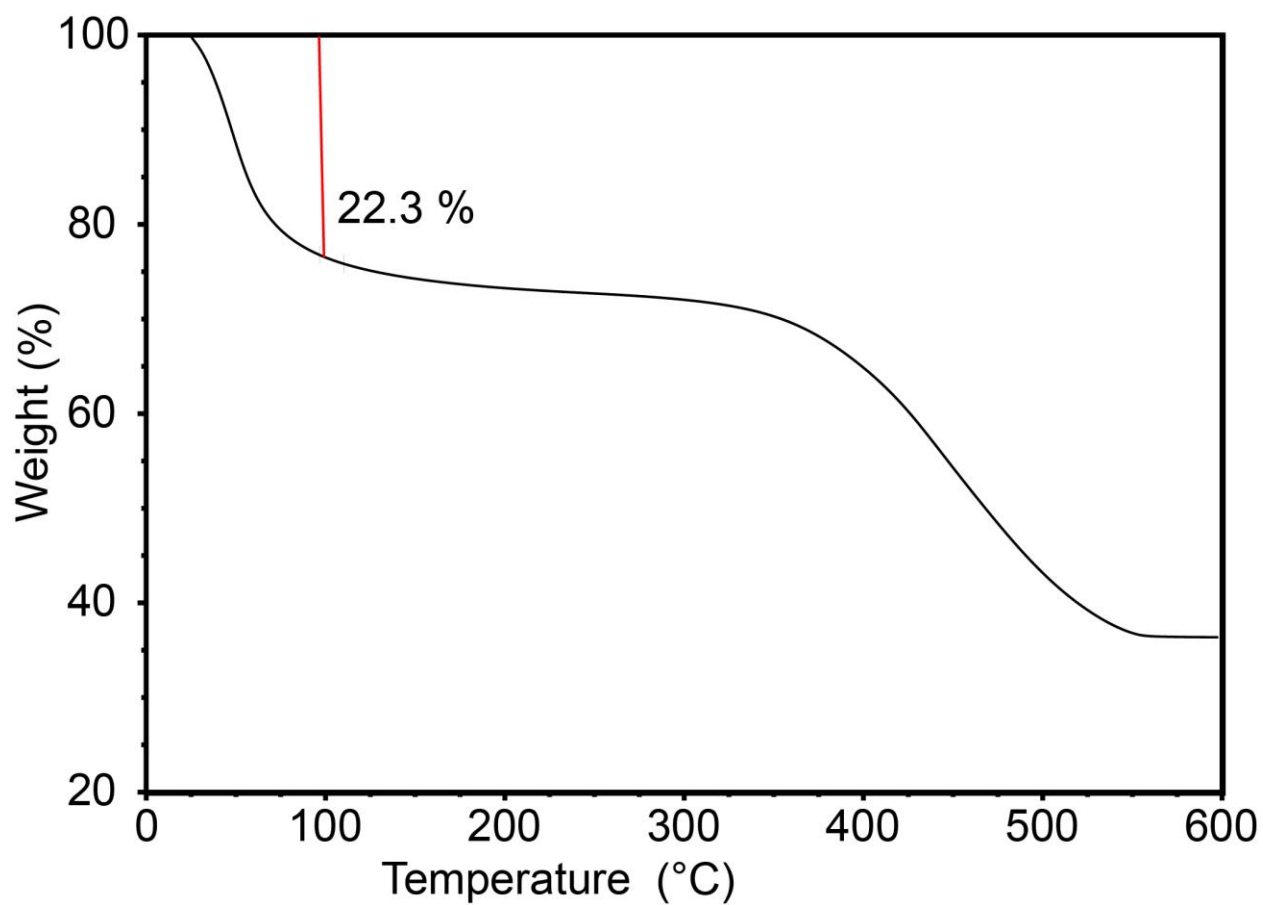


Figure S34. TGA for MeOH soaked sample of **3** measured at a ramp rate of 5 °C/min under flowing N₂ (50 mL/min).

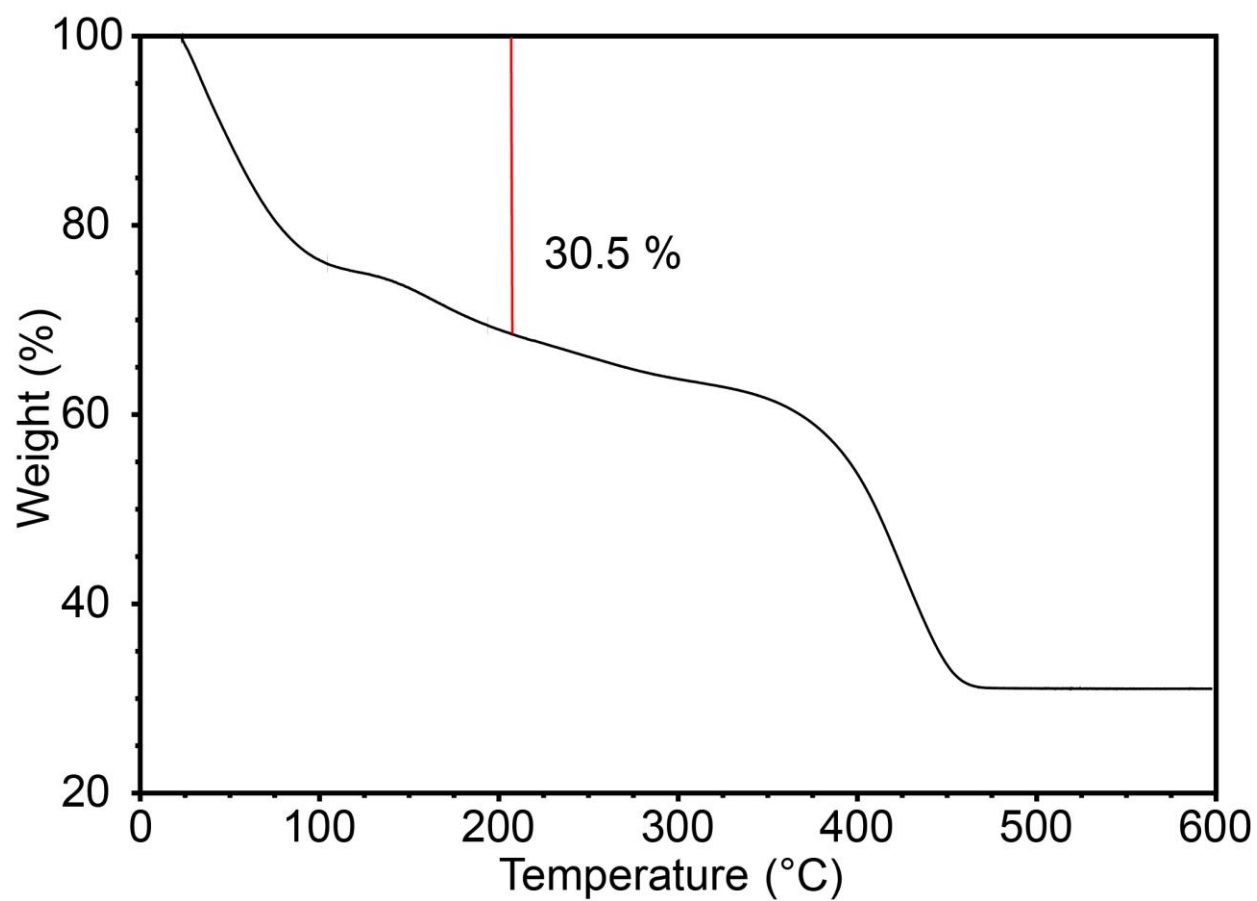


Figure S35. TGA for THF-exchanged sample of **2** measured at ramp rate of 5 °C/min under flowing N₂ (50 mL/min). ¹H NMR analysis of THF-exchanged MOF prior to TGA showed the presence of both THF and DMF solvents. As a result, 30.5 % mass loss up to 200 °C is attributed to volatilization of these solvents.

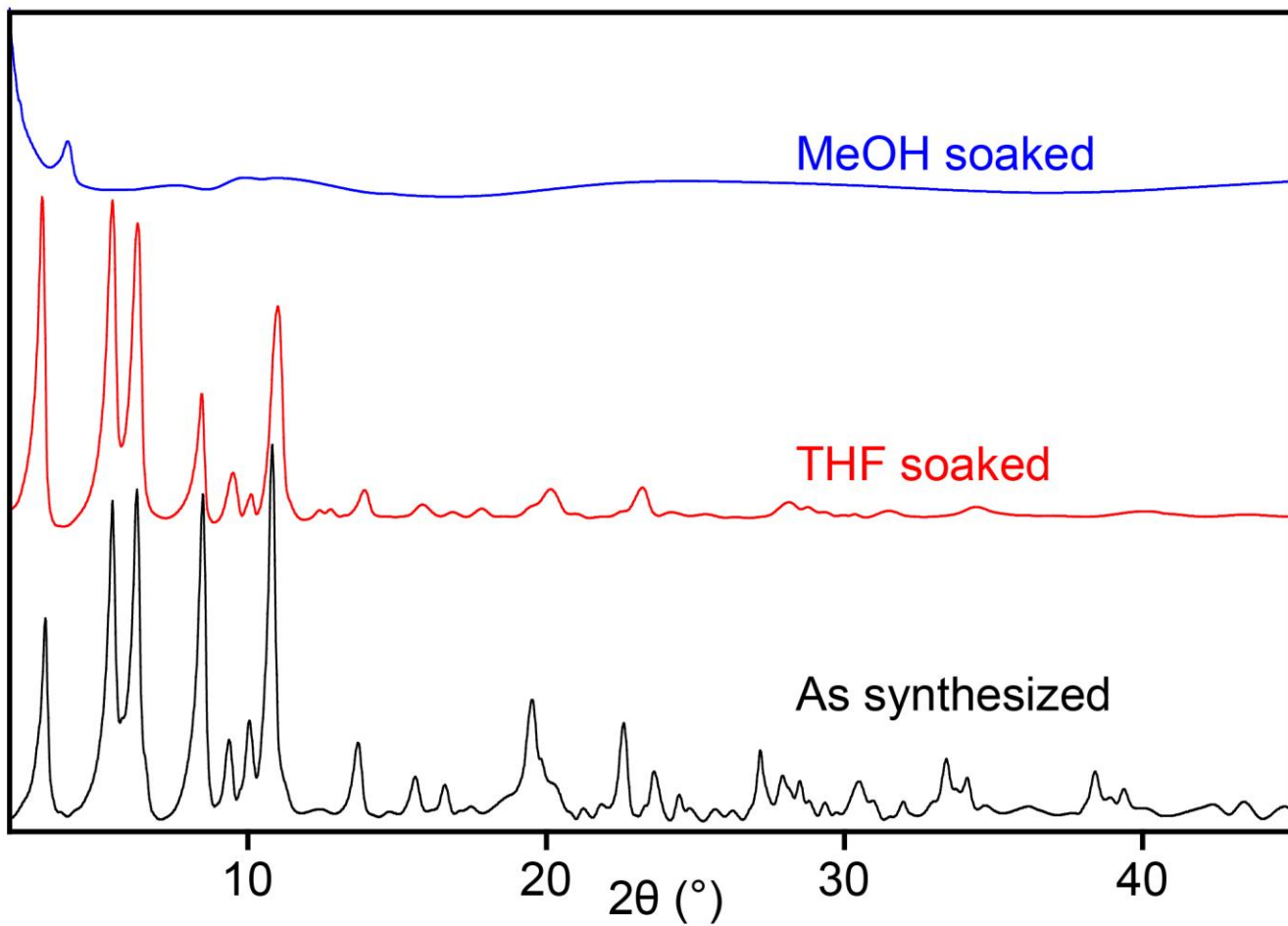


Figure S36. XRPD patterns (Cu-K α radiation, $\lambda = 1.5418 \text{ \AA}$) for as synthesized, THF and MeOH solvent exchanged samples of **2**.

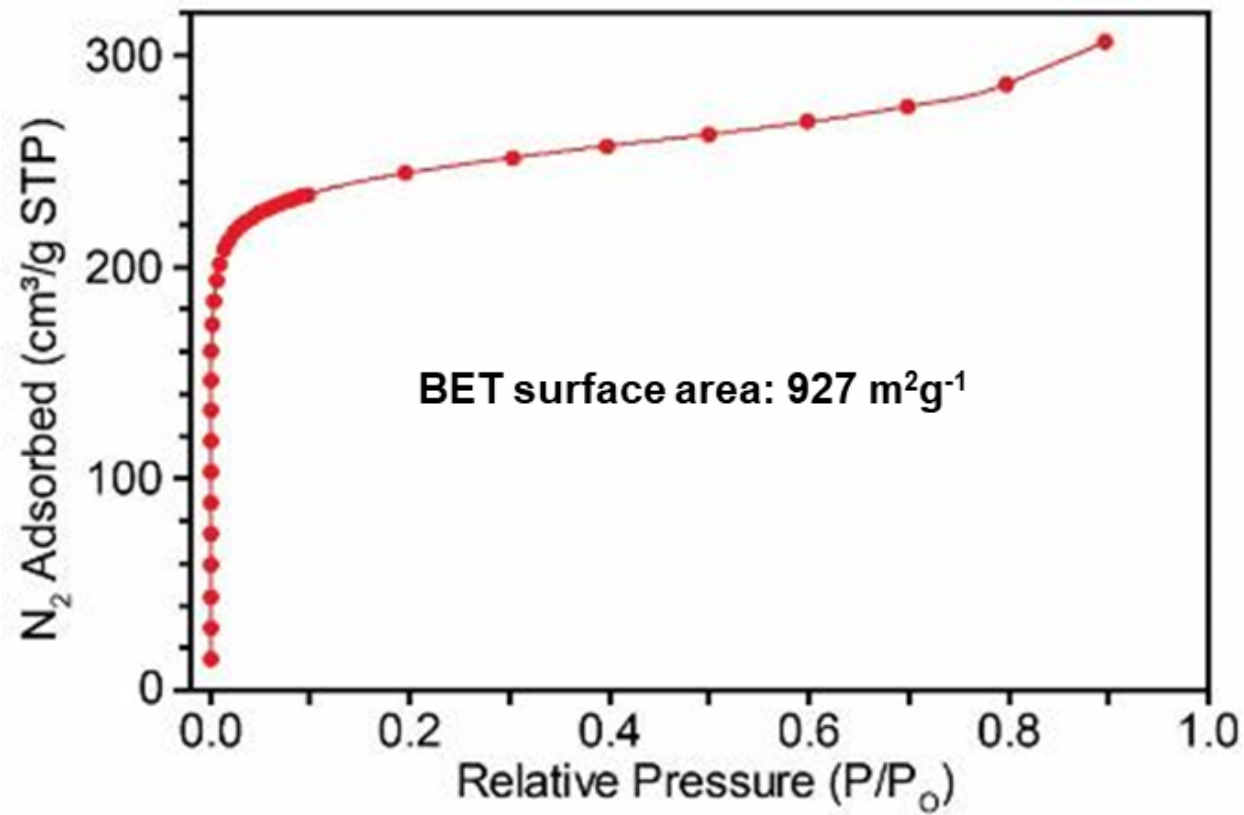


Figure S37. N_2 adsorption isotherm (77 K) for MeOH soaked sample of **1** after desolvation at 100 °C and 10^{-4} torr for 16 h.

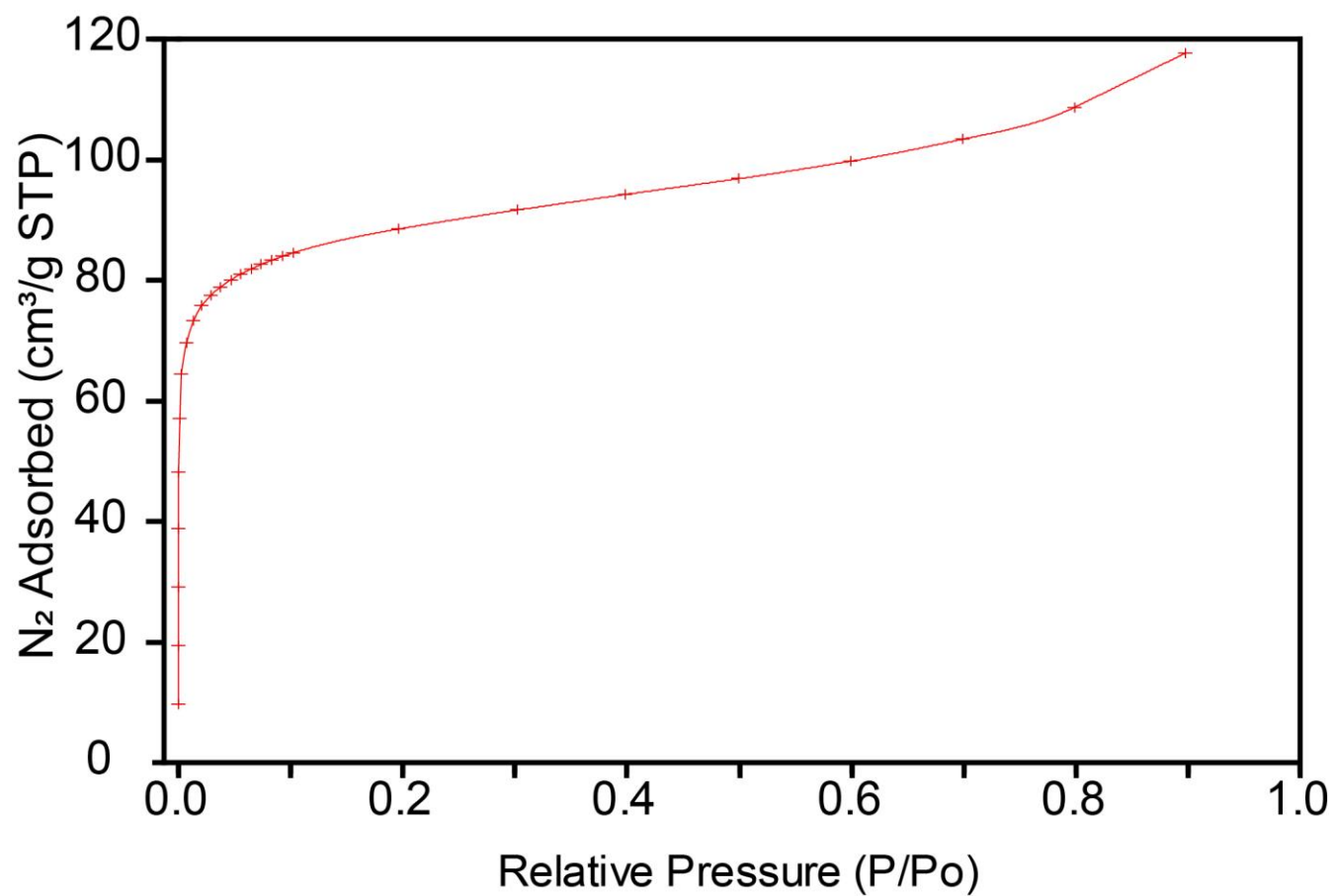


Figure S38. N₂ adsorption isotherm (77 K) for THF soaked sample of **2** after desolvation at 100 °C and 10⁻⁴ torr for 16 h.

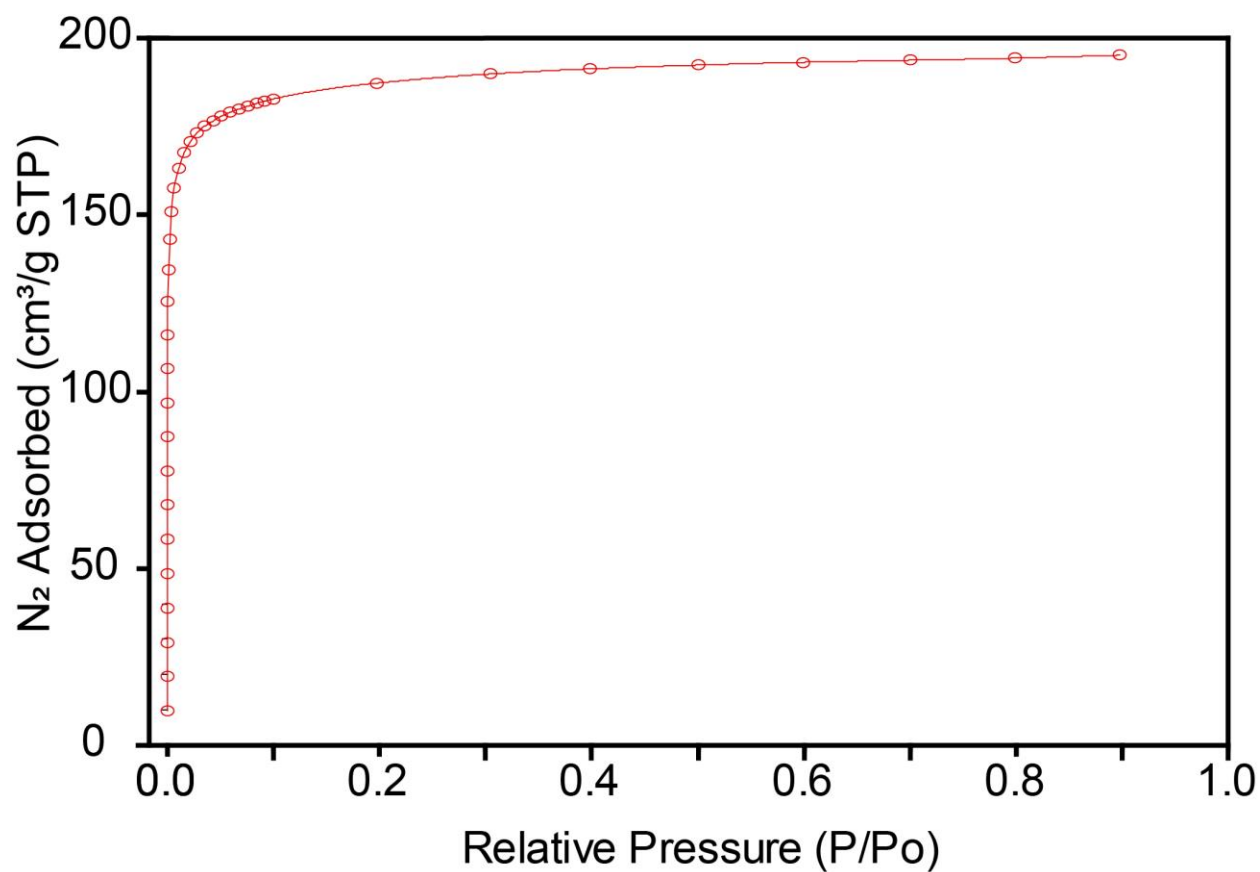


Figure S39. N₂ adsorption isotherm (77 K) for MeOH soaked sample of **3** after desolvation at 100 °C and 10⁻⁴ torr for 16 h.

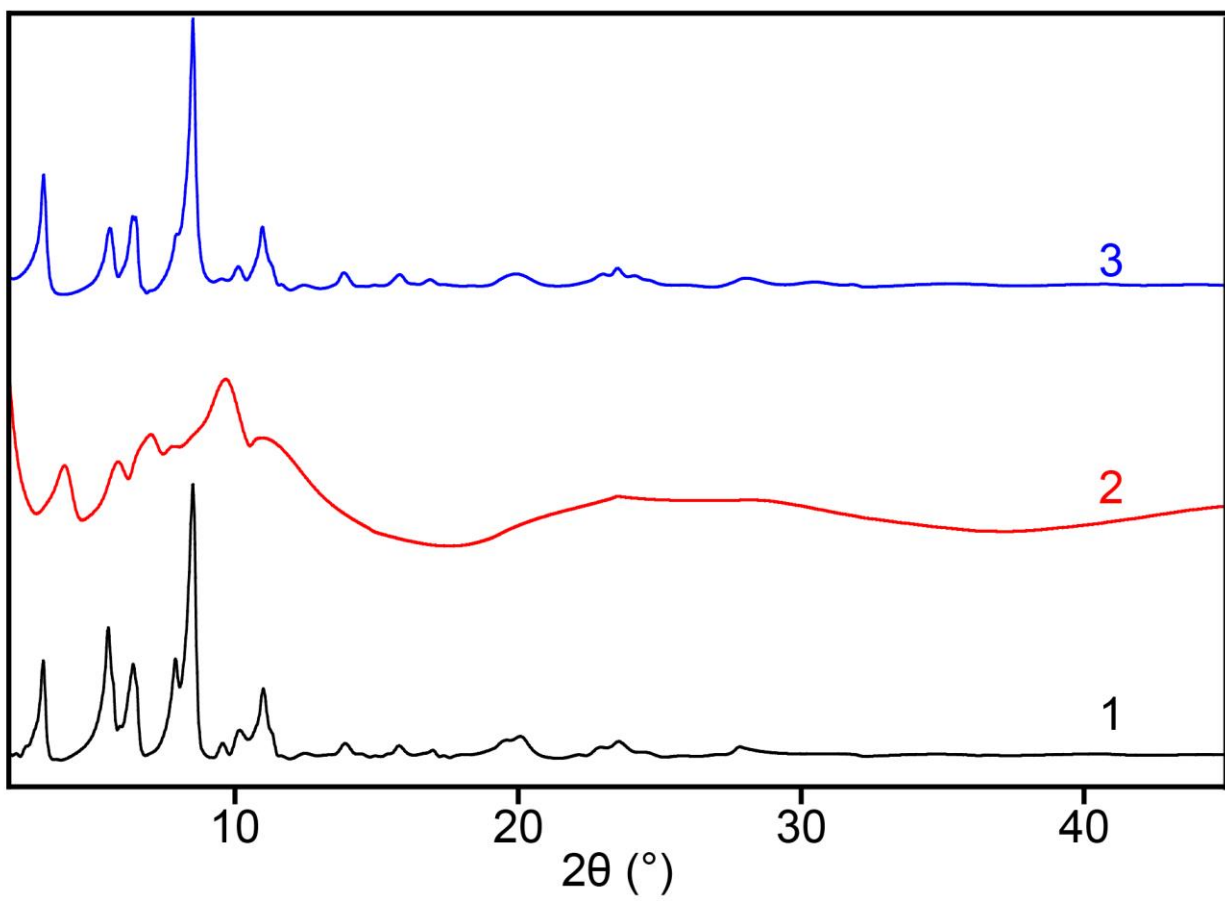


Figure S40. XRPD patterns (Cu-K α radiation, $\lambda = 1.5418 \text{ \AA}$) for activated samples of **1**, **2** and **3**.

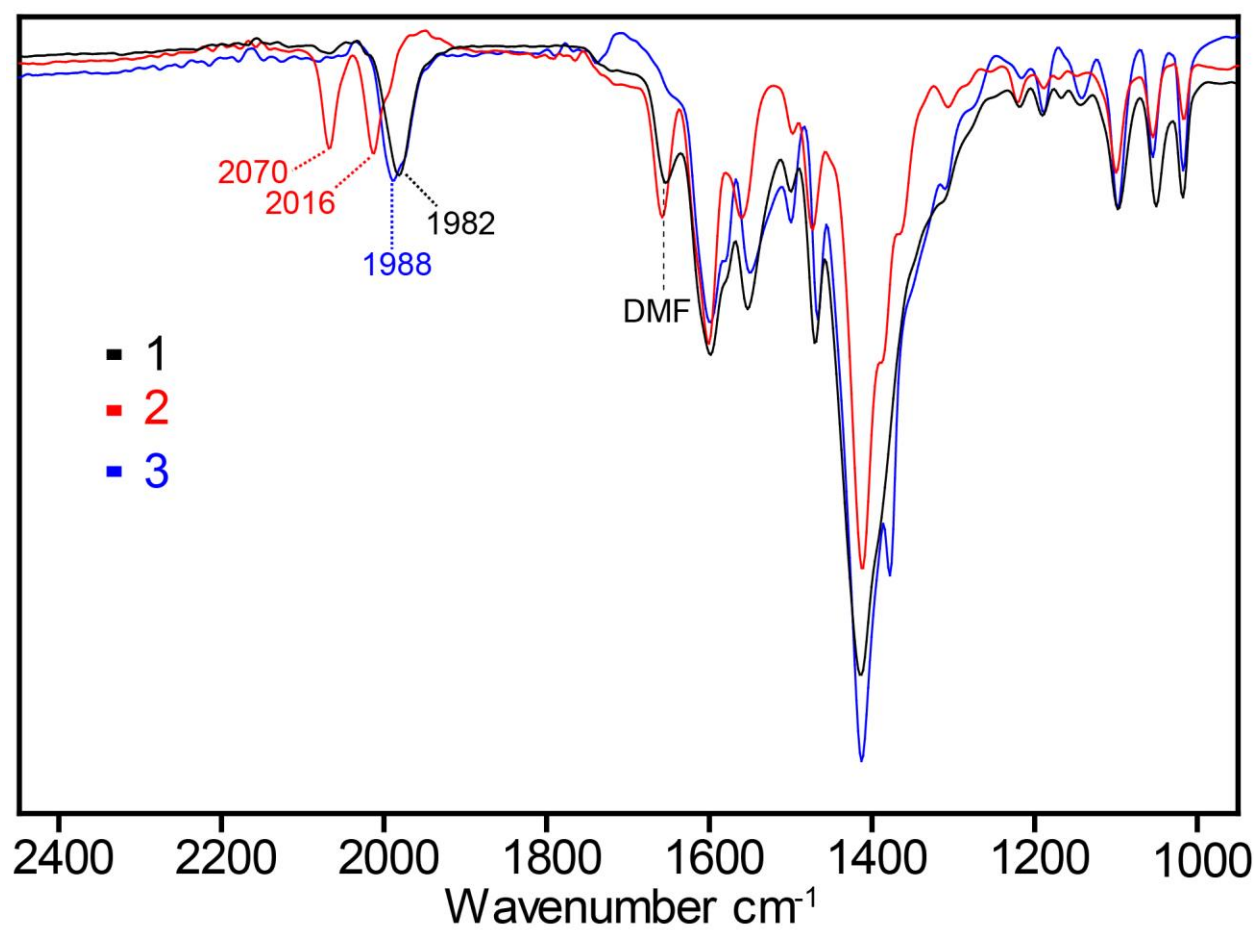


Figure S41. ATR-IR spectra for samples of **1**, **3** (MeOH soaked), and **2** (THF soaked).

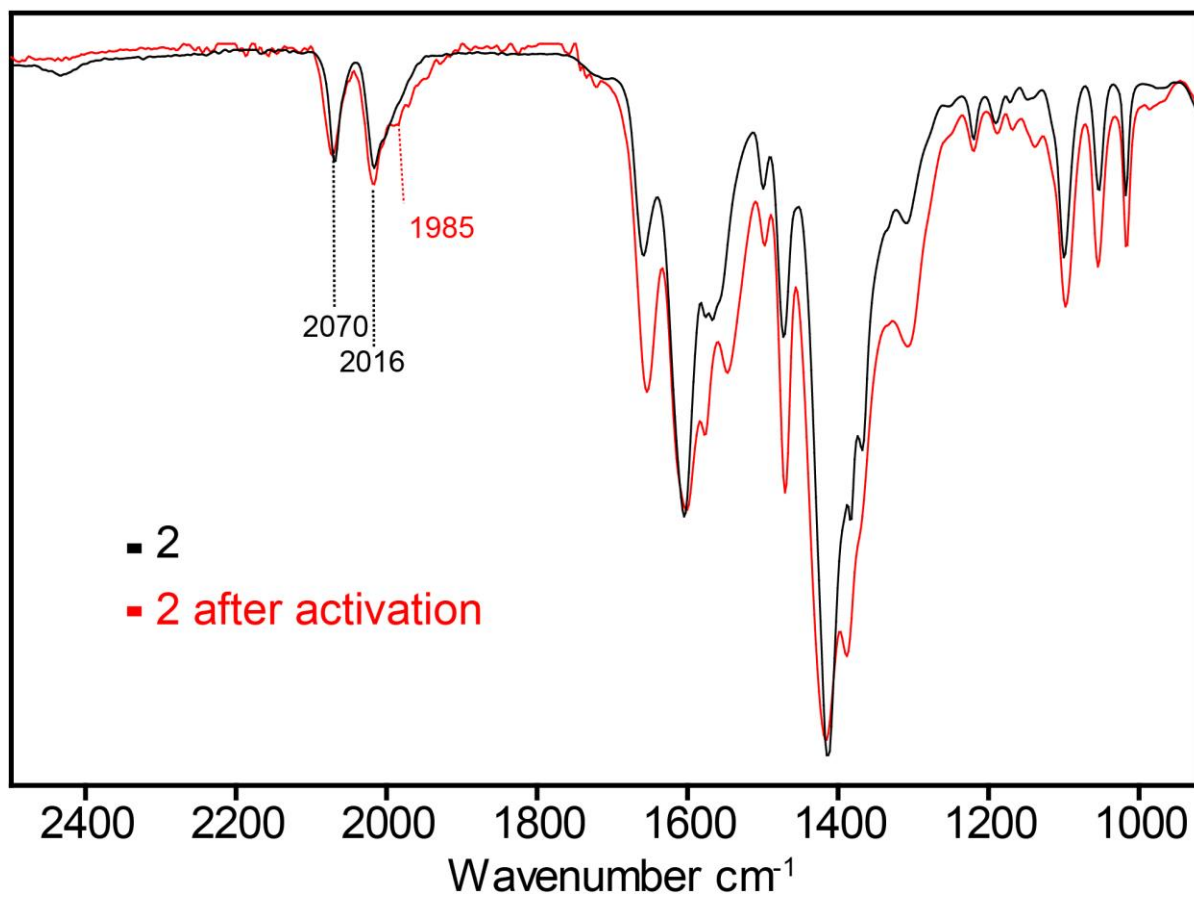


Figure S42. ATR-IR spectra for **2** before and after activation.

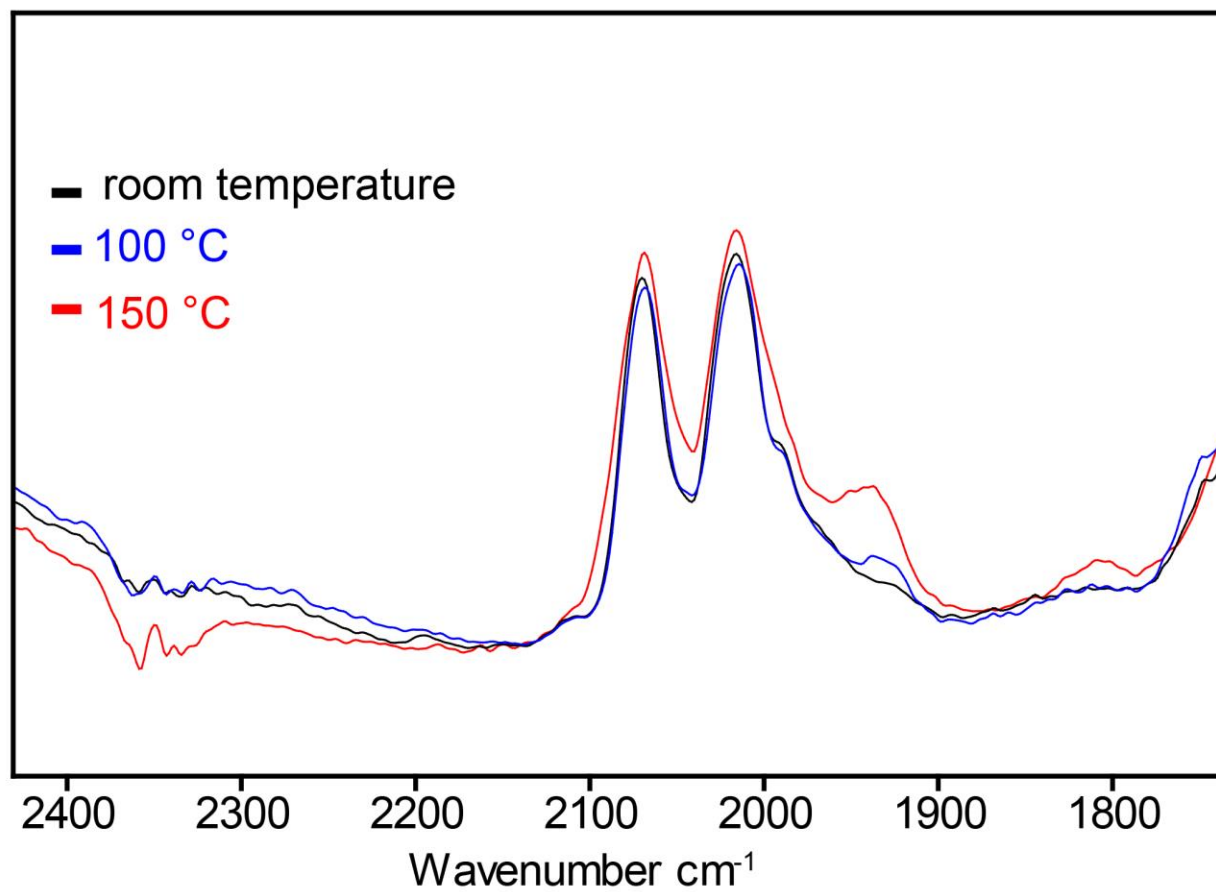


Figure S43. Diffuse reflectance IR spectra of **2** at room temperature and have heating to 100 and 150 °C under an N₂ atmosphere.

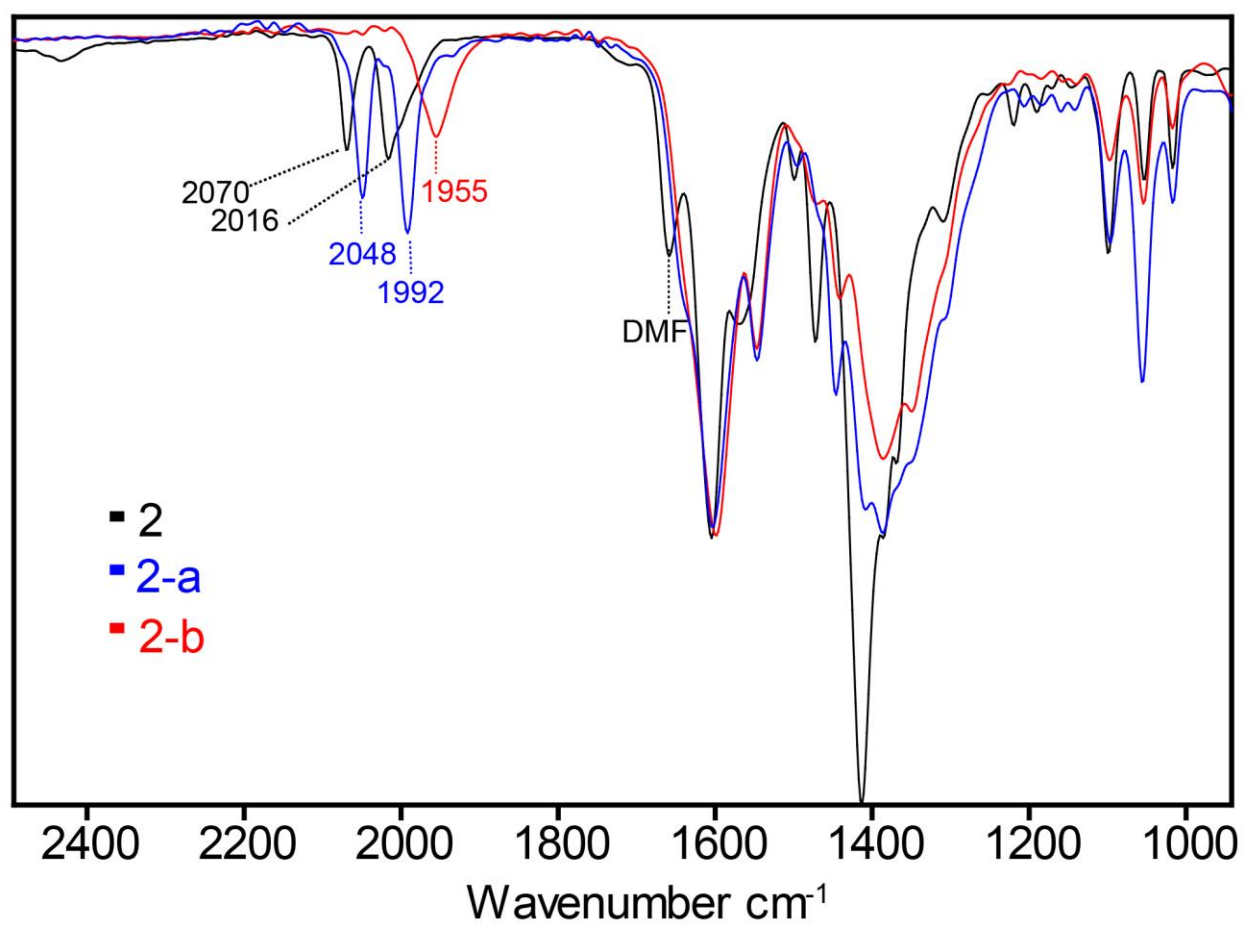


Figure S44. ATR-IR spectra of **2**, **2-a**, and **2-b**.

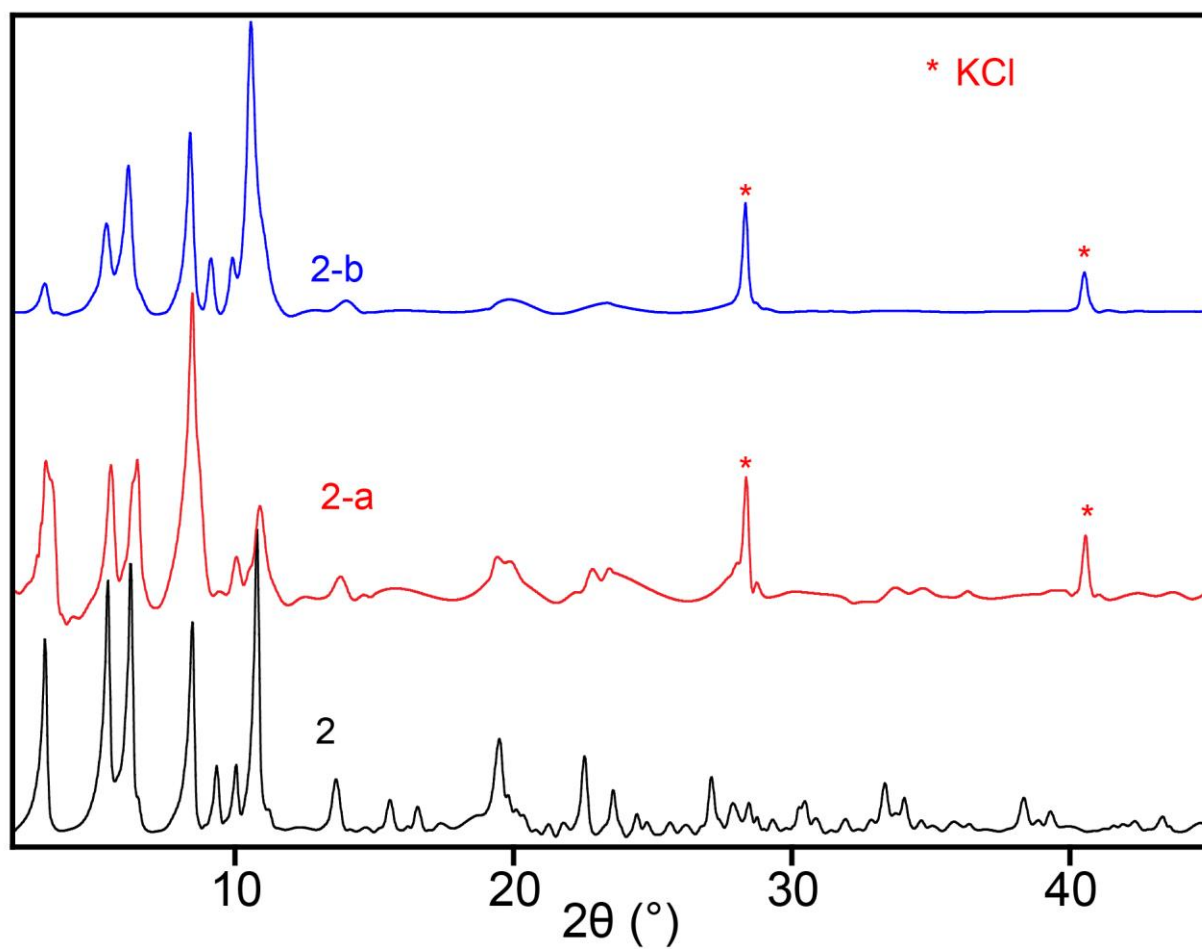


Figure S45. XRPD patterns (Cu-K α radiation, $\lambda = 1.5418 \text{ \AA}$) of **2**, **2-a** and **2-b**.

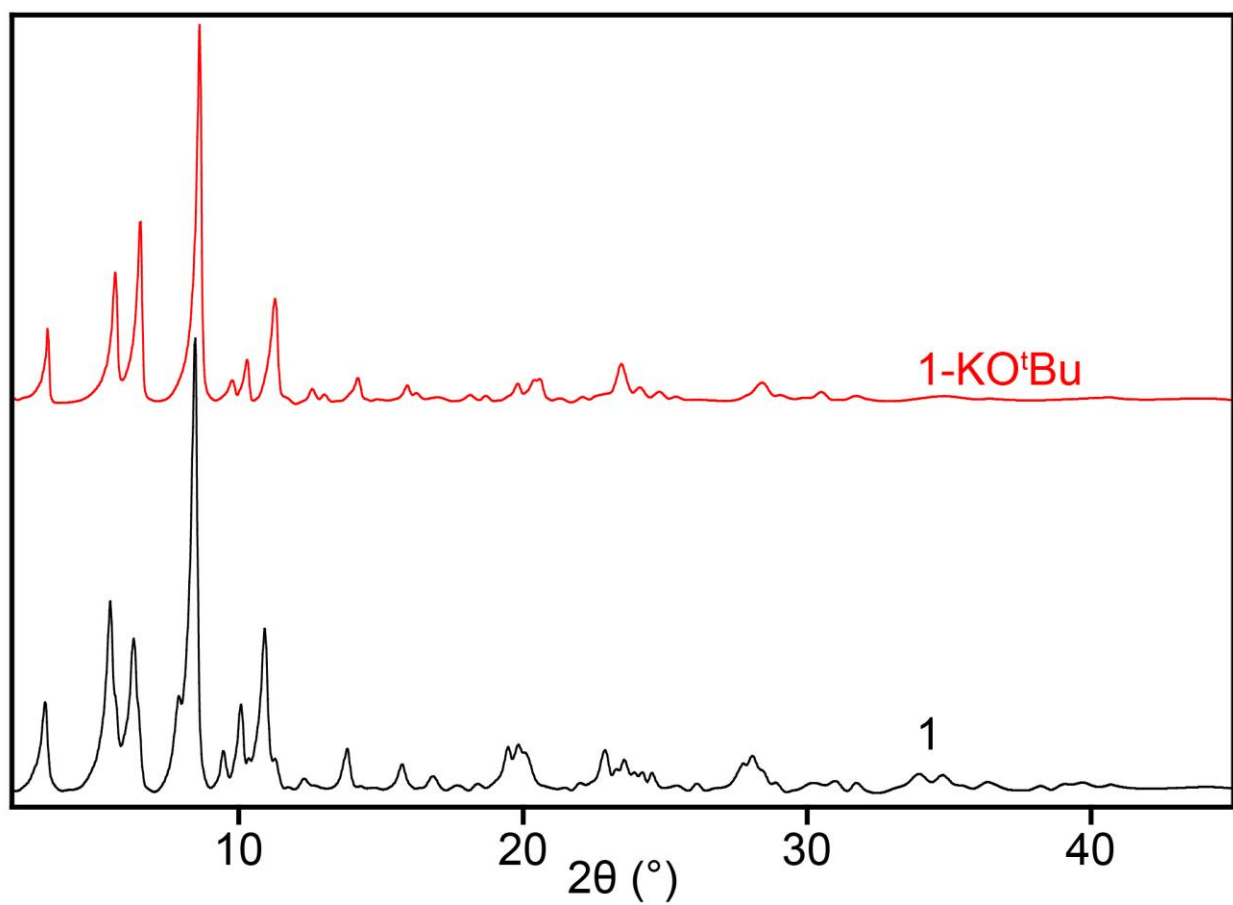


Figure S46. XRPD patterns (Cu-K α radiation, $\lambda = 1.5418 \text{ \AA}$) of **1** and **1-KO^tBu**.

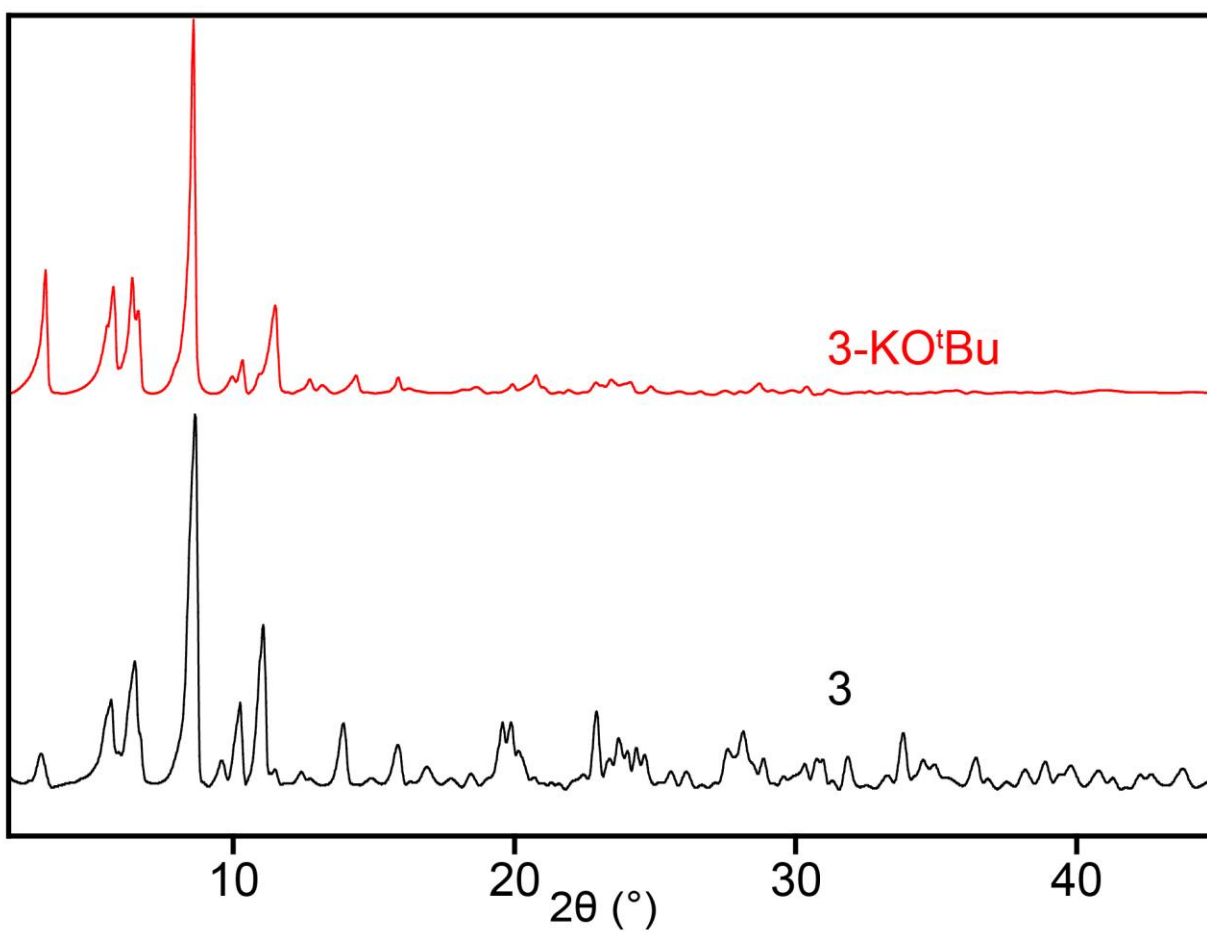


Figure S47. XRPD patterns (Cu-K α radiation, $\lambda = 1.5418 \text{ \AA}$) of **3** and **3-KO^tBu**.

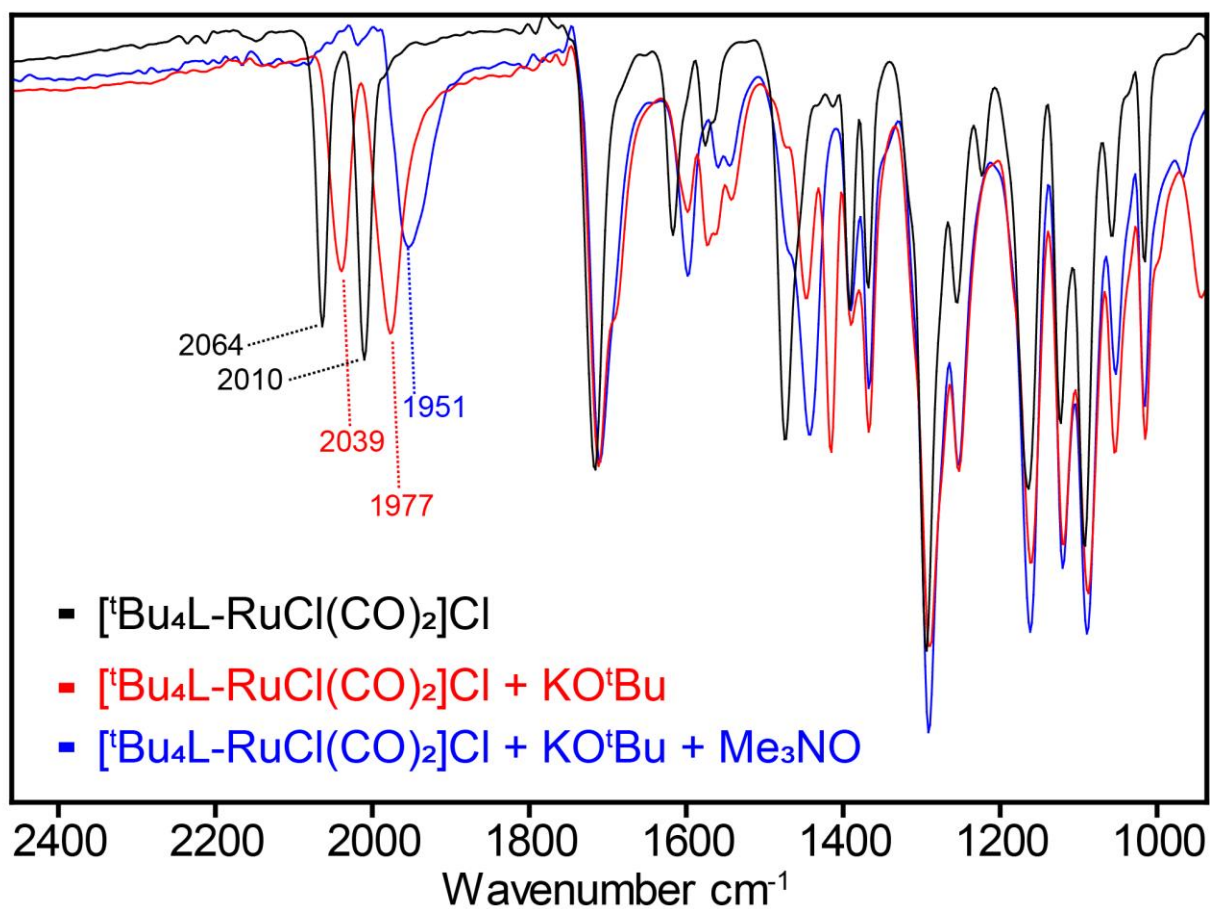


Figure S48. ATR-IR spectra for $[\text{tBu}_4\text{L-RuCl}(\text{CO})_2]\text{Cl}$ reaction with KO^tBu and Me_3NO .

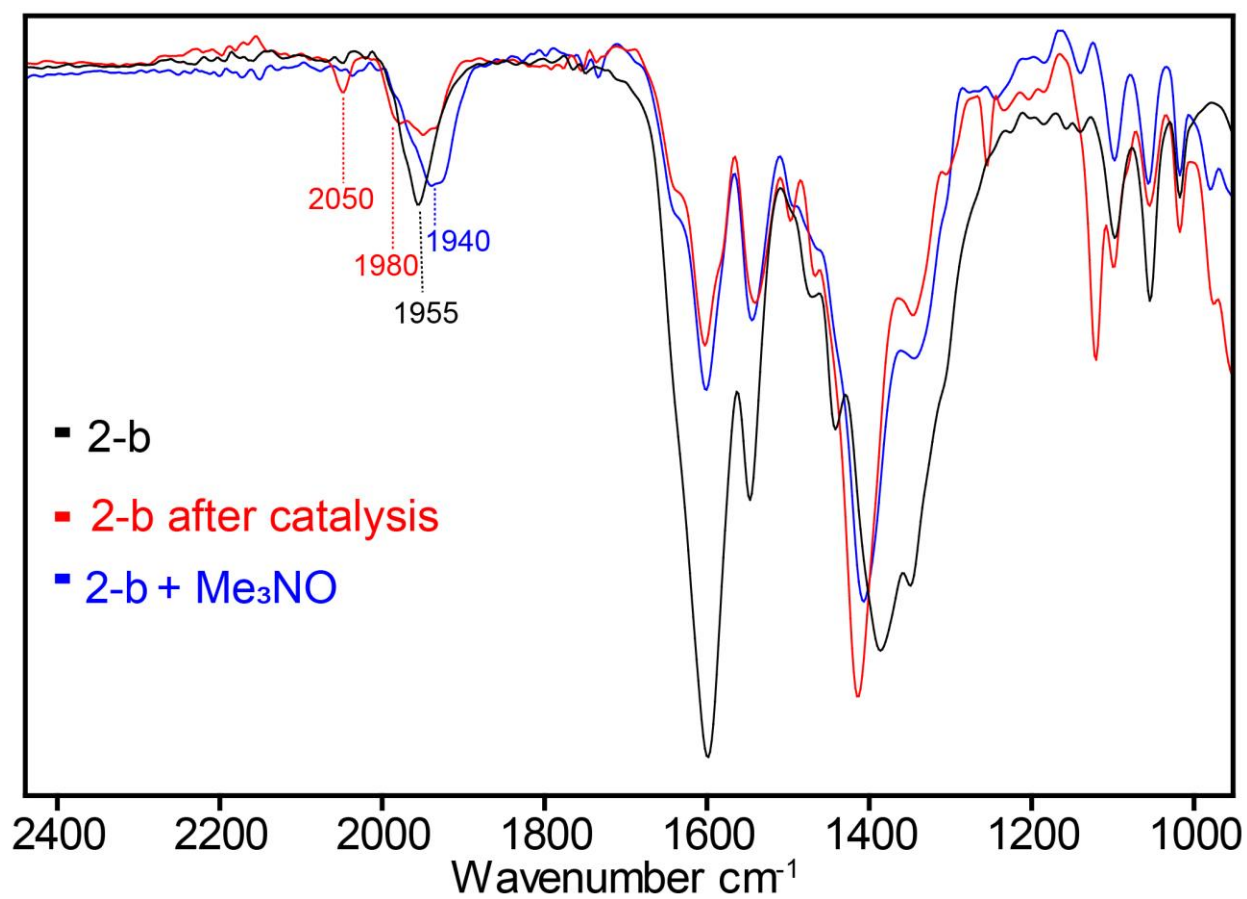
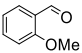
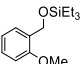
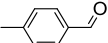
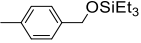
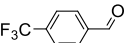
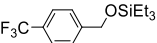
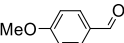
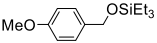
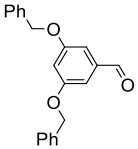
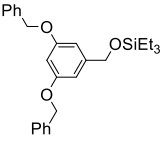
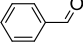
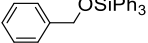


Figure S49. ATR-IR spectra for **2-b** before and after catalysis, and regeneration of **2-b** with Me₃NO.

Table S3. Hydrosilylation of aryl aldehydes catalyzed by **2-b**^a

$\text{Ar}-\text{CHO} + \text{R}_3\text{SiH} \xrightarrow[\text{100 } ^\circ\text{C, 12 h}]{\text{5 mol \% [Ru], 1,4-dioxane}} \text{Ar}-\text{CH}_2\text{OSiR}_3$ (2 equiv.)			
Entry	Substrate	Product	% Yield ^b
1			91
2			86
3			92
4			69
5			9
6 ^c			< 5

^aReaction conditions: substrate (0.2 mmol), catalyst (0.01 mmol), Et₃SiH (0.4 mmol), 1,4-dioxane (1 mL), 12 h, 100 °C. ^bYields were determined by ¹H NMR with respect to an internal standard (hexamethylbenzene). ^cPh₃SiH (0.4 mmol) was used in place of Et₃SiH.

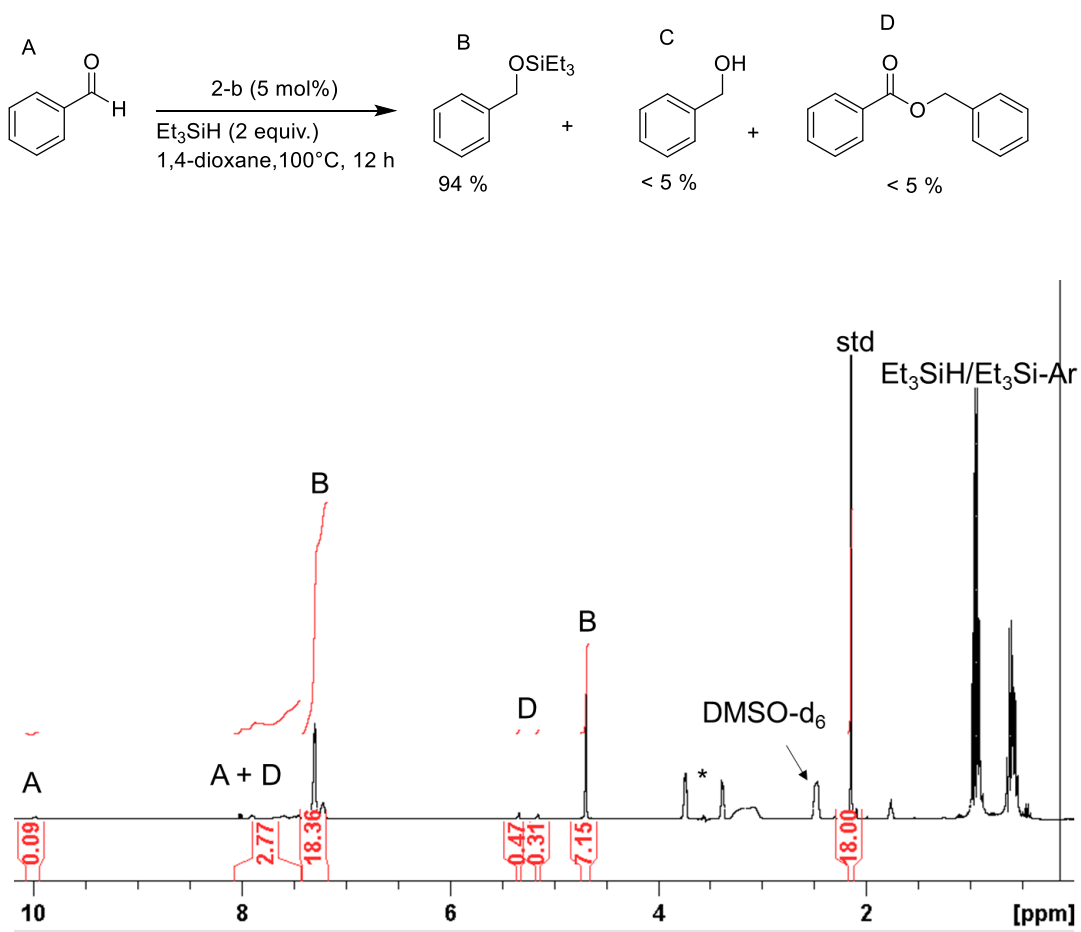


Figure S50. ^1H NMR spectrum for hydrosilylation of benzaldehyde with **2-b**. (Substrate: hexamethylbenzene = 3.8:1). Asterisk (*) is used to denote suppressed 1,4-dioxane.

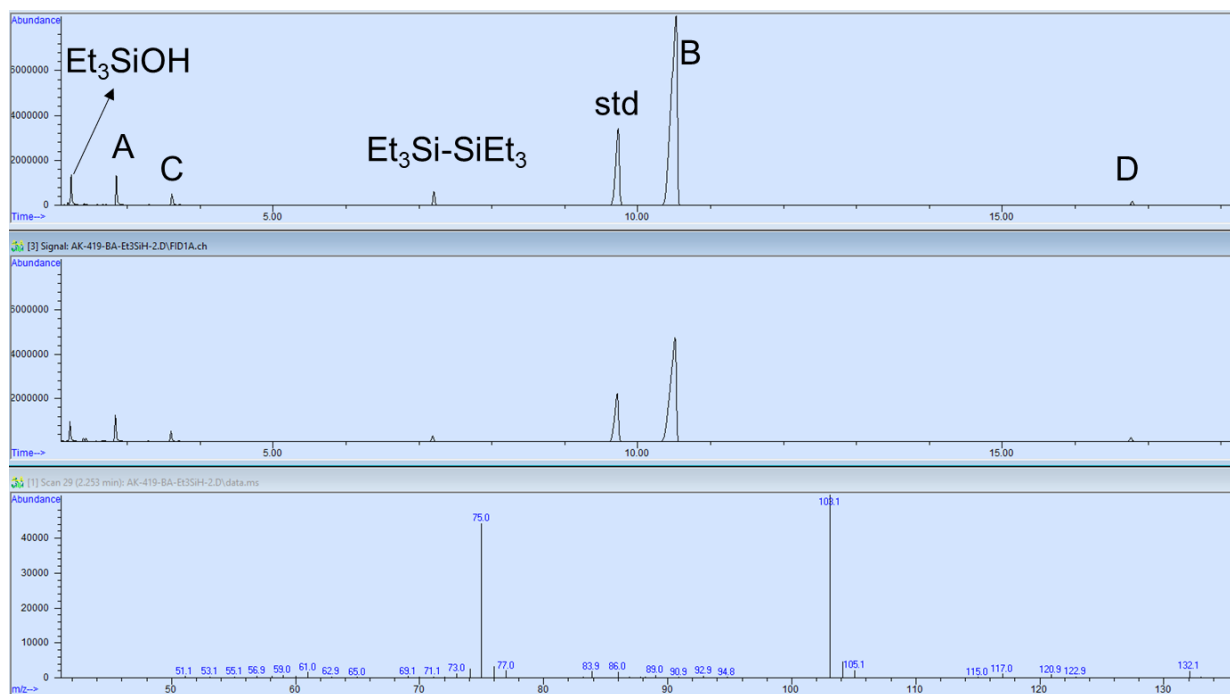
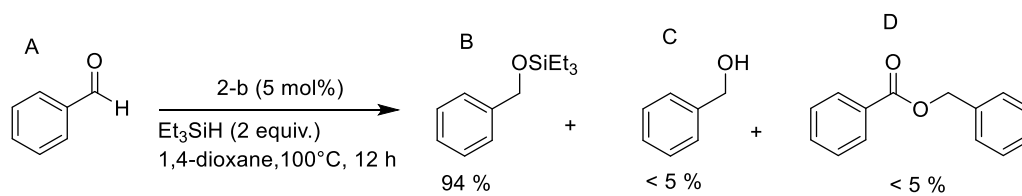


Figure S51. GC/MS chromatogram for the hydrosilylation of benzaldehyde with **2-b**.

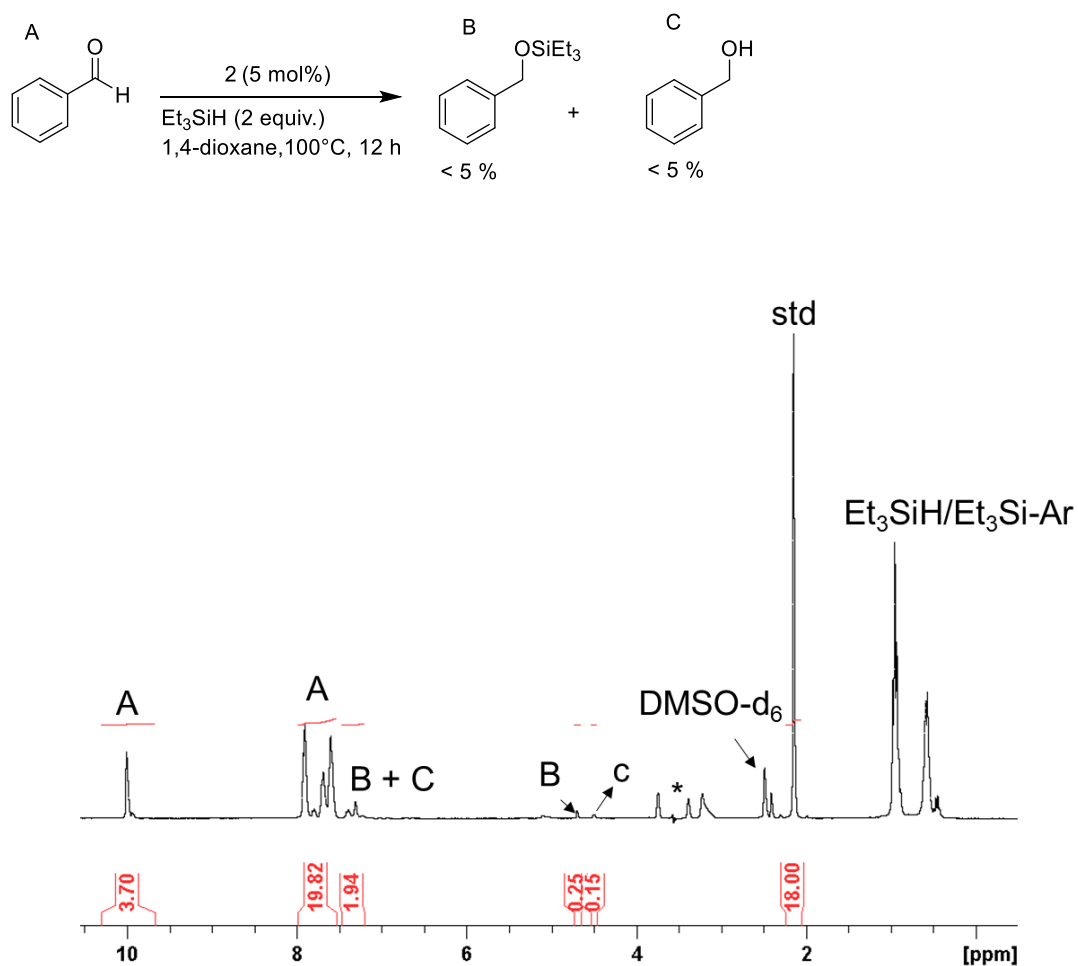


Figure S52. ^1H NMR spectrum for hydrosilylation of benzaldehyde with **2**. (Substrate: hexamethylbenzene = 3.8:1). Asterisk (*) is used to denote suppressed 1,4-dioxane.

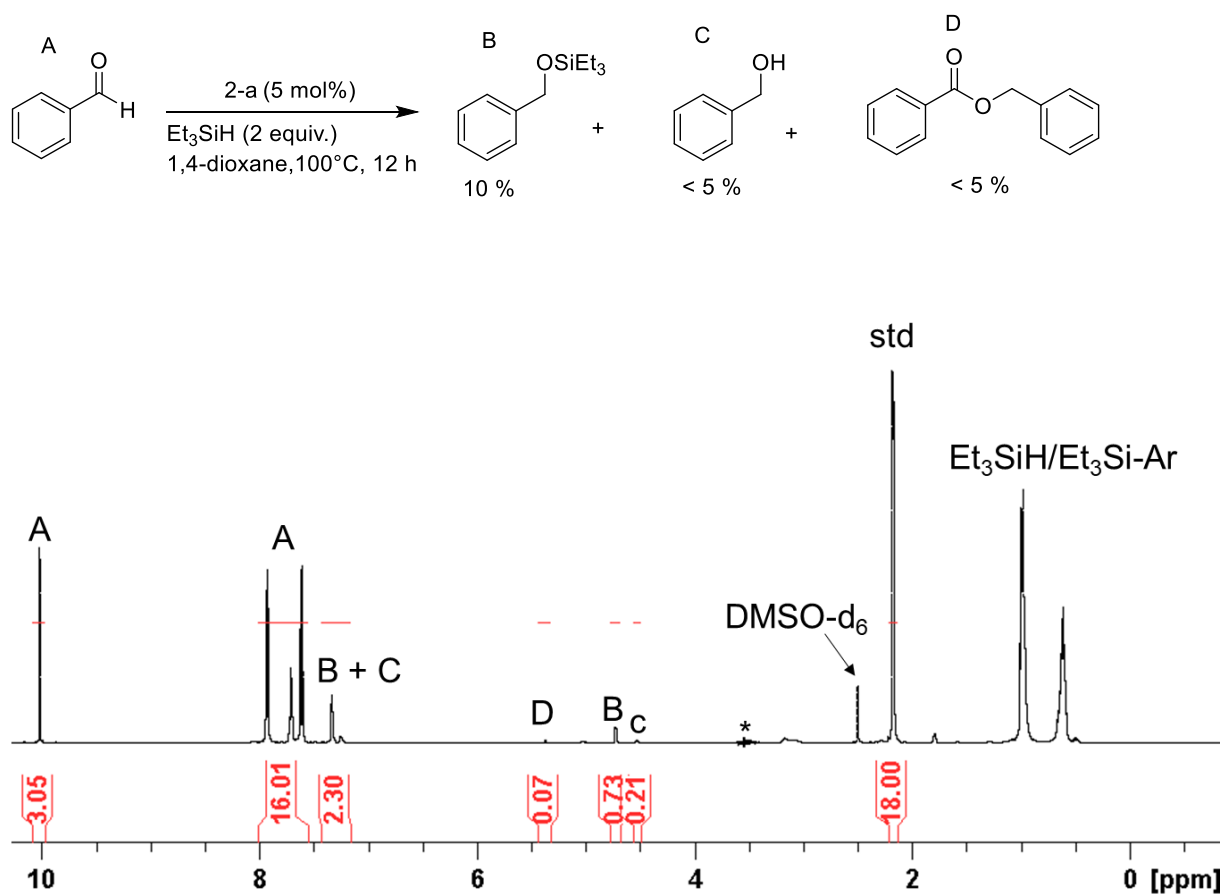


Figure S53. ^1H NMR spectrum for hydrosilylation of benzaldehyde with **2-a**. (Substrate: hexamethylbenzene = 3.8:1). Asterisk (*) is used to denote suppressed 1,4-dioxane.

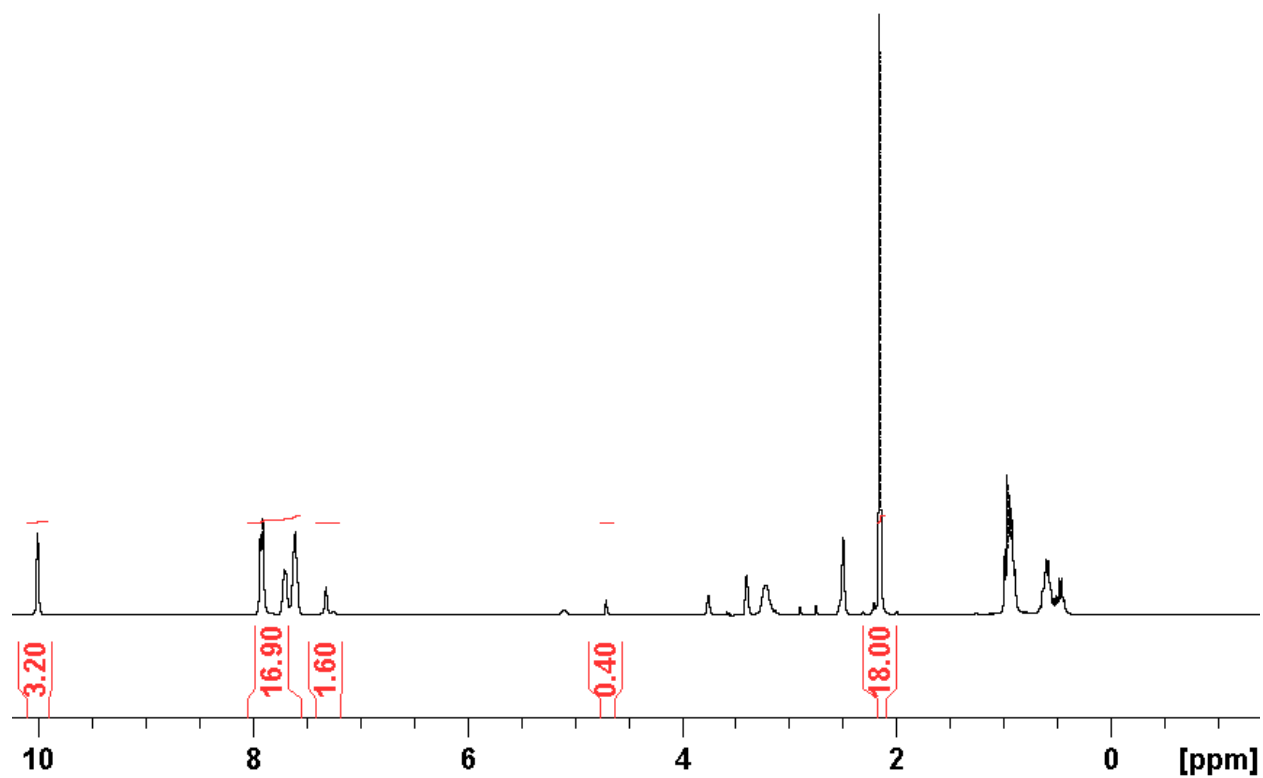
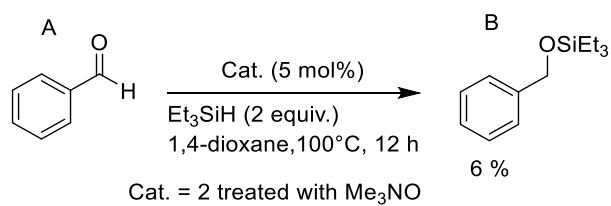


Figure S54. ¹H NMR spectrum for hydrosilylation of benzaldehyde with **2** treated with Me₃NO. (Substrate: hexamethylbenzene = 3.3:1).

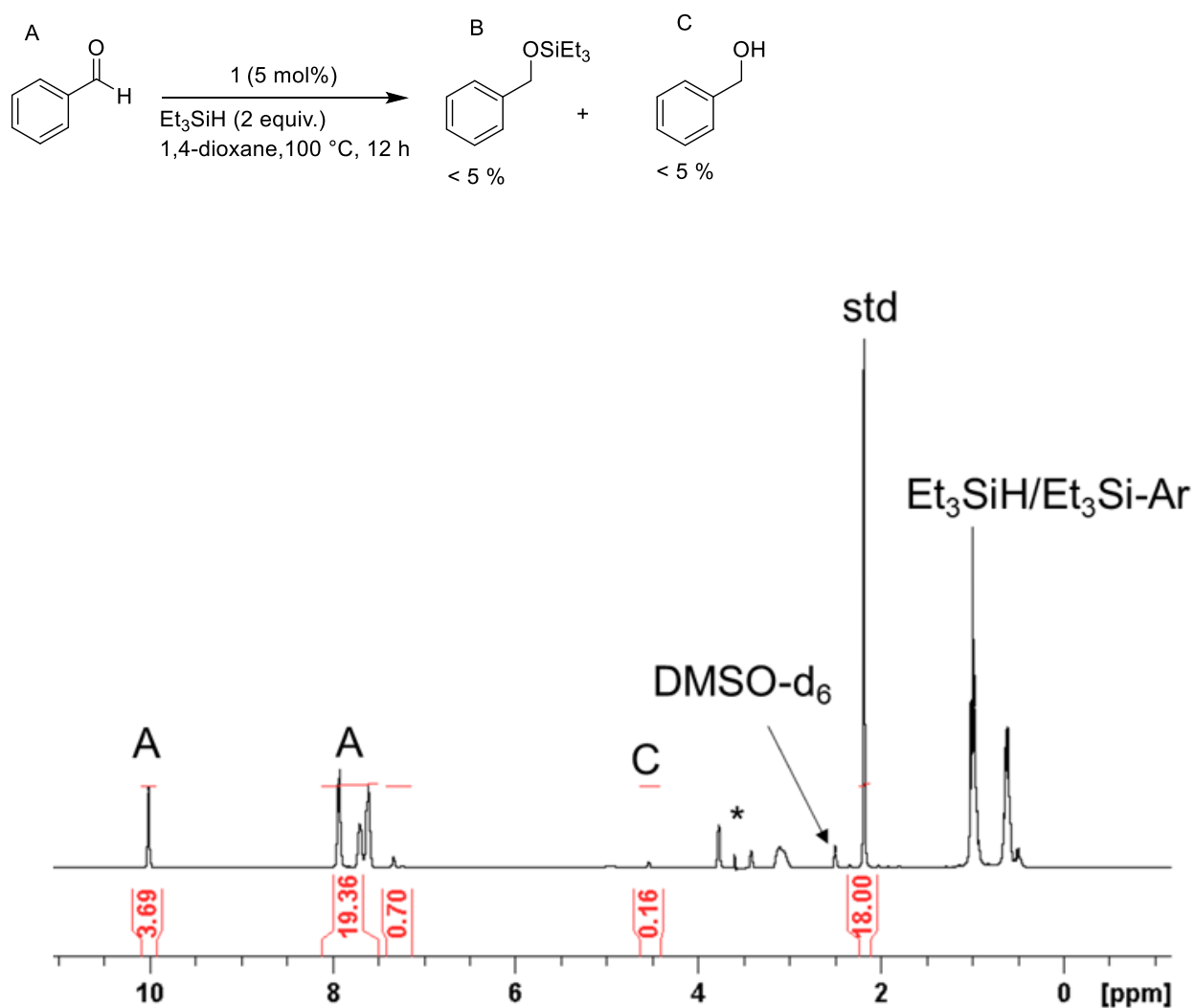


Figure S55. ^1H NMR spectrum for hydrosilylation of benzaldehyde with **1**. (Substrate: hexamethylbenzene = 3.98:1). Asterisk (*) is used to denote suppressed 1,4-dioxane.

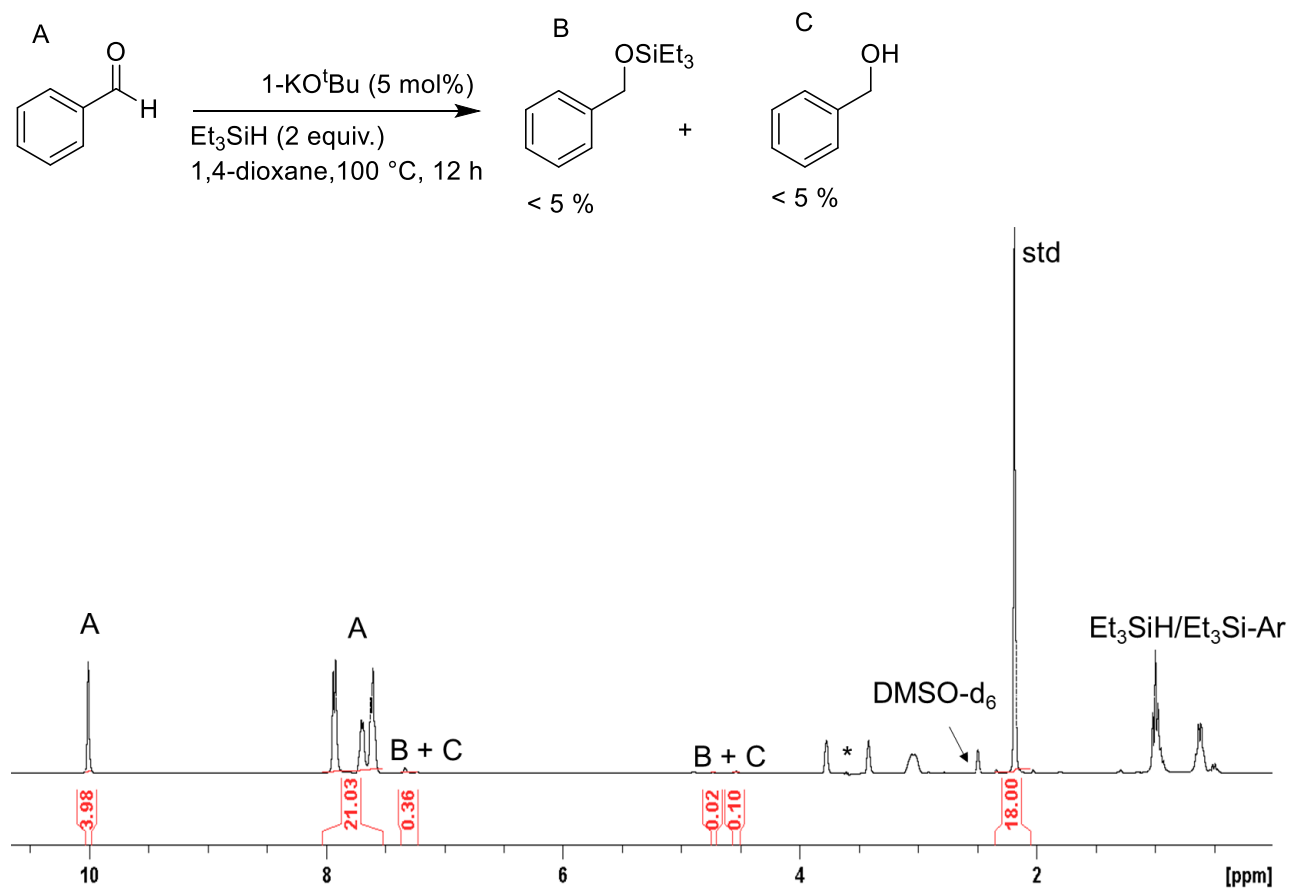


Figure S56. ^1H NMR spectrum for hydrosilylation of benzaldehyde with $1\text{-KO}^t\text{Bu}$. (Substrate: hexamethylbenzene = 4:1). Asterisk (*) is used to denote suppressed 1,4-dioxane.

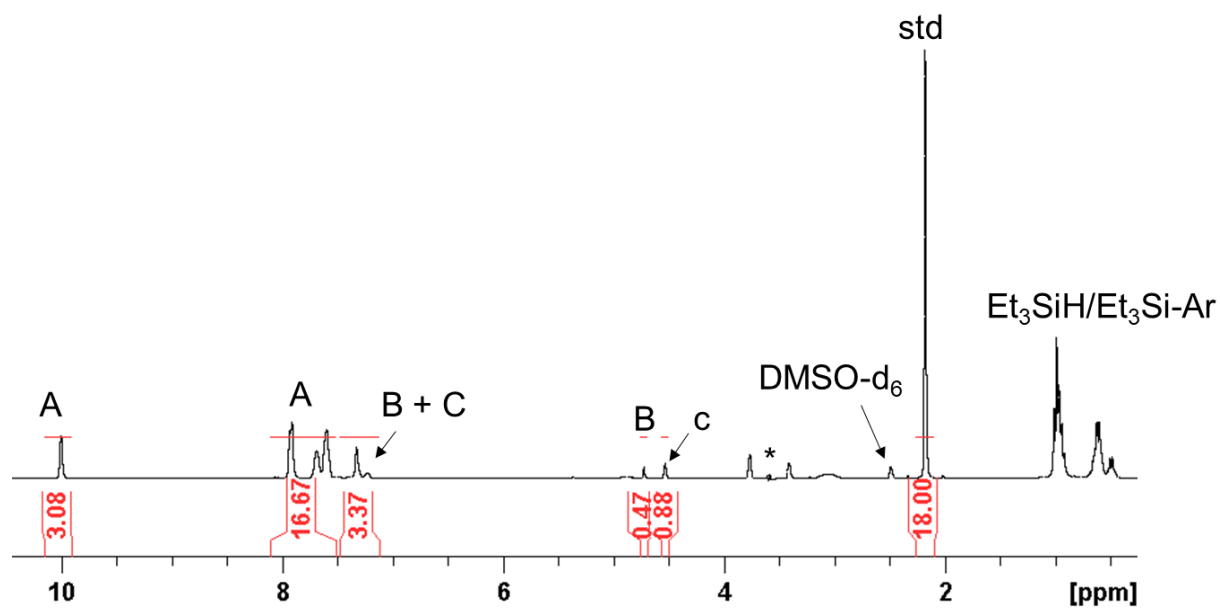
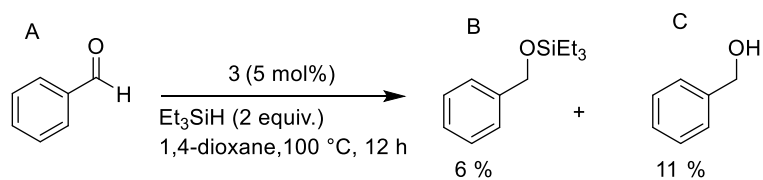


Figure S57. ^1H NMR spectrum for hydrosilylation of benzaldehyde with **3**. (Substrate: hexamethylbenzene = 3.8:1). Asterisk is used to denote suppressed 1,4-dioxane.

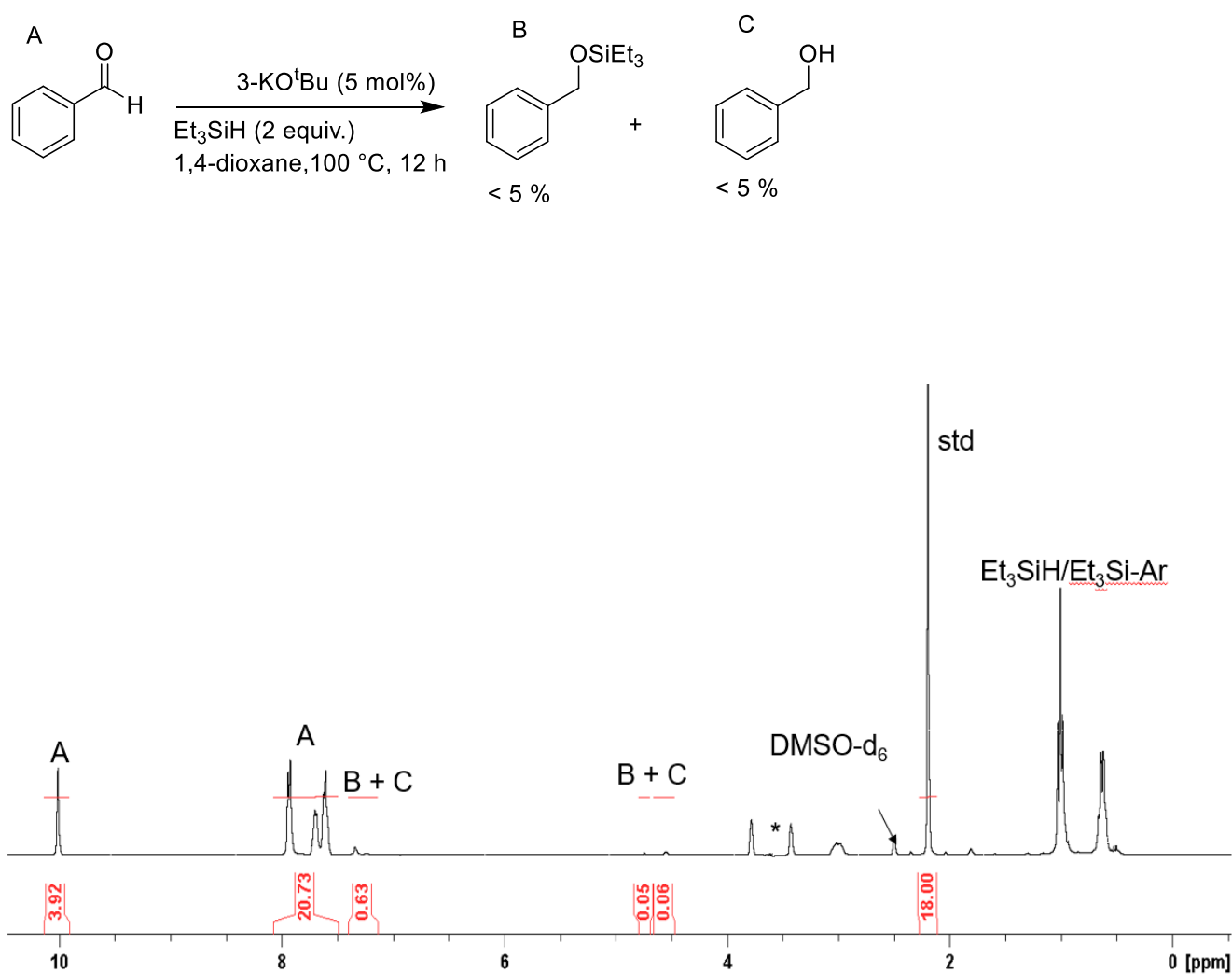


Figure S58. ^1H NMR spectrum for hydrosilylation of benzaldehyde with **3-KO^tBu**. (Substrate: hexamethylbenzene = 4:1). Asterisk is used to denote suppressed 1,4-dioxane.

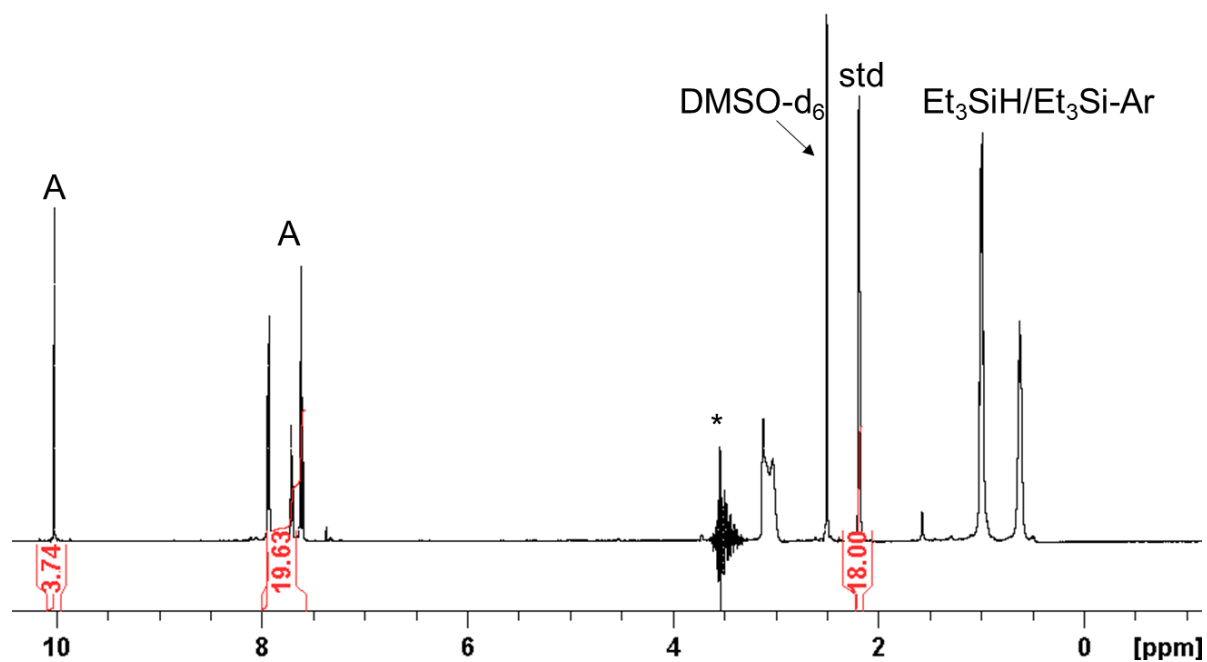
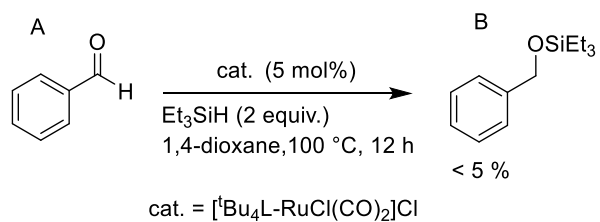


Figure S59. ^1H NMR spectrum for hydrosilylation of benzaldehyde with $[\text{tBu}_4\text{L-RuCl(CO)}_2]\text{Cl}$. (Substrate: hexamethylbenzene = 3.8:1). Asterisk (*) is used to denote suppressed 1,4-dioxane.

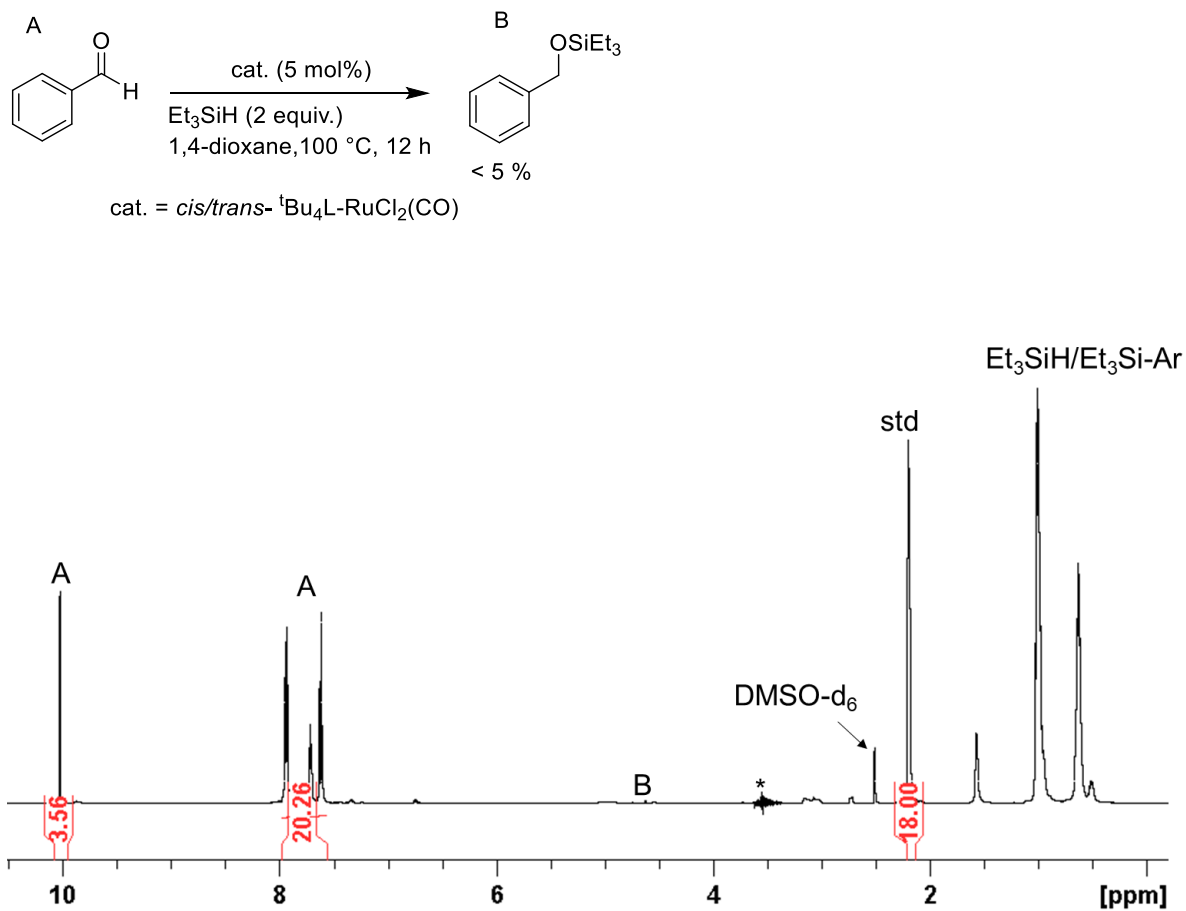


Figure S60. ¹H NMR spectrum for hydrosilylation of benzaldehyde with *cis/trans*-^tBu₄L-RuCl₂(CO). (Substrate: hexamethylbenzene = 3.8:1). Asterisk (*) is used to denote suppressed 1,4-dioxane.

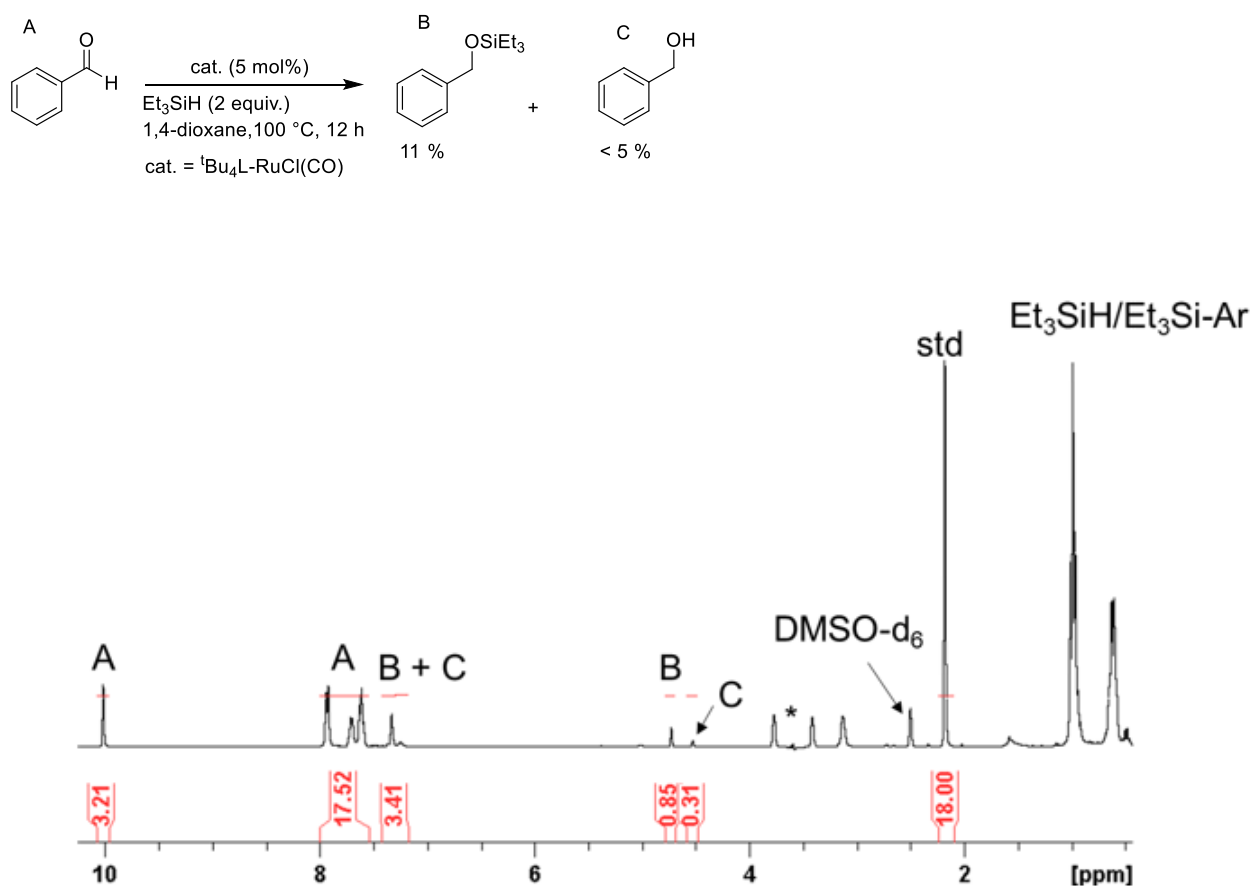


Figure S61. ^1H NMR spectrum for hydrosilylation of benzaldehyde with $[\text{tBu}_4\text{L-RuCl}(\text{CO})_2]\text{Cl}$ pretreated with KO^tBu and Me_3NO . (Substrate: hexamethylbenzene = 3.8:1). Asterisk (*) is used to denote suppressed 1,4-dioxane.

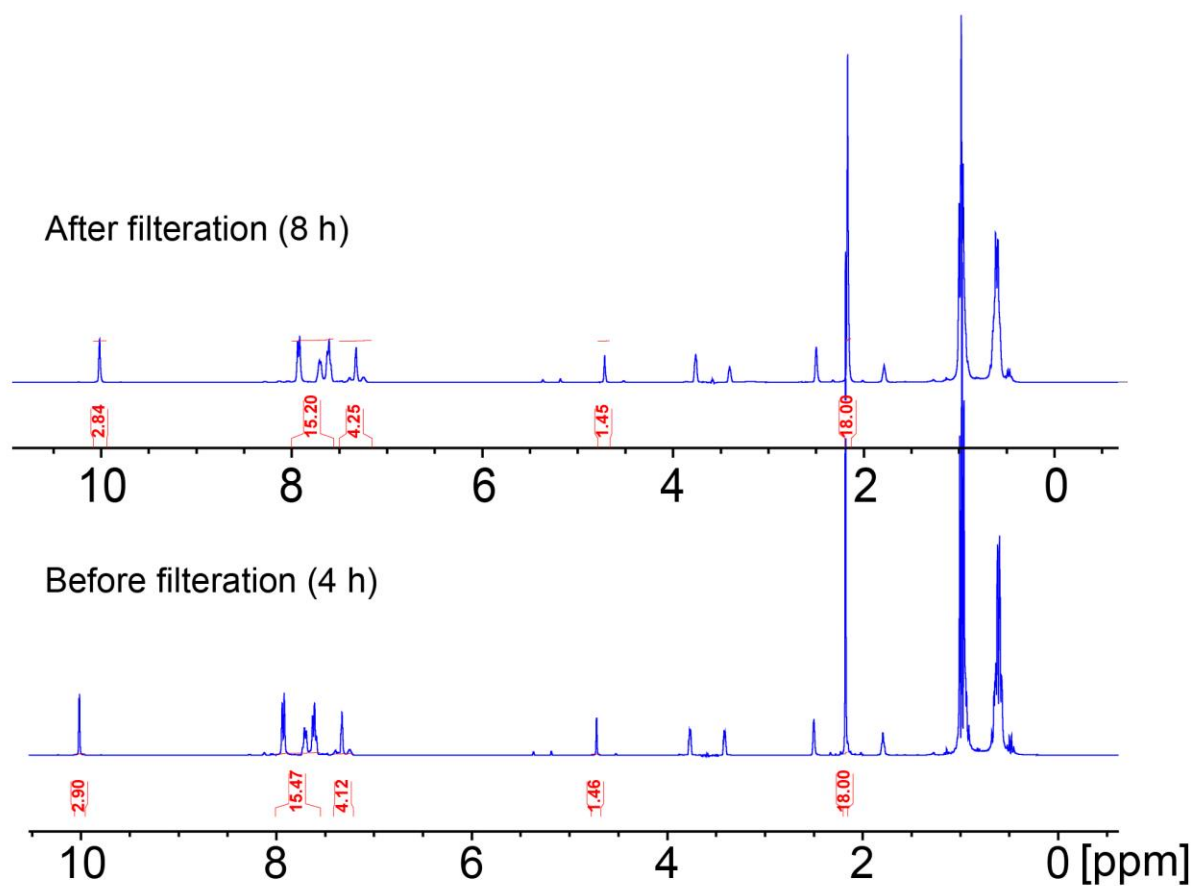
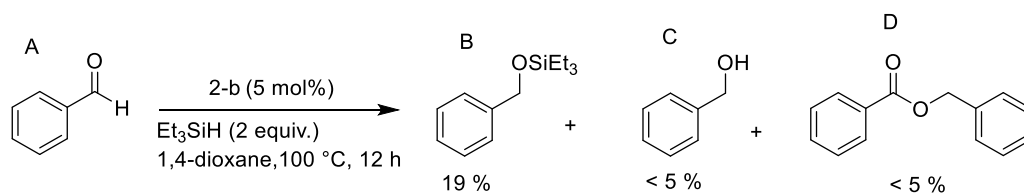


Figure S62. ^1H NMR spectra before (bottom) and after (top) hot filtration for hydrosilylation of benzaldehyde with **2-b**. (Substrate: hexamethylbenzene = 3.8:1). Asterisk (*) is used to denote suppressed 1,4-dioxane.

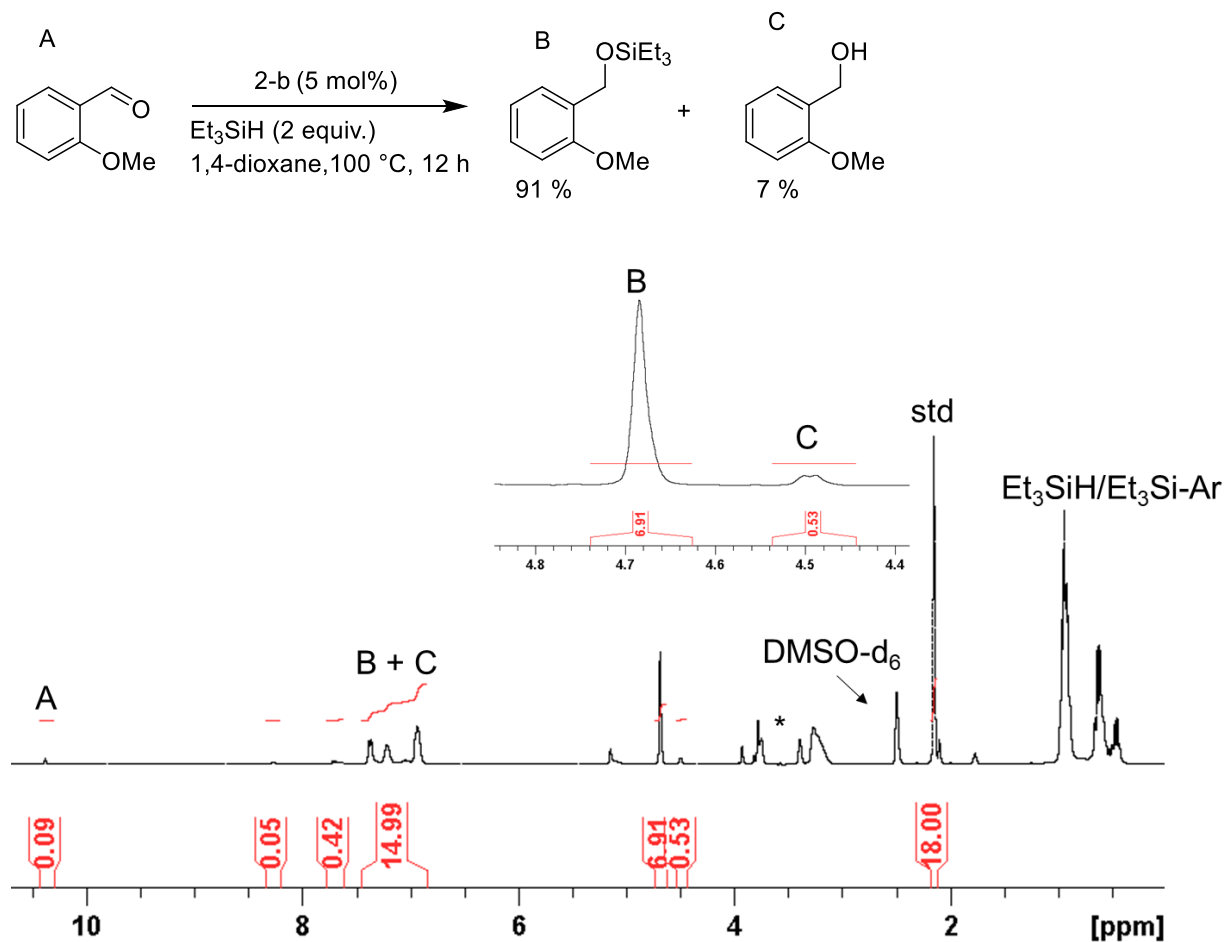


Figure S63. ¹H NMR spectrum for hydrosilylation of o-anisaldehyde with **2-b**. (Substrate: hexamethylbenzene = 3.8:1). Asterisk (*) is used to denote suppressed 1,4-dioxane.

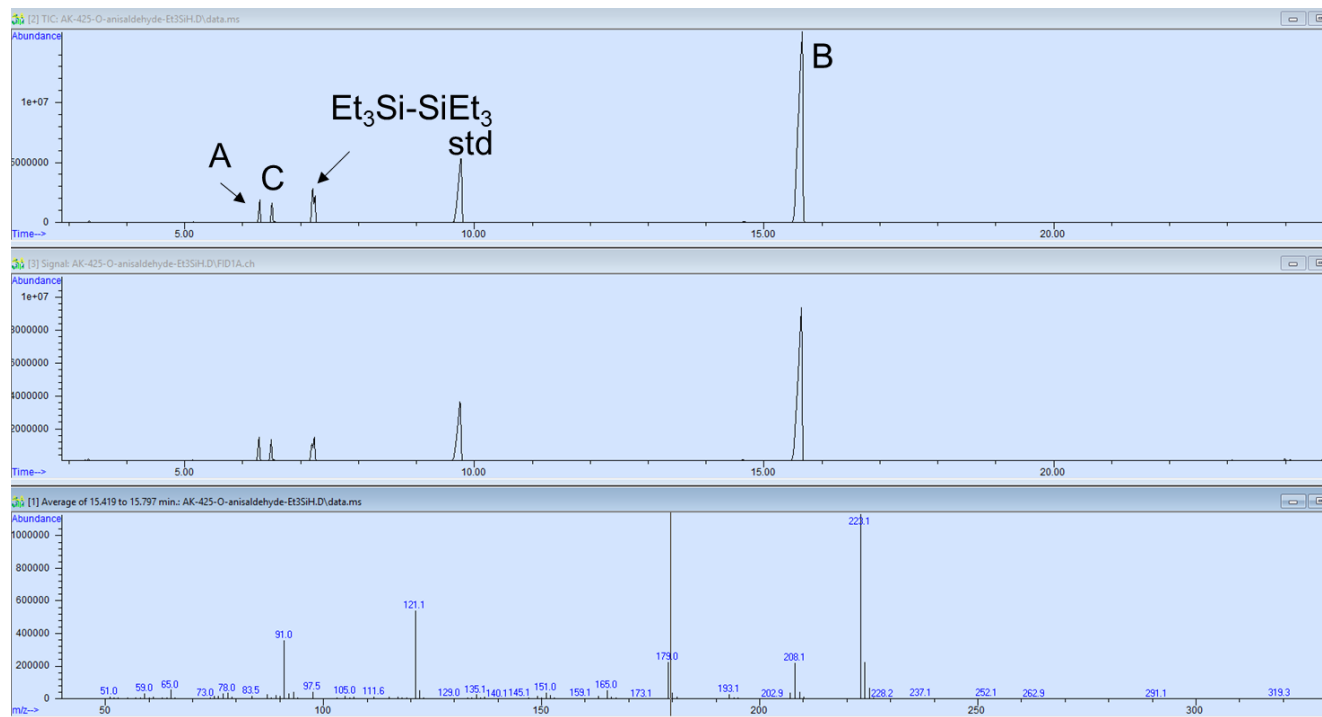
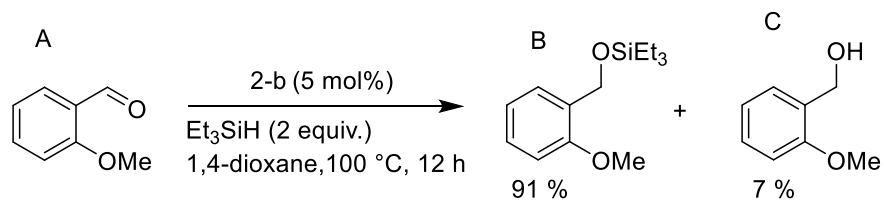


Figure S64. GC/MS chromatogram for the hydrosilylation of O-anisaldehyde with **2-b**.

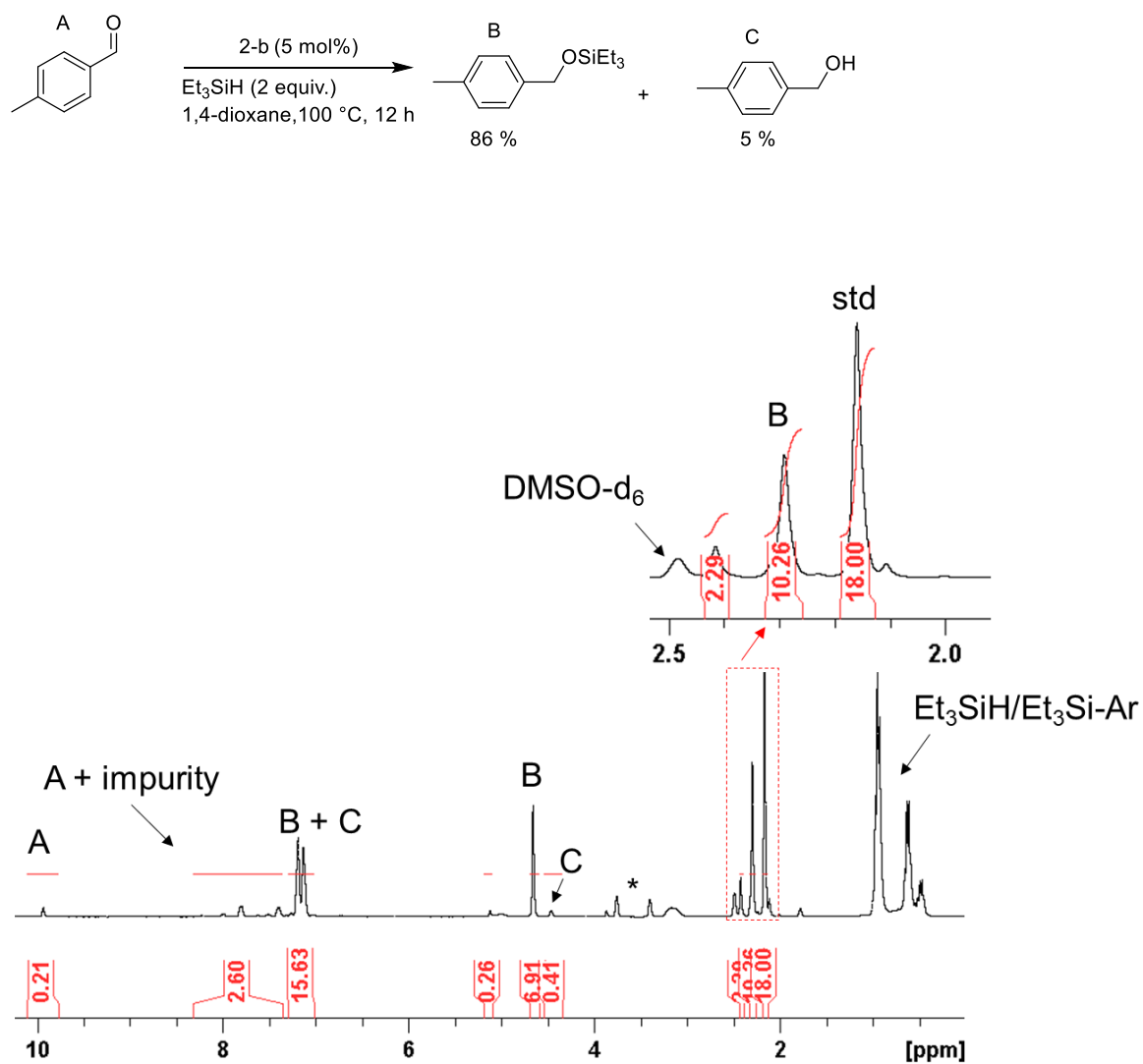


Figure S65. ^1H NMR spectrum for hydrosilylation of 4-methylbenzaldehyde with **2-b**. (Substrate: hexamethylbenzene = 4:1). The substrate had some impurity that was not removed after distillation. GC/MS analysis of the substrate predicts the impurity as methyl benzoate. Asterisk (*) is used to denote suppressed 1,4-dioxane.

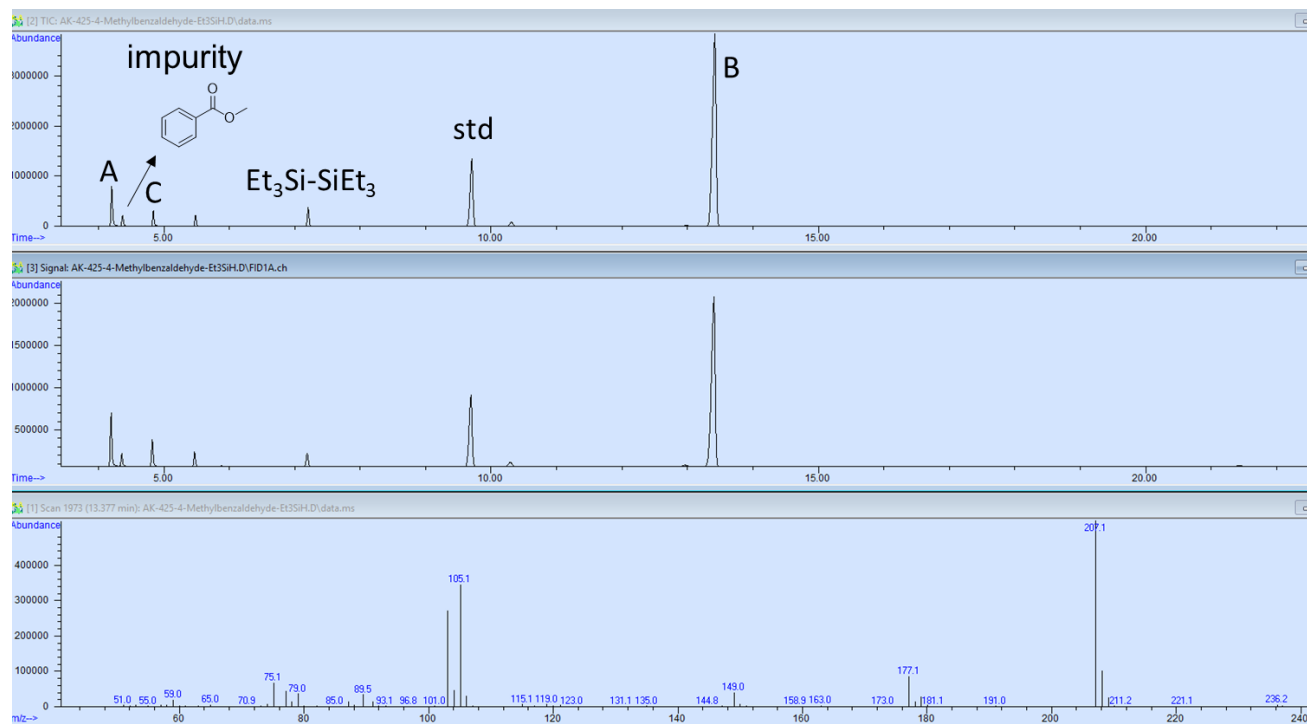
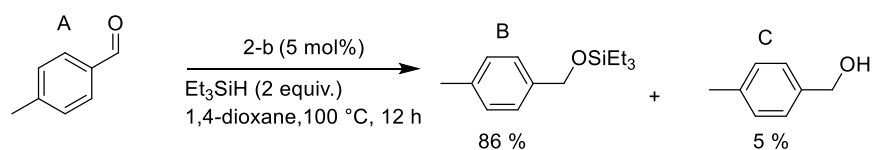


Figure S66. GC/MS chromatogram for the hydrosilylation of 4-methylbenzaldehyde with **2-b**.

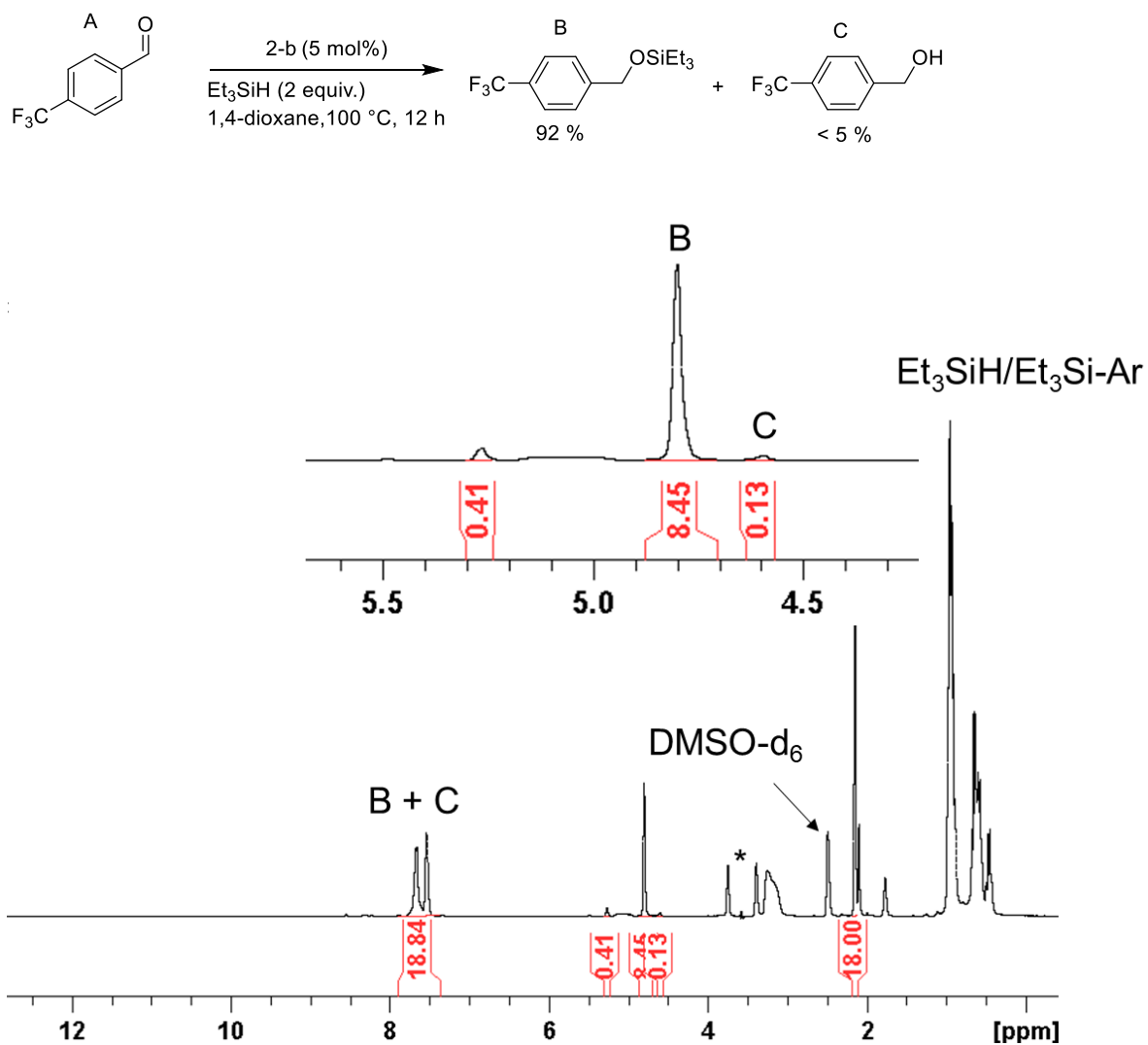


Figure S67. ^1H NMR spectrum for hydrosilylation of 4-(Trifluoromethyl)benzaldehyde with **2-b**. (Substrate: hexamethylbenzene = 4.6:1). Asterisk (*) is used to denote suppressed 1,4-dioxane.

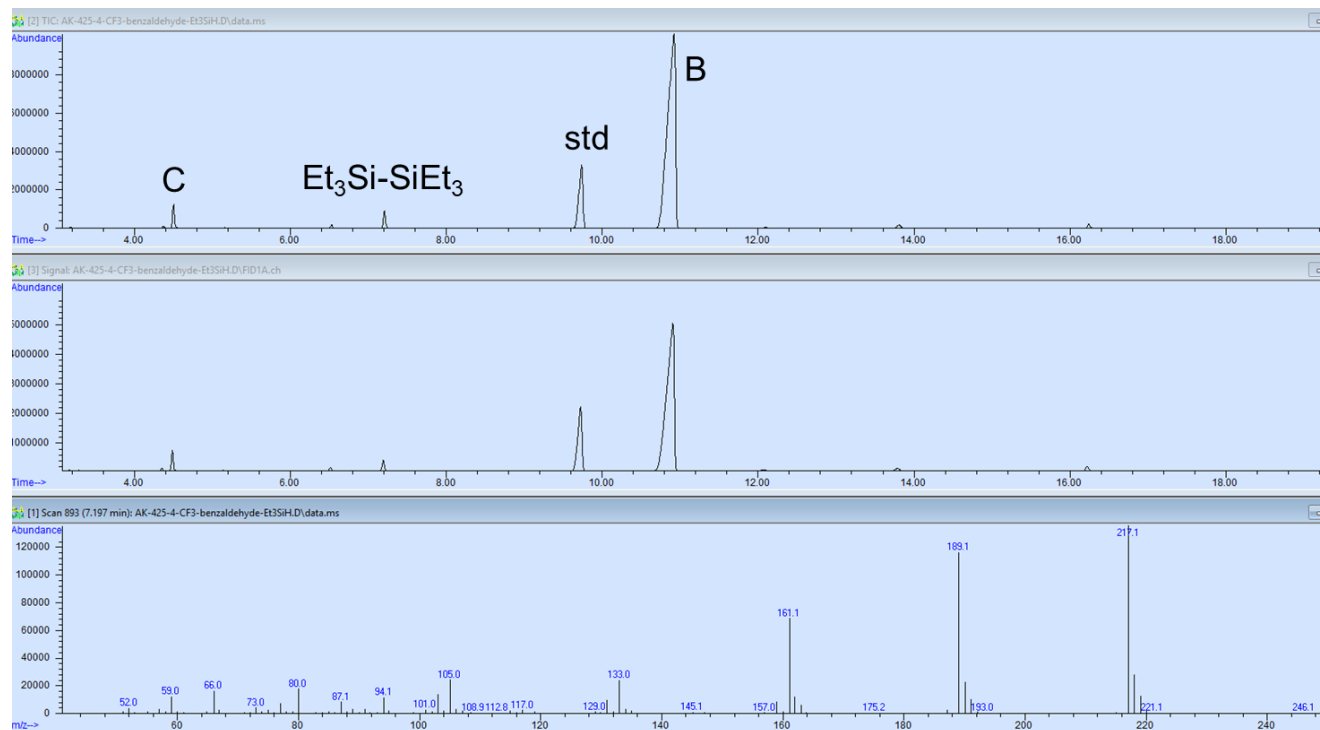
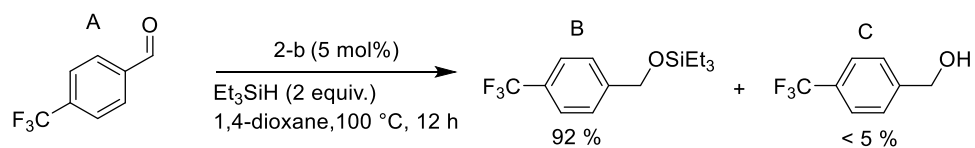


Figure S68. GC/MS chromatogram for the hydrosilylation of 4-(Trifluoromethyl)benzaldehyde with **2-b**.

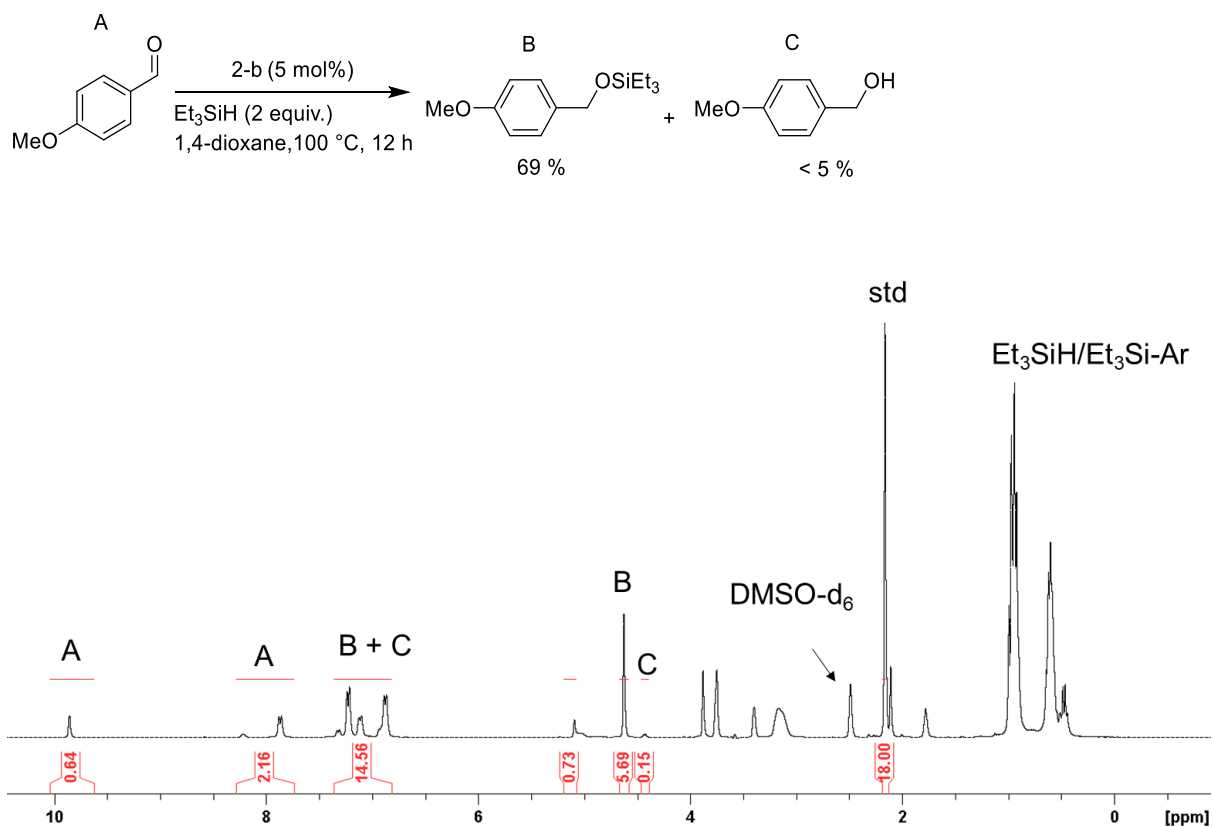


Figure S69. ^1H NMR spectrum for the hydrosilylation of 4-methoxybenzaldehyde with **2-b**. (Substrate: hexamethylbenzene = 4.1:1). Asterisk (*) is used to denote suppressed 1,4-dioxane.

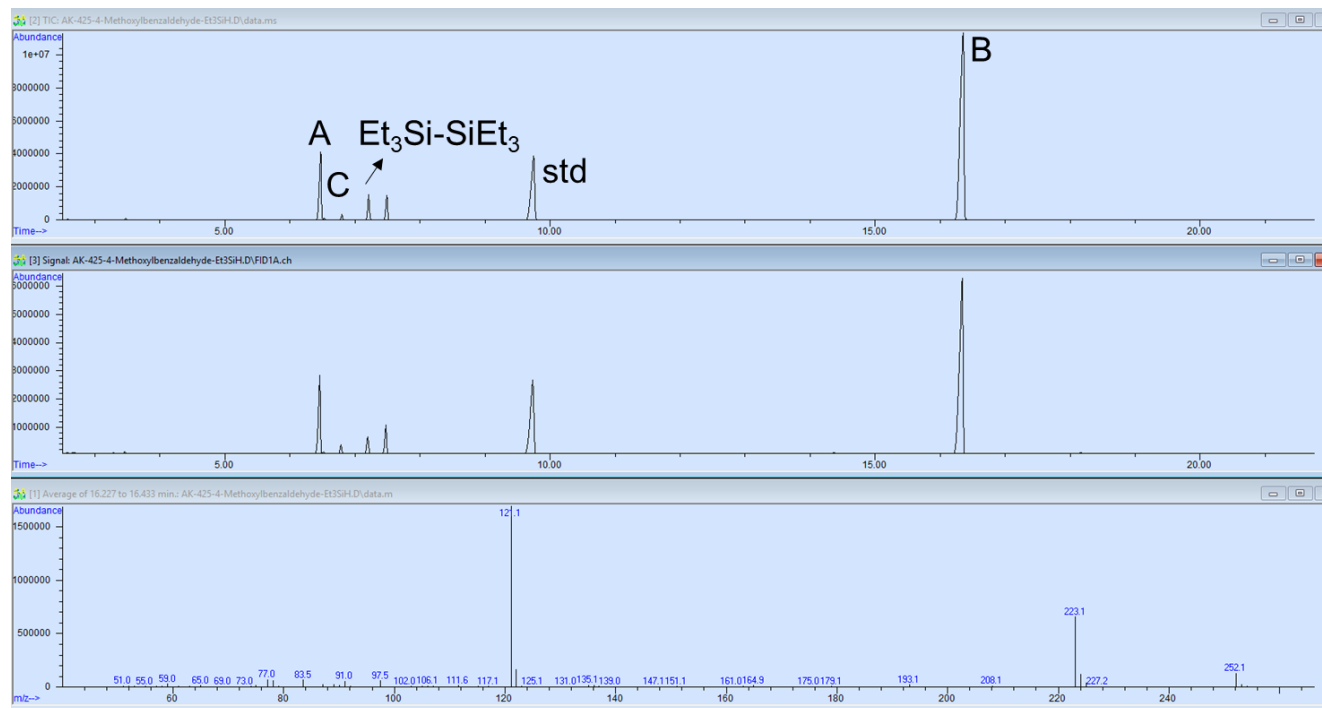
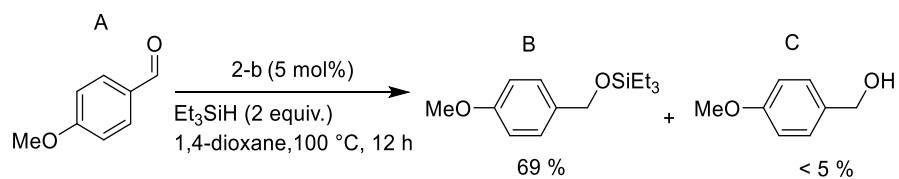


Figure S70. GC/MS chromatogram for the hydrosilylation of 4-methoxybenzaldehyde with **2-b**.

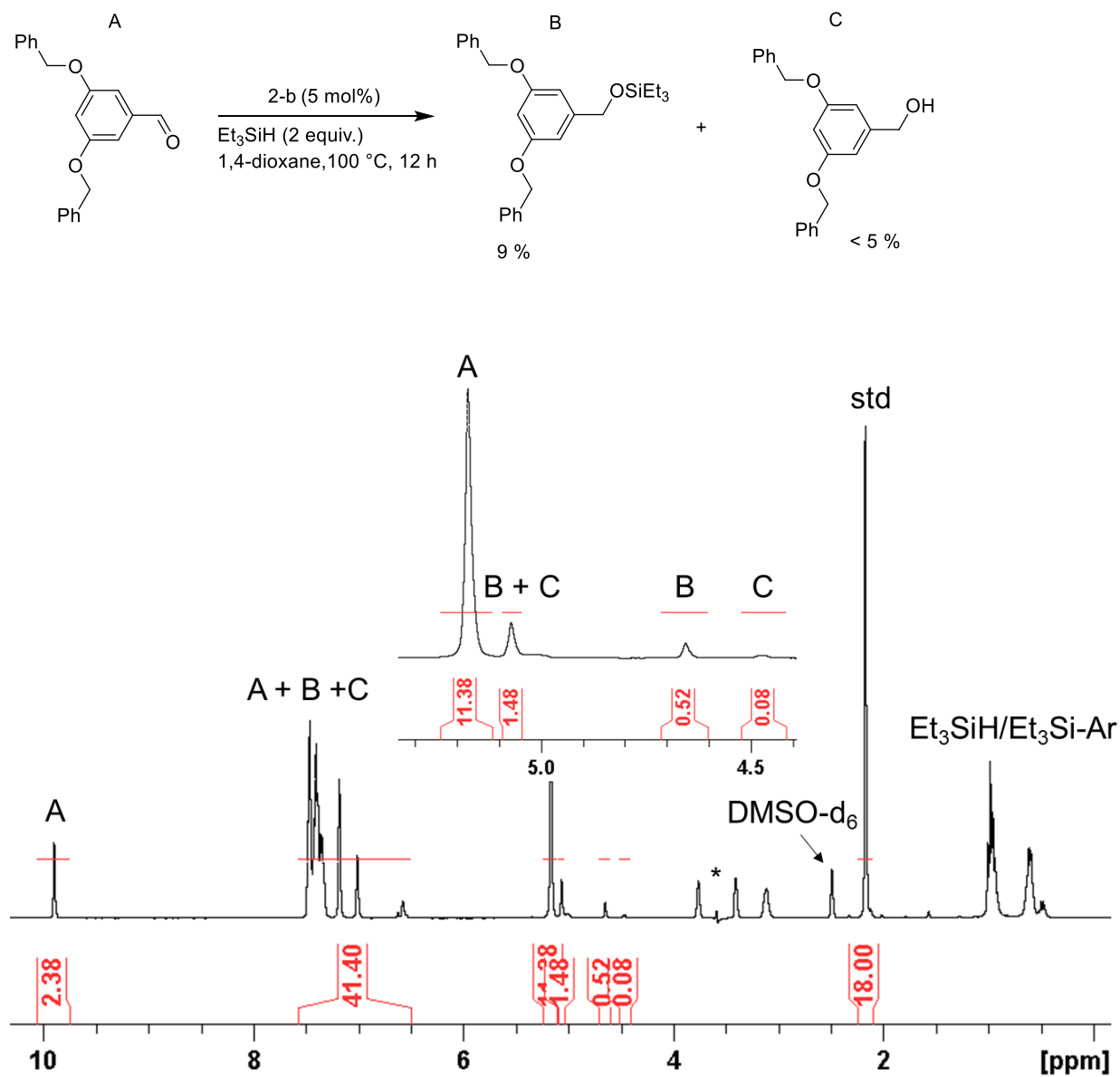


Figure S71. ^1H NMR spectrum for the hydrosilylation of 3,5-dibenzoyloxybenzaldehyde with 2-b. (Substrate: hexamethylbenzene = 2.9:1)

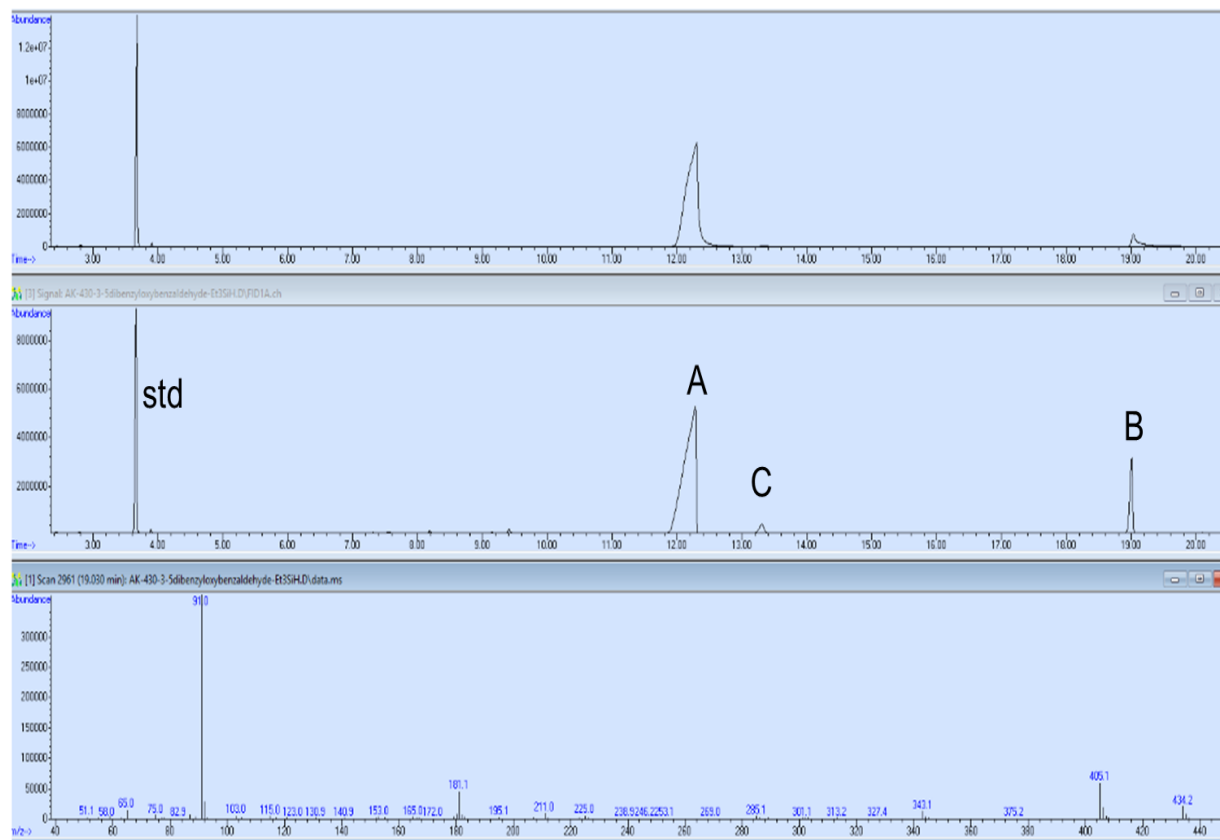
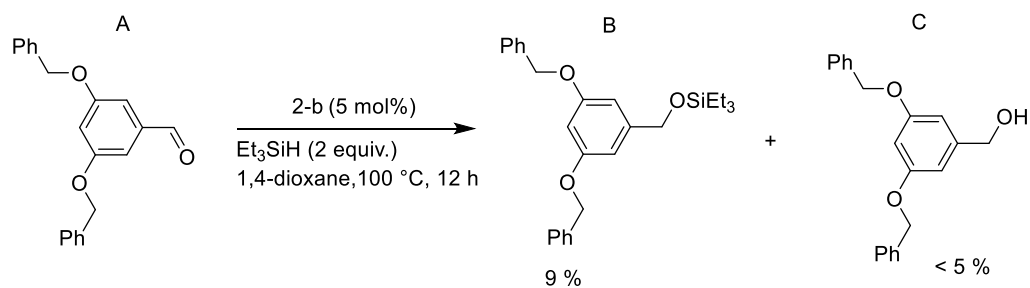


Figure S72. GC/MS chromatogram for the hydrosilylation of 3,5-dibenzoyloxybenzaldehyde with 2-b.

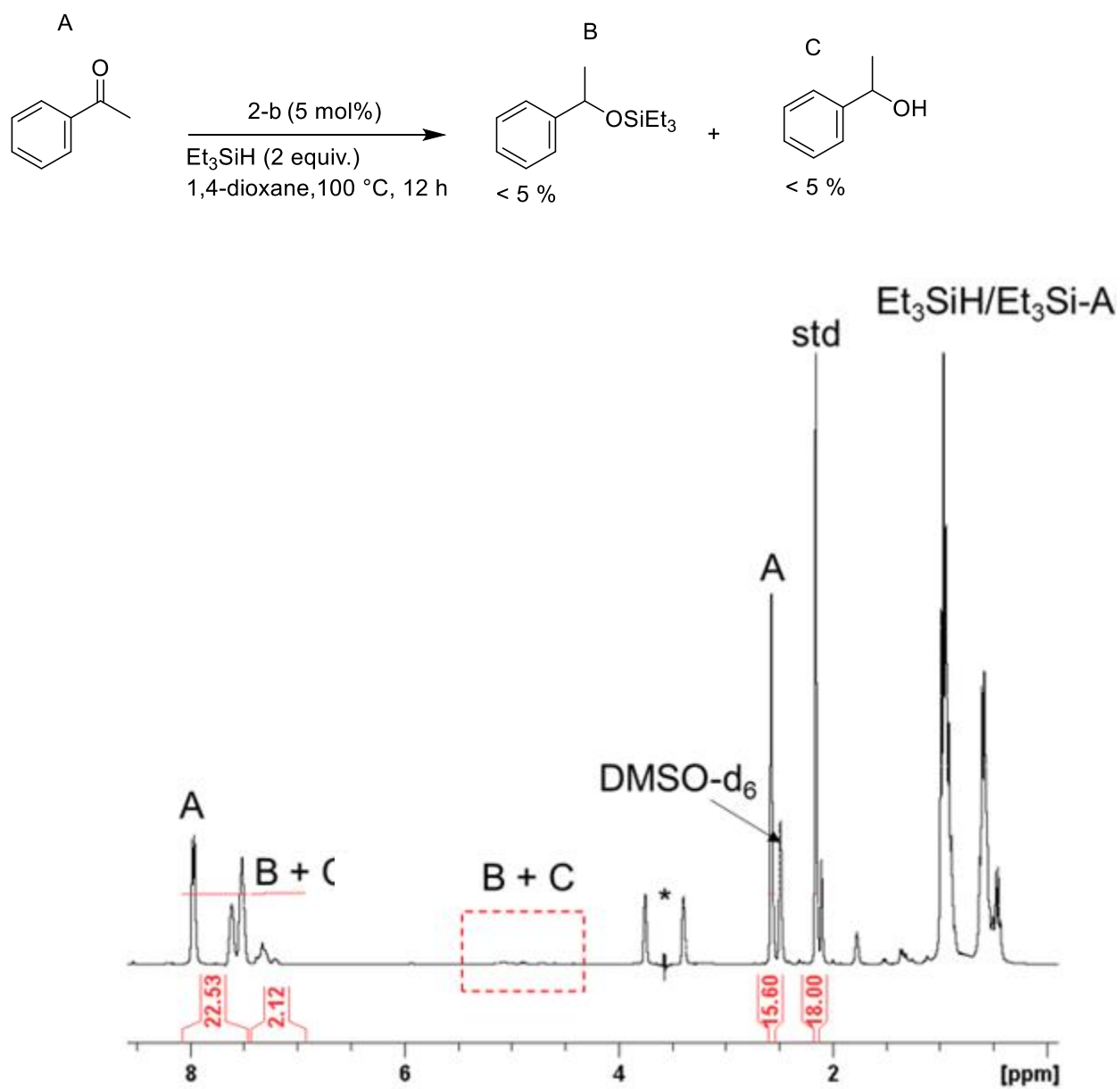


Figure S73. ^1H NMR spectrum for the hydrosilylation of acetophenone with **2-b**. (Substrate: hexamethylbenzene = 4.6:1)

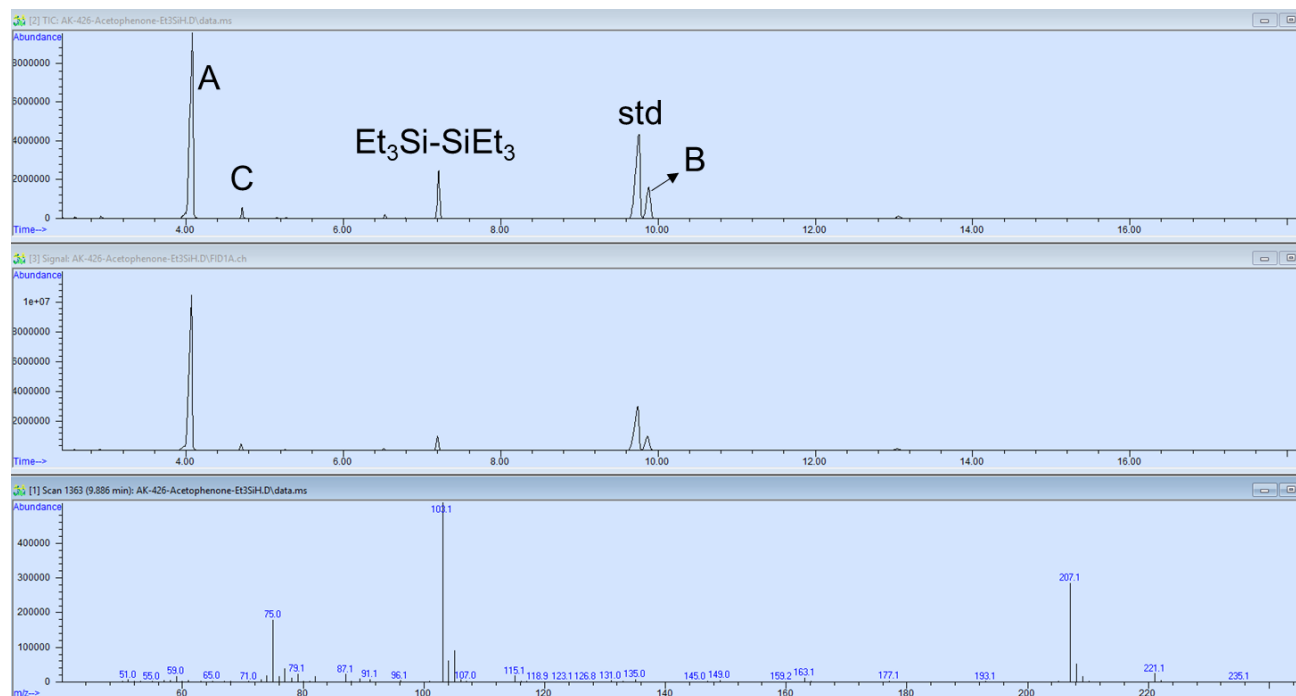
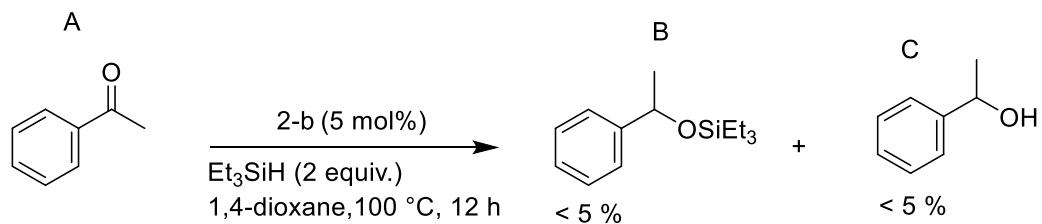


Figure S74. GC/MS chromatogram for the hydrosilylation of acetophenone with **2-b**.

REFERENCES

- (1) Kassie, A. A.; Duan, P.; McClure, E. T.; Schmidt-Rohr, K.; Woodward, P. M.; Wade, C. R. Postsynthetic Metal Exchange in a Metal–Organic Framework Assembled from Co(III) Diphosphine Pincer Complexes. *Inorg. Chem.* **2019**, 58, 3227–3236.